LMS/RBL/S09152

Modeling of Flow and Transport Induced by Gas Production Wells near the Project Rio Blanco Site, Piceance Basin, Colorado

June 2013

Approved for public release; further dissemination unlimited

U.S. DEPARTMENT OF ENERGY | Legacy Management

Available for sale to the public from:

U.S. Department of Commerce
National Technical Information Service
5301 Shawnee Road
Alexandria, VA 22312
Telephone: 800.553.6847
Fax: 703.605.6900
E-mail: orders@ntis.gov
Online Ordering: *http://www.ntis.gov/help/ordermethods.aspx*

Available electronically at *http://www.osti.gov/scitech/*

Available for a processing fee to U.S. Department of Energy and its contractors, in paper, from:

U.S. Department of Energy
Office of Scientific and Technical Information
P.O. Box 62
Oak Ridge, TN 37831-0062
Phone: 865.576.8401
Fax: 865.576.5728
Email: reports@adonis.osti.gov

Reference herein to any specific commercial product, process, or service by trade name, trademark, manufacturer, or otherwise, does not necessarily constitute or imply its endorsement, recommendation, or favoring by the United States Government or any agency thereof or its contractors or subcontractors.

LMS/RBL/S09152

Modeling of Flow and Transport Induced by Gas Production Wells near the Project Rio Blanco Site, Piceance Basin, Colorado

June 2013

Approved for public release; further dissemination unlimited

This page intentionally left blank

Contents

Abbreviations iv
Executive Summary v
1.0 Introduction 1
1.1 Modeling Objectives 4
1.1.1 Summary of Past Modeling 4
1.1.2 Rationale for Rio Blanco Modeling 4
1.2 Geologic Setting 5
1.3 Nuclear Test Description 6
1.4 Radionuclide Source and Potential Migration Pathways 8
1.4.1 Radionuclides Removed by Production Testing, Upper and Lower Chimneys 10
1.4.2 Radionuclide Disposition 13
2.0 Conceptual and Numerical Model of Flow and Transport within the Mesaverde 14
2.1 Numerical Modeling Code 15
3.0 Rio Blanco Model Construction 15
3.1 Rio Blanco Model Domain and Discretization 15
3.2 Formation Lithologic Distribution 19
3.3 Rio Blanco Detonation Zones 21
3.4 Hydrofracturing of Wells 24
3.5 ROCK (Material) Parameters 25
3.5.1 Permeability and Porosity 26
3.5.2 Capillary Pressure and Relative Permeability 26
3.6 Boundary Conditions 29
3.7 Initial Concentration and Partitioning of Tritiated Water (THO) Between Gas and Aqueous Phases 29
3.8 Initial Conditions 32
3.8.1 Formation 33
3.8.2 Detonation Zones 33
3.9 Decay and Diffusion 35
3.10 Well Treatment (Sources and Sinks) 36
3.10.1 Reentry Wells 36
3.10.2 Gas Wells 38
4.0 Model Calibration 38
4.1 Upper Chimney Reentry Well Calibration 39
4.2 Other Significant Well Data Considered for Calibration 40
5.0 Rio Blanco Simulation Results 41
5.1 Simulations from Post-Detonation to 2015 Conditions 41
5.2 Consideration of Recompleting Well RB-U4 53
5.3 Simulation of Future Drilling near Rio Blanco 55
6.0 Summary and Conclusions 63
7.0 References 64

Figures

Figure 1. Delineation of the Piceance Basin 2
Figure 2. Institutional Control Boundary 3
Figure 3. Piceance Basin Cross Section 6
Figure 4. Generalized Cross Section of Rio Blanco 7
Figure 5. Schematic of Reentry Well AR-1 11
Figure 6. Concentration of Tritium and ^{85}Kr in Dry Gas 12
Figure 7. Concentration of Tritium in Separator Water 13
Figure 8. Horizontal Extent of Current Model Domains 16
Figure 9. Map of the Rio Blanco Model Area in Real Coordinates (Feet, State Plane Colorado Central, NAD 27), Including Lot Boundaries, Current Wells, and Element Centers (Dark Blue) 17
Figure 10. Map of the Rio Blanco Model in Model Coordinates, Including Site Wells, Simulated Hypothetical Wells, and Element Centers 18
Figure 11. Vertical Extent of the Rulison Model with Model Depth, Elevation, and Vertical Extent of Previous Models 19
Figure 12. Rio Blanco Model Lithologic Distribution 20
Figure 13. Vertical (Side View) Slice of the Model Chimneys and Nuclear Fractured Regions 22
Figure 14. Horizontal (Top View) Slices of the Model Chimneys and Nuclear Fractured Regions That Resulted from the Upper and Middle Detonations 23
Figure 15. Sliced Model Domain Showing Several Hydrofractured Wells (Simulated Potential Future) and Detonation Zones 25
Figure 16. Capillary Pressure Curves for the Modeled ROCK Types 27
Figure 17. Gas Relative Permeability Curves for the Modeled ROCK Types 28
Figure 18. Inverse Vapor Pressure of Water Relative to Temperature 30
Figure 19. Effects of Molecular Weight and Temperature on the Initial Partitioning of THO from the Aqueous Phase to the Gas Phase 32
Figure 20. Initial Liquid Saturation Conditions (Flood) 34
Figure 21. Initial Temperature Distribution 35
Figure 22. Pressure Decline Curve for the Upper Chimney Reentry Well Production 37
Figure 23. Pressure Decline Curve for the Lower Chimney Reentry Well Production 37
Figure 24. Simulated Mass Rate Removed 38
Figure 25. Overlay of Calibrated Simulated Pressure Curve with Observed Pressure 39
Figure 26. Plot of Results of Parameter Calibration Simulations 40
Figure 27X. Initialized Mass Fraction of THO in the Gas Phase (Xthogas) After the Detonation 43
Figure 27P. Initialized Pressure Distribution After the Detonation 43
Figure 28X. Mass Fraction of THO Gas Beginning of Production Testing 44
Figure 28P. Pressure Distribution at Beginning of Production Testing 44
Figure 29X. Mass Fraction of THO After First Production Test, AR-1 45
Figure 29P. Pressure Distribution After First Production Test, AR-1 45
Figure 30X. Mass Fraction of THO After Second Production Test, AR-1 46
Figure 30P. Pressure Distribution After Second Production Test, AR-1 46
Figure 31X. Mass Fraction of THO Beginning AR-2 Testing 47
Figure 31P. Pressure Distribution Beginning AR-2 Testing 47
Figure 32X. Mass Fraction of THO End of AR-2 Testing 48

Figure 32P. Pressure Distribution End of AR-2 Testing 48
Figure 33X. Mass Fraction of THO 1000 days After Detonations 49
Figure 33P. Pressure Distribution 422 days After End of Production Testing of AR-2 49
Figure 34X. Mass Fraction of THO in 2015 50
Figure 34P. Pressure Distribution in 2015 50
Figure 35. Initial Temperature Distribution 52
Figure 36. Temperature Distribution in 2015 52
Figure 37. Simulated Concentration Distribution Relative to Well RB-U4 in 2015 53
Figure 38. "As Is" Diagram of Well RB-U4 54
Figure 39X. Mass Fraction of THO in 2016 (y45) 56
Figure 39P. Pressure Distribution in 2016 56
Figure 40X. Mass Fraction of THO in 2020 (y45, x97) 57
Figure 40P. Pressure Distribution in 2020 57
Figure 41X. Mass Fraction of THO in 2035 (y41, x97) 58
Figure 41P. Pressure Distribution in 2035 58
Figure 42X. Mass Fraction of THO in 2040 (y45, x70, x97) 59
Figure 42P. Pressure Distribution in 2040 59
Figure 43X. Mass Fraction of THO in 2055 (y45, x70, x97) 60
Figure 43P. Pressure Distribution in 2055 60
Figure 44. Pressure Distribution in 2040 with Well RB-U4 (looking SE) 61
Figure 45. Pressure Distribution in 2055 With Well FCG #1 (looking NW) 61
Figure 46. Simulated Temperature Distribution in 2055 63

Tables

Table 1. Gas-Phase Components and Potential Radionuclides 8
Table 2. ^{85}Kr: Created by Detonation, Removed by Testing, Remains in 2012 After Decay 9
Table 3. Tritium: Created by the Detonation, Removed by Testing, Remains in 2012 After Decay 9
Table 4. Model Coordinates and Ellipsoid Radii of Chimneys and Nuclear Fracture Extents 21
Table 5. ROCK types used in the Rulison and Rio Blanco Models 26
Table 6. Parameters from Calibration That Provided the Best Fit for One Realization 39
Table 7. Range of Parameters Used in the Sensitivity Runs 40
Table 8. Key Steps in Simulating Post-detonation to 2015 42
Table 9. Milestones in the Rio Blanco Simulation 55

Appendixes

Appendix A Summary Reports on Projects Rio Blanco and Rulison from 2001 through 2010
Appendix B Method Used to Create Sandstone - Shale Realizations

Abbreviations

^{14}C	carbon-14
Ci	curie
DOE	U.S. Department of Energy
DRI	Desert Research Institute
ft	feet
g/mol	grams per mole
^{85}Kr	krypton-85
LM	Office of Legacy Management
m	meters
MCF	thousand cubic feet
MMCF	million cubic feet
MPa	megapascals
N/S	north/south
psi	pounds per square inch
SGZ	surface ground zero
THO	tritiated water

Executive Summary

The 1973 Project Rio Blanco nuclear test in the Piceance Basin of western Colorado was the third and last natural gas stimulation experiment in the Plowshare Program. It was designed to use three simultaneously detonated nuclear devices to fracture low-permeability, gas-bearing rock and create a single connected chimney to enhance natural gas production. Following the detonations, testing on the reentry well into the upper chimney produced gas at rates greater than those of conventional wells of the time but significantly less than the earlier Project Rulison test, which also took place in the Piceance Basin. Testing on the reentry well into the lower chimney produced even less gas, and the test was abandoned. Based on the reentry well data, it was determined that the three chimneys failed to connect and that the higher water content of the formations targeted by the Rio Blanco test was too high for the nuclear stimulation to be successful. The Rulison detonation was in the underlying section, which has a lower water content and is the target of current gas development. Recent advances in hydrofracturing technology have made it feasible to extract natural gas from low-permeability reservoirs and have led to a significant increase in drilling in the area. Drilling activity near the Rio Blanco and Rulison sites has raised concerns that remnant radioactivity in the detonation zones could migrate to nearby producing wells and enter the natural gas distribution system. Radionuclides that can exist in the gas phase and were created in significant amounts by the detonations are of primary concern because of their potential mobility. The relative permeability of the gas phase is orders of magnitude greater than that of liquids in the natural-gas-producing reservoirs at the Rio Blanco site. The primary gas-phase radionuclide of concern is tritium as tritiated water vapor. Tritiated liquid water in the detonation zone acts as a source that partitions from the low-mobility aqueous phase to the higher-mobility gas phase.

Numerical modeling can be used to make predictions about a site's flow system and contaminant transport potential by quantitatively replicating the site conceptual model and various aspects of the system, allowing past, current, and future scenarios to be tested. The modeling effort for the Rulison site has been employed at Rio Blanco. The Rio Blanco model was initialized to conditions following the detonations and used to simulate the reentry well production testing, the subsequent pressure recovery after testing ended, migration of contamination from the detonation zone to its current extent, and the potential effects on the flow system of future gas wells. The model was calibrated to the historical reentry well data from the upper chimney. Attempts were made to be conservative by elongating the detonation zone, both the chimney and surrounding nuclear fractured region, in the direction of the natural fracture trend in the area and by using a conservatively high estimate of mobile tritium in the detonation zone. The model was used to simulate the effects of a staged drilling approach at Rio Blanco similar to that recommended in the Rulison Path Forward document (DOE 2010). The simulation results indicate that contamination, in the form of tritiated water, is contained within the institutional control boundary and does not migrate beyond well RB-U4 (600 feet from the detonations). Simulations of future wells producing in the underlying gas-bearing section reduce pressures in that section but do not create a pressure gradient sufficient to induce migration from the detonation zone to a producing well. The modeling provides quantifiable results that allow the effects of gas production on the flow system and the potential for contaminant migration to be visualized at the Rio Blanco site.

This page intentionally left blank

1.0 Introduction

The Piceance Basin in western Colorado contains significant reserves of natural gas in poorly connected, low-permeability (tight) sandstone lenses of the Mesaverde Group. The ability to enhance the production of natural gas in this area has long been a goal of the oil and gas industry. The U.S. Atomic Energy Commission, predecessor agency to the U.S. Department of Energy (DOE) and the U.S. Nuclear Regulatory Commission, participated in three tests using nuclear detonations to fracture gas-bearing formations in an effort to enhance gas production. The tests were conducted under Project Plowshare, a program designed to identify peaceful, beneficial uses for nuclear explosives. The first, Project Gasbuggy, was conducted in 1967 in the San Juan Basin of New Mexico. The 29-kiloton fission-fusion device produced significant amounts of tritium (38,000 curies [Ci], Sokol 1970) in the subsurface. The two subsequent tests in the Piceance Basin of Colorado (Figure 1), Project Rulison in 1969 and Project Rio Blanco in 1973, were designed to limit the amount of tritium produced by using fission devices and enhanced shielding. The 40-kiloton Rulison device (DOE 2000) produced 10,000 Ci of tritium (Reynolds 1971), and the three simultaneously detonated 33-kiloton devices at Rio Blanco produced 1,000 Ci each, for a total of 3,000 Ci (Toman 1974). Among the many radionuclides created by the detonations, tritium (an isotope of hydrogen with two neutrons) is considered the most likely radionuclide that could feasibly migrate to nearby gas-producing wells due to its occurrence in both the gas and liquid phases, its abundance relative to other mobile radionuclides, and its relatively long half-life.

The ability to enhance natural gas production from tight sands has become practical through advances in hydrofracturing technology. Fluids with entrained sand are pumped into gas reservoirs at high pressure, creating fractures that extend outward from the wellbore. After fracturing, the fluid is extracted, and the sand remains, keeping the fractures propped open, enhancing reservoir permeability and gas flow to a well. The ability to hydrofracture tight sandstones has enabled gas development in the Piceance Basin. An increase in drilling activity near the Rulison and Rio Blanco sites has raised concerns that contamination currently contained in the subsurface could be released through a gas well drilled too close to the site.

As wells are drilled nearer the Rulison and Rio Blanco sites, the DOE Office of Legacy Management (LM) has taken the approach outlined in the June 2010 Rulison Path Forward document (DOE 2010, available on the LM website: http://www.lm.doe.gov/Rulison/Documents.aspx). The Path Forward recommends that drillers adopt a conservative, staged approach to gas development. They are encouraged to drill wells in areas with a low likelihood of encountering contamination (both distance and direction from the detonation zone are factors) and to collect data from these wells prior to drilling nearer the sites. The Path Forward relies in part on the results from a numerical modeling effort that indicate contamination has been contained within the institutional control boundary (Figure 2). The Path Forward document couples the model predictions with the monitoring of gas and produced water from the gas wells and the monitoring of shallow groundwater near the site (see the Rulison Monitoring Plan on the LM website). In coordination with the Colorado Oil and Gas Conservation Commission, DOE reviews applications to drill within 3 miles of Rulison. Drilling near the Rio Blanco site has progressed more slowly than at Rulison, but it is expected that a path forward similar to that at Rulison will be recommended for Rio Blanco and will incorporate both the similarities and differences between the two sites.

Figure 1. Delineation of the Piceance Basin
(based on the contact between Tertiary and Upper Cretaceous rocks, Green 1996)

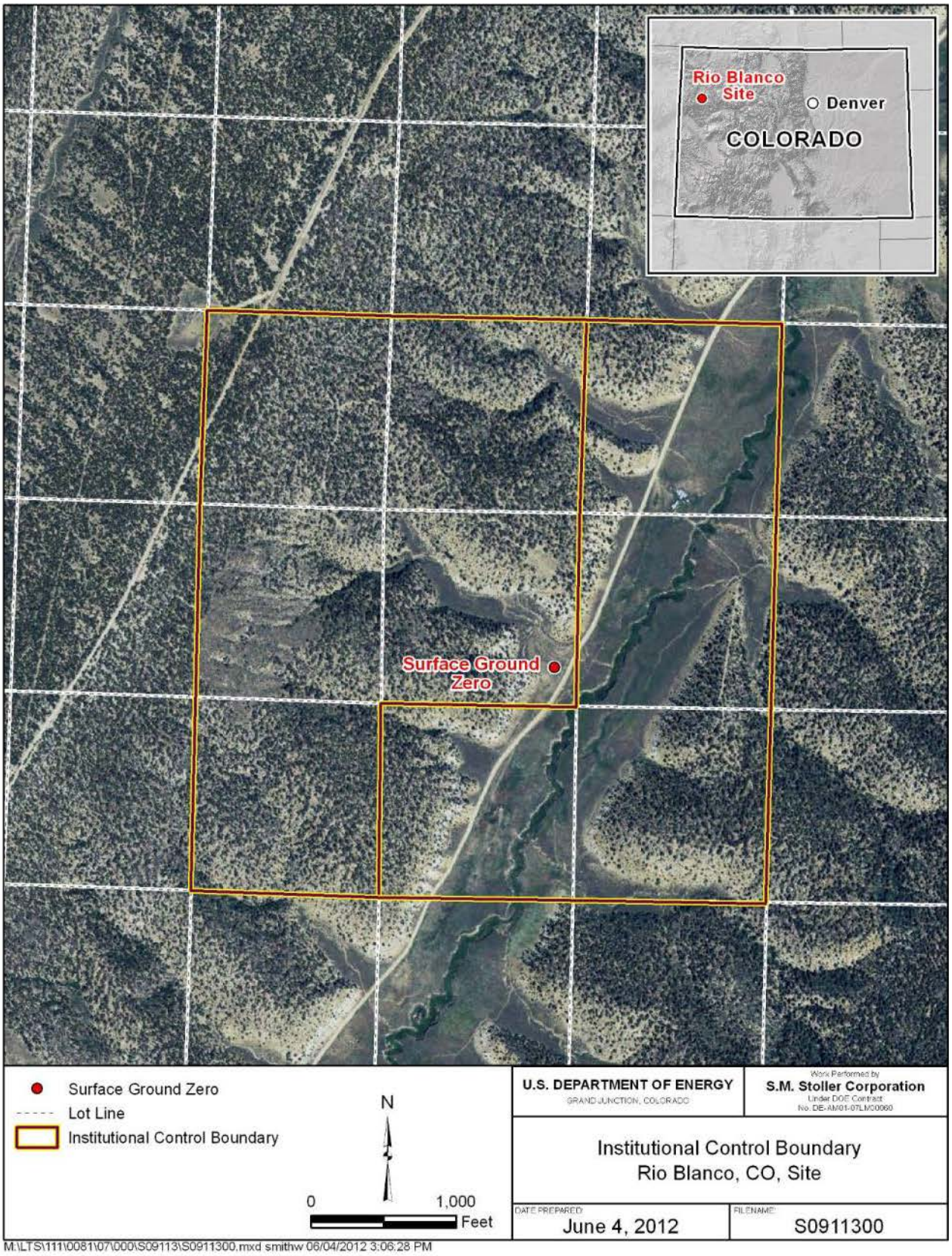

Figure 2. Institutional Control Boundary
(left permanent, right till October 3, 2046)

1.1 Modeling Objectives

A numerical model is a tool that incorporates hydrogeologic data for a given site to make quantitative predictions on fluid flow and potential contaminant transport. The various models of both Rulison and Rio Blanco were used to estimate the current extent of contamination, simulate the flow of fluids to one or more producing wells as they are drilled nearer the detonations, and evaluate the potential for contaminant migration from the detonation zone to the wells.

1.1.1 Summary of Past Modeling

The Rio Blanco flow and tritium transport numerical model, performed by Desert Research Institute (Cooper et al. 2005), simulated that following the nuclear detonation, tritiated water vapor would travel only about 100 meters (m) radially outward from the center of the chimney/cavity. Simulations of krypton-85 (^{85}Kr, a noble gas) showed behavior similar to that of tritium, primarily due to the similar half-lives of tritium and ^{85}Kr. Numerical simulations were also conducted in which a gas production well was located 292 m from the center of the chimney, with a production interval at the same elevation as the middle of the three simultaneous detonations. Monte Carlo techniques were used in an attempt to quantify the variability of flow and transport parameters. For a reference simulation with the "best" estimate of reservoir parameters, tritium was shown to travel only 100 m (the same as for the diffusive-only case) beyond the center of the chimney. Simulations to test the effects of fracture spacing were also conducted on a 2D model using the MINC (multiple interacting continua) mesh generator. Results indicated that a fracture spacing of 20 m or less performed similarly to the equivalent porous media model used for the 3D simulations.

Reviewers of the model expressed concerns that it was constructed with layers that did not adequately represent the discontinuous interbedded sandstone and shale lenses at the site. The subsequent modeling of the Rulison site (Cooper et al. 2007), also in the Williams Fork Formation of the Piceance Basin, used a spatially correlated sand-shale distribution to add subsurface heterogeneity. The Rulison model was improved in a follow-up addendum (Cooper et al. 2009) to address concerns with the value of the partitioning coefficient controlling the distribution of tritiated water between the liquid and vapor phases, the assignment of effective porosity to hydraulically generated fractures surrounding a hypothetical production well, and the treatment of molecular diffusion in the partially saturated reservoir. A concern not addressed by the addendum was the limited use of data from the site in constructing the Rulison model. The model was updated again in 2010 (Cooper et al. 2010) to address this concern. The updated model used sandstone and shale ratios from nearby wells (less than 0.5 mile from the model domain) and was calibrated to historical data from the reentry well production tests performed in 1970 and 1971. The latest revision to the Rulison model expands the domain horizontally to include active production wells and vertically to include the entire gas-producing section. The latest Rulison model, which was used as a blueprint for this Rio Blanco modeling study, is being released concurrently with this study. A summary of the past Rio Blanco and Rulison modeling is provided in Appendix A.

1.1.2 Rationale for Rio Blanco Modeling

The Rio Blanco model was based on the methods used to develop the Rulison model that simulates the staged approach to drilling recommended in the Rulison Path Forward document

(DOE 2010). Reading the Rulison model report would be beneficial to understanding the approach taken for the Rio Blanco modeling. The Rio Blanco and Rulison sites have many similarities that initially suggest one model could suffice for both sites. Both are in the Piceance Basin, and drilling near both sites targets the same productive interval. The primary differences are that three simultaneous detonations occurred at Rio Blanco, the detonations were in the stratigraphic interval above the current producing interval (the Rulison detonation was in the productive interval), and post-detonation reentry well testing was limited at Rio Blanco relative to the Rulison production testing. Wells drilled near Rio Blanco to exploit the deeper gas zones drill through the detonation interval, and modeling provides an estimate of the extent that contamination could migrate away from the detonations by diffusion. Modeling can also predict the likelihood that nearby production wells could induce contaminant migration from the detonation zones. In a fashion similar to the Rulison modeling, which simulates the enactment of the Rulison Path Forward, the Rio Blanco model can be used to simulate the effects of a series of wells drilled progressively closer to the site and producing from the current gas production zone. This report is the first update to the Rio Blanco model since new conceptualizations and methodologies were developed in the Rulison modeling efforts.

1.2 Geologic Setting

The Tertiary and Cretaceous strata of the Piceance Basin contain significant hydrocarbon reserves. The Green River Formation is estimated to contain up to 1.45 trillion barrels of oil in place (http://www.ogj.com/articles/2011/10/green-river-shale-oil-in-place-put-at-1-45-trillion-bbl.html), half of which is in the Piceance Basin. Gas reserves in the Upper Cretaceous Mesaverde Group (Figure 3) are estimated at 300 trillion cubic feet (http://oilshalegas.com/piceancebasin.html). The Williams Fork Formation of the Mesaverde Group is composed of low-permeability, discontinuous, interbedded fluviodeltaic sandstones and shales. There is a general east-west trend of natural fractures in the lower Tertiary and Upper Cretaceous section that varies somewhat with depth and location within the basin. The tight sandstones in the lower two-thirds of the Williams Fork can be stimulated by hydrofracturing to enhance production. Gas-bearing sandstones in the upper third of the Williams Fork and the overlying Ft. Union Formation are more continuous, but are not production targets due to their higher water content, which lowers the relative permeability of the gas phase and causes water production to be excessive compared to the amount of gas that can be produced. After hydrofracture stimulation of sandstones in the productive interval, a well typically drains about 10 to 40 acres. The different estimates are due to differences in interpretations by operating companies, and the success of the recent adoption of the closer 10-acre spacing near Rulison will be evaluated after a sufficient production history is available.

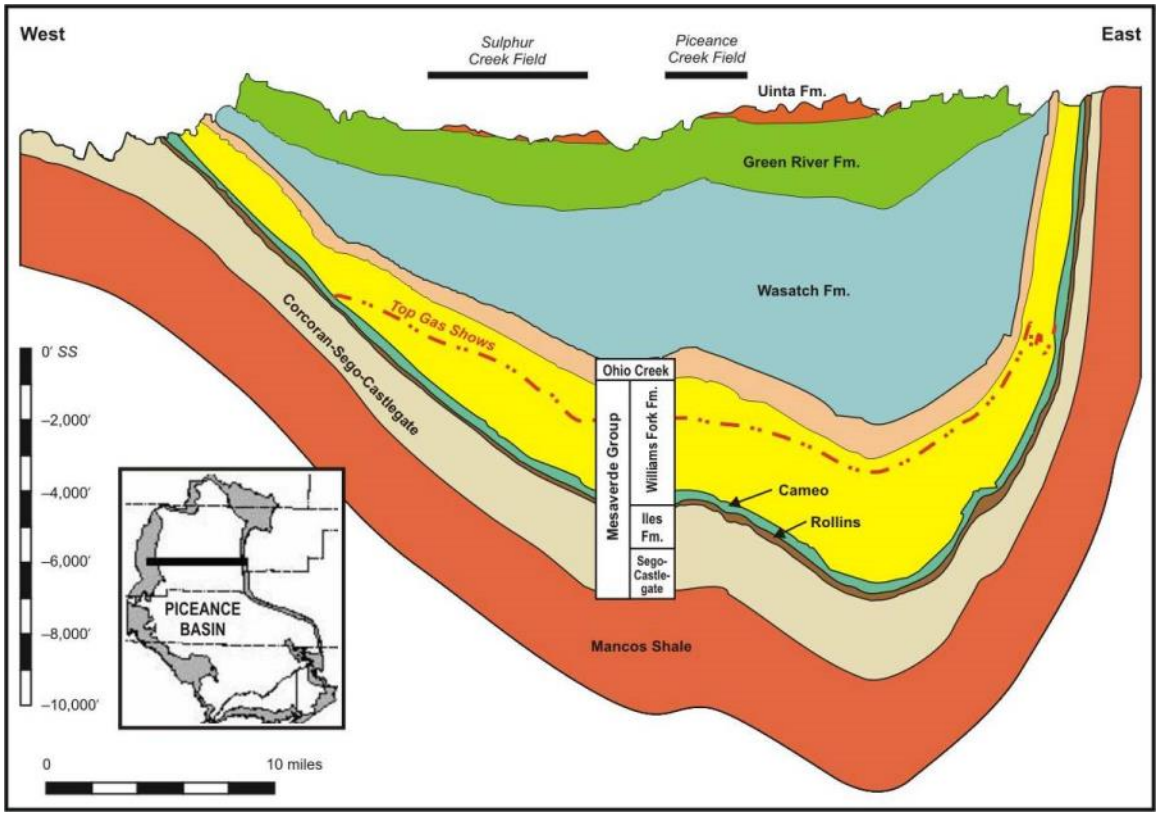

(modified from Yurewicz 2003)

Figure 3. Piceance Basin Cross Section

1.3 Nuclear Test Description

The extremely high temperatures associated with a subsurface nuclear detonation vaporize a volume of rock and produce a roughly spherical cavity surrounding the blast point. A high-pressure shock wave spreads from the blast, fracturing the rock beyond the cavity wall to a distance related to the yield of the device, depth of burial, and the rock properties. As the high temperatures decrease, the vaporized rock condenses to a liquid melt that flows to the base of the cavity. Within minutes to hours after the detonation, the fractured rock above the cavity usually collapses, forming a rubble-filled chimney. The chimney region extends upward from the base of the former cavity to where open fractures end and a stable vaulted ceiling forms. The rubble zone with rock fragments entrained in a glassy matrix forms when the cavity collapses into the basal melt zone. The relatively rapid rate of cooling causes the solidified melt rock to have a vitreous texture (melt glass).

At Rio Blanco, there were three simultaneous 33-kiloton detonations at depths of 5,840 feet (ft), 6,230 ft, and 6,690 ft below ground surface (Figure 4), each with an initial cavity radius of 66 ft (Toman 1974). There was partial fluid loss at 265 ft and complete fluid loss at 248 ft above the upper detonation during the drilling of the reentry well to the upper chimney, which formed from collapse into the estimated 66 ft radius cavity. Formation permeability was believed to be increased 10 to 30 times to a distance of 3 cavity radii (198 ft). The production testing indicated that there was very little communication between the uppermost chimney and the lower ones. At

the end of a second drawdown test, small amounts of xenon and krypton (tracers in the middle and lower detonations) were detected (Toman 1974).

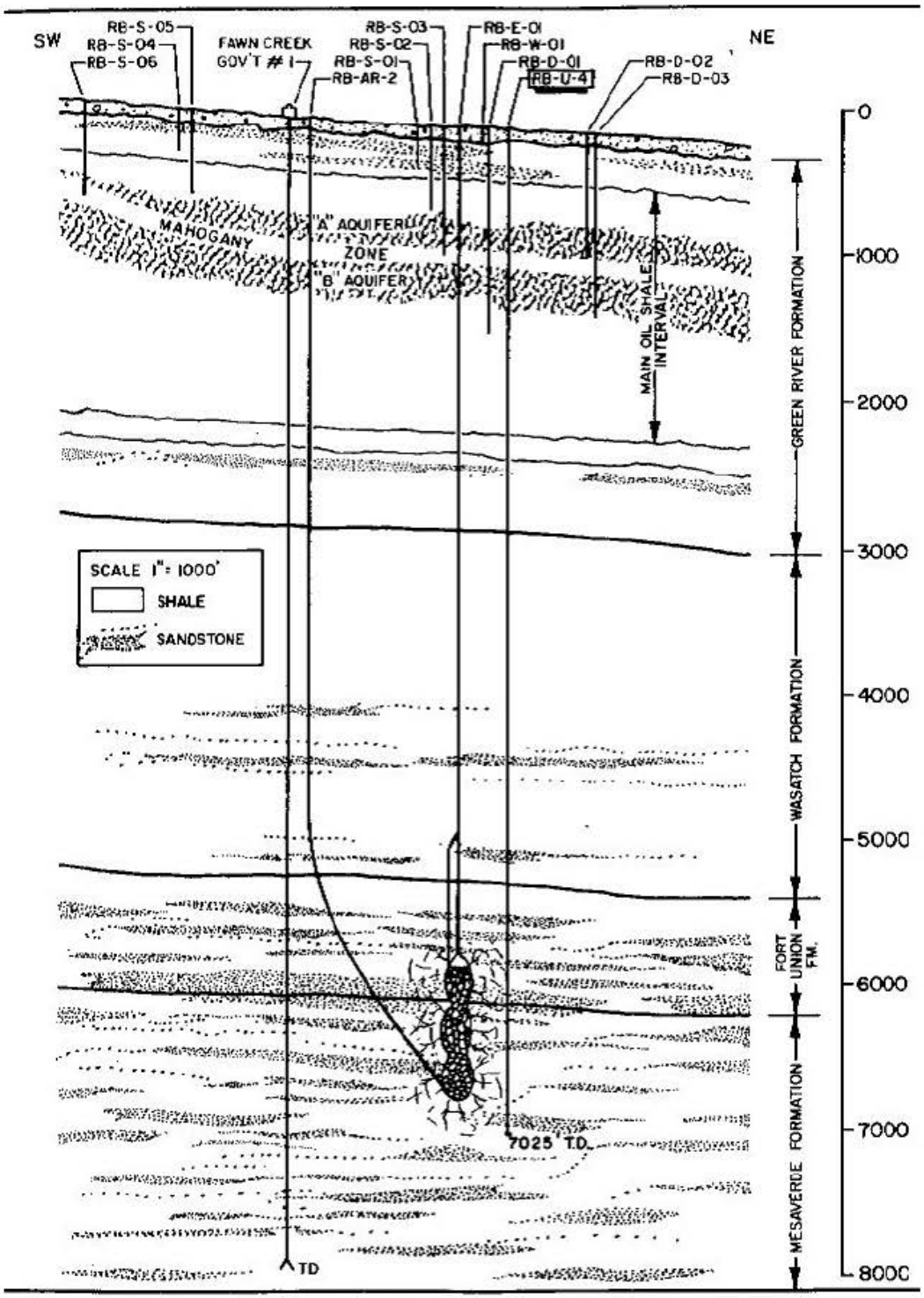

Source: ERDA 1975

Figure 4. Generalized Cross Section of Rio Blanco

1.4 Radionuclide Source and Potential Migration Pathways

An underground nuclear detonation produces a number of radionuclide contaminants with the potential to migrate with passing fluids (liquid and gas). The radionuclides include unburned fissile fuel such as uranium and plutonium isotopes, fission products such as cesium-137 and strontium-90, activation products from neutron bombardment of device hardware and the surrounding lithology, and tritium (Bowen et al. 2001). Not all radionuclides produced by a detonation pose a long-term hazard. Radionuclides with short half-lives that quickly decay to undetectable levels and those produced in amounts so small that they never exceed regulatory limits can safely be disregarded. Radionuclides with properties that make them essentially immobile in certain geologic environments are also of less concern than those that are more mobile in the subsurface. Each radionuclide exists as a solid, liquid, or gas under various temperature and pressure conditions depending on its chemical properties. For instance, most radionuclides have a high melting point, causing them to solidify with and become entrained in the melt rock as it cools. In water-saturated environments, the melt rock can be subject to dissolution, which could potentially lead to the slow release of radionuclides into passing groundwater. Many radionuclides strongly sorb to mineral grains, causing their migration rate to be much slower than the rate of groundwater movement. The migration of radionuclides from melt rock dissolution has been shown to be limited in saturated environments, and in unsaturated environments where formation water is practically immobile (as at the Rio Blanco and Rulison sites), dissolved radionuclides are not expected to move beyond the detonation zone. For all practical purposes, isotopes of uranium, plutonium, cesium, and strontium are immobile in the geologic environment surrounding the Rulison and Rio Blanco detonation zones and are protected from direct access by the existing institutional control areas.

Radionuclides that can exist in the gas phase (Table 1) and were created in significant amounts by the detonations are of primary concern because of their potential mobility. The relative permeability of the gas phase is orders of magnitude greater than that of liquids in the natural-gas-producing reservoirs of the Williams Fork Formation. Though, in the section where the Rio Blanco detonations occurred (higher water content, lower gas relative permeability), the mobility of the gas phase over the liquid phase is less than in the productive interval (lower water content, higher gas relative permeability). The gas phase largely consists of methane with smaller amounts of ethane, propane, carbon dioxide, water vapor, and other minor constituents. Gas-phase radionuclides produced by the Rio Blanco detonations (Toman 1974) in order of abundance were estimated at approximately 1,000 Ci of tritium per detonation (3,000 total), approximately 775 Ci of ^{85}Kr per detonation (2,325 total), and minor amounts of argon isotopes and carbon-14 (^{14}C).

Table 1. Gas-Phase Components and Potential Radionuclides

Gas Component	Possible Radionuclides
Carbon dioxide (CO_2)	$^{14}CO_2$
Natural gas: methane (CH_4), water vapor (H_2O)	THO, $^{14}CH_4$, CTH_3
Hydrogen gas (H_2)	HT
Noble gases	^{85}Kr, ^{37}Ar, ^{39}Ar

THO = tritiated water; CTH_3 = tritiated methane; HT = tritiated hydrogen gas; Ar = argon

The original design for the Rio Blanco test was for the three simultaneous detonations to create one connected chimney composed of the three separate chimneys. Production test results indicated that the chimneys did not interconnect and remained essentially separated (Toman 1974). Many of the gas-phase radionuclides in the upper chimney, other than tritium, were largely removed by production testing (described below) of the reentry well (AR-1, alternate reentry well 1). The depletion of tritiated methane by the production testing leaves tritiated water (as vapor or liquid) as the primary mobile contaminant source for the upper Rio Blanco chimney. A second reentry well, AR-2, was drilled into the lower chimney. It produced poorly, and testing was limited to about 27 million cubic feet (MMCF) of gas. Only about a third of the ^{85}Kr was removed from the lower chimney. No reentry well was drilled into the middle chimney. The estimated amount of ^{85}Kr and tritium remaining in the three chimneys after removal by production testing and radioactive decay is given Table 2 and Table 3. Tritium is considered the greater risk due its ability to be incorporated into the body, whereas ^{85}Kr is a noble gas and is not retained in the body. The current modeling focuses on tritiated water vapor as the contaminant of concern, though ^{85}Kr has the potential to migrate slightly farther than tritiated water vapor. Partitioning between the mobile gas phase and the much less mobile aqueous phase retards tritiated water vapor migration, and dissolution of ^{85}Kr into the aqueous phase retards its movement. The presence of tritiated methane is also a concern due to the limited removal by production testing and its greater mobility with respect to tritiated water, though it is produced in smaller quantities than tritiated water. The detonation oxidizes much of the methane in the cavity/chimney to carbon dioxide and water. Due to its relative abundance and greater ability to be retained in the body, this study focused on tritiated water as the primary contaminant of concern.

Table 2. ^{85}Kr: Created by Detonation, Removed by Testing, Remains in 2012 After Decay

^{85}Krypton (Curies)	Created	Testing Removed	Remains in 2012
Rulison	1,113[a]	1,062	Trace
Rio Blanco (upper)	775[b]	775	Trace
Rio Blanco (middle)	775[c]	0	75
Rio Blanco (lower)	775[c]	244	55

[a] Precise number from integration of concentration data (AEC 1973), typically rounded to 1,100 Ci
[b] Estimate for upper chimney, ± 80 Ci (Toman 1974)
[c] Estimate for upper chimney used for middle and lower chimneys

Table 3. Tritium: Created by the Detonation, Removed by Testing, Remains in 2012 After Decay

Tritium (Curies)	Created	Testing Removed	Remains in 2012
Rulison	10,000	3,000	600
Rio Blanco (upper)	1,000	202[a]	80
Rio Blanco (middle)	1,000	0	100
Rio Blanco (lower)	1,000	51[b]	100

[a] 150 Ci (liquid water) injected into Fawn Creek Govt #1 well (CER 1975)
[b] 28 Ci (liquid water) injected into Fawn Creek Govt #1 well
20 of the 178 total curies injected would remain in 2012 after decay

The most likely transport mechanism to the surface for tritiated water vapor (or ^{85}Kr) in or near the detonation zone is with natural gas extracted from a nearby production well. To be of concern, the well would have to be close enough to interact with the potentially contaminated

region. Wells in the Piceance Basin typically drain an area of roughly 1,200 ft by 300 ft (10 acres), with the long axis oriented east-west, along the natural fracture trend in the Williams Fork Formation. In practice, this requires four wells per quarter-quarter section (centered east-west and aligned north-south) to drain each 40-acre parcel. The majority of wells installed at this spacing have not interacted with one another or with wells in adjacent 40-acre lots. It is evident that wells east and west of the site would be in the most susceptible transport direction due to the increased permeability in that direction and the tendency of fractures to propagate in that direction. The 10-acre spacing for wells is thus far supported by production data from wells near the Rulison site, though operators near Rio Blanco continue to locate wells on a 40-acre spacing. Considering that the wells near Rulison have only been in production for a few years of an expected 20–25 year life-cycle, the possibility exists that a greater percentage of wells may interact in the future, reducing the ultimate recovery per well.

Shortly after the detonations, gas-phase contaminants were spread through the nuclear chimneys and likely through the adjacent nuclear fractured regions. Reentry well production testing created an inward pressure gradient that persisted for years, drawing contaminants back from the nuclear fractured region of the upper detonation (and to a lesser extent the lower) to the chimney and out the wellbore during testing. It is predicted that as the inward pressure gradient of the testing dissipated, tritium likely spread by gaseous diffusion back throughout the region of increased permeability and possibly beyond. The middle chimney was not reentered and would not have had an induced inward pressure gradient.

1.4.1 Radionuclides Removed by Production Testing, Upper and Lower Chimneys

Reentry well AR-1 (Figure 5) was drilled into the upper Rio Blanco chimney and tested to determine the success of the detonations at improving gas production. The well produced 97.7 MMCF of dry gas over 28 days of testing that took place from November 1973 through February 1974 in two separate flow tests (AEC 1974). The produced gas was flared to the atmosphere, and samples of the produced gas and produced water were collected and analyzed to determine the degree to which radioactivity levels changed as testing progressed. All releases during drilling and testing were monitored by the U.S. Environmental Protection Agency National Environmental Respiratory Center and the Colorado Department of Health to protect workers at the site, the public, and the environment. As expected, the radioactivity levels decreased throughout the testing as gas from the chimney region was produced, burned, and replenished by uncontaminated gas from the surrounding formation. Sample analysis indicated that approximately 771 to 775 of the 775 Ci of ^{85}Kr were removed by the production testing (Toman 1974). The concentration of ^{85}Kr in the produced gas (assumed well mixed throughout the detonation zone due to its inert nature) was closely monitored throughout the testing to determine when radioactive gas from the detonation zone was depleted. Due to radioactive decay, less than 7 percent of any ^{85}Kr that was not removed by testing would remain in 2013.

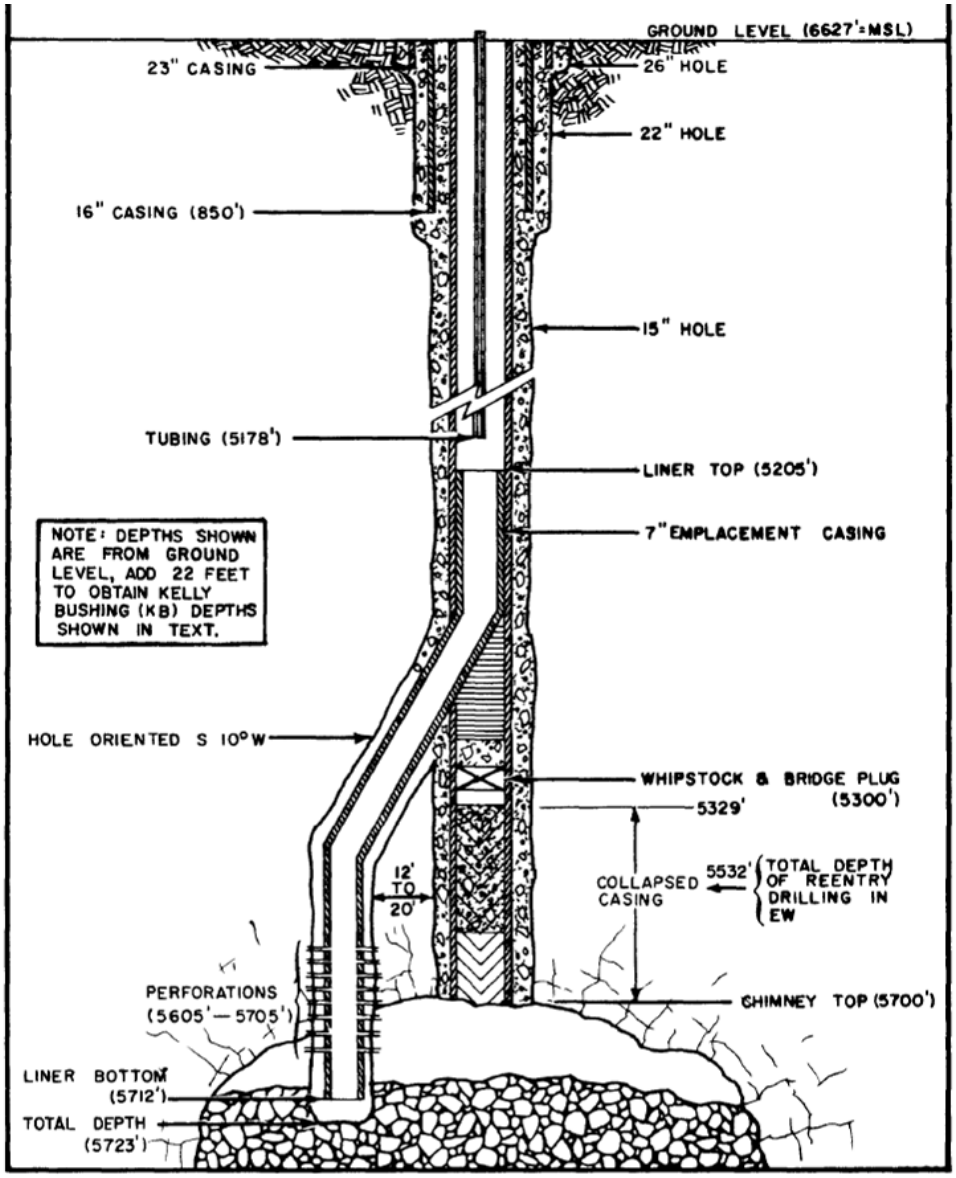

Source: CER 1975

Figure 5. Schematic of Reentry Well AR-1

Reentry well AR-2 was drilled into the lower chimney at Rio Blanco and tested to determine the success of the detonations at creating a continuous chimney. The well produced 27 MMCF of dry gas over 7 days of testing that took place in December 1974 (CER 1975). The testing confirmed the results from testing on the upper chimney, that the chimneys created by the three simultaneous detonations were not interconnected. Each chimney contained a tracer (neon, xenon, and krypton in the upper, middle, and lower) that was virtually absent from the production tests (except for the tracer in the chimney being tested). Additionally, the pressure-volume calculations and the amount of ^{85}Kr from the production testing were consistent with the interpretation of separate chimneys.

Table 2 provides an estimate of the ^{85}Kr inventory for Rio Blanco (each detonation) and the inventory of Rulison for comparison. Table 3 provides an estimate of the tritium created by the detonations and of tritium removed by production testing and subsequent decay. Figure 6 shows the decline in concentrations of ^{85}Kr and tritium in dry gas (as tritiated methane [CH_3T] or as tritiated hydrogen gas [HT]) relative to the cumulative amount of gas produced for both the upper and lower chimney production testing. Figure 7 shows the tritium concentration in the separator water relative to the cumulative amount of gas produced for both the upper (AR-1) and lower (AR-2) chimney production testing. Note that the values of tritium in separator water from AR-2 were scaled up by 1,000, assuming a unit mistake in the source document (CER 1975).

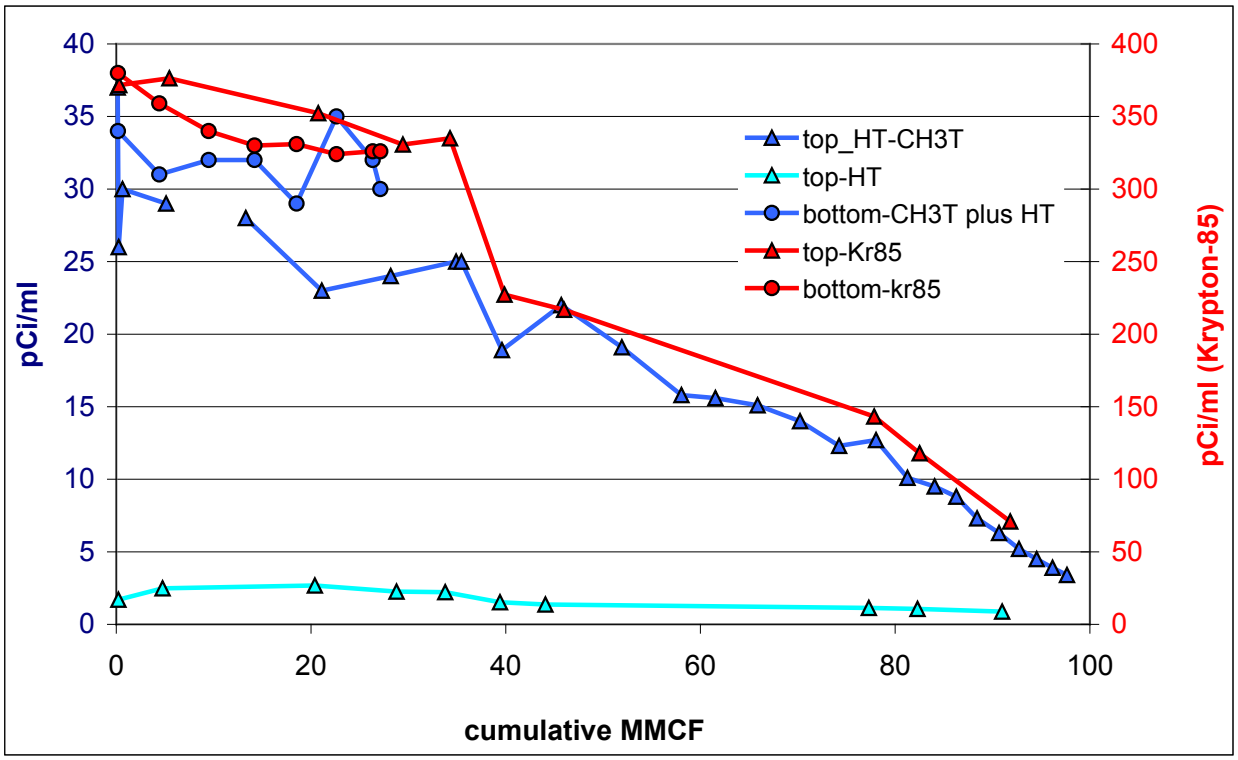

Note: MMSCF = million standard cubic feet
pCi/mL = picocuries per milliliter

Source: Toman 1974 and CER Geonuclear 1975

Figure 6. Concentration of Tritium and ^{85}Kr in Dry Gas

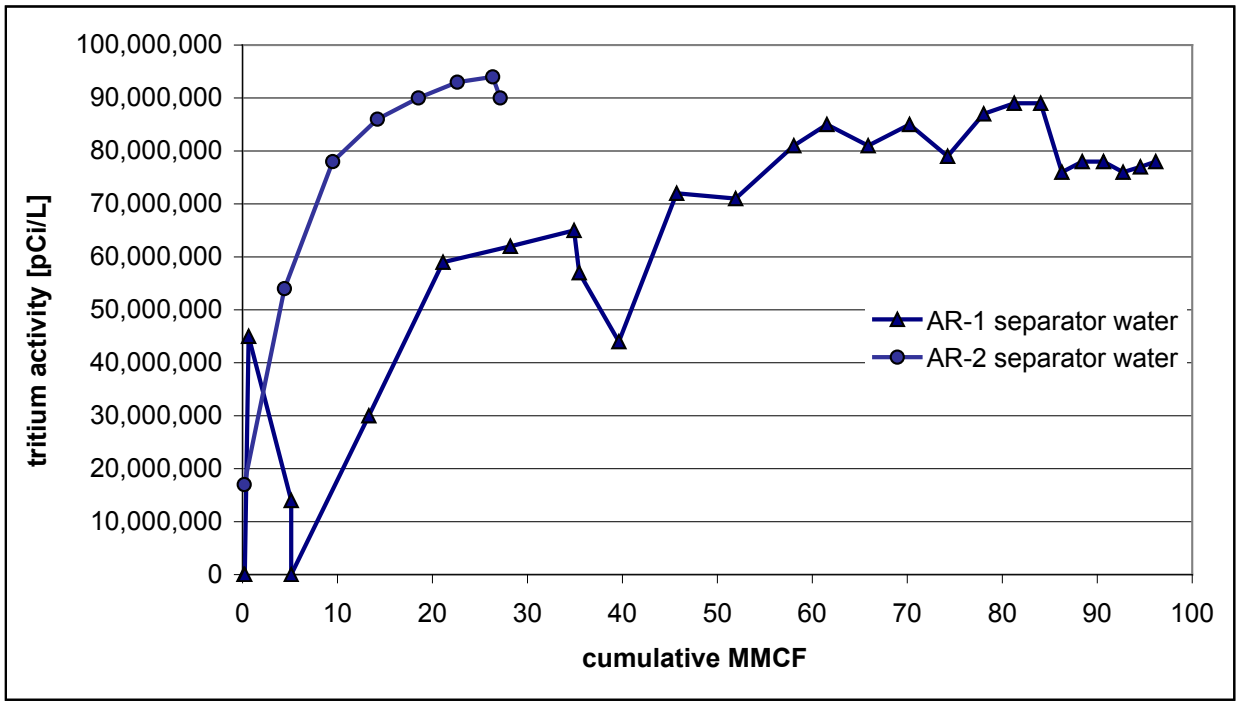

Note: MMSCF = million standard cubic feet
pCi/L = picocuries per liter

Source: Toman 1974 and CER Geonuclear 1975

Figure 7. Concentration of Tritium in Separator Water

Tritium was initially present, after the detonations, in hydrocarbons (mostly methane with lesser amounts of ethane and propane), hydrogen gas, and water (vapor and liquid) in the chimneys. Unlike Rulison, where most of the gas-phase radionuclides were removed by production testing, testing was limited at Rio Blanco because of relatively poor production and the isolation of radionuclides in three separate chimneys. The dry gas tritium (as tritiated hydrogen gas and tritiated methane) in the upper chimney was mostly removed by the production testing, as evidenced by the declining concentrations during testing (Figure 6). The concentrations of tritiated water had just leveled off at the end of the testing (Figure 7), which was abbreviated relative to Rulison because of limited inflow of natural gas from the formation. Unlike the upper chimney, which is most analogous to Rulison in that the remaining mobile radionuclide is tritiated water (the vapor being mobile), the middle and lower chimneys still have significant amounts of ^{85}Kr and tritiated methane in addition to tritiated water.

1.4.2 Radionuclide Disposition

At the end of production testing in December 1974, aggregate quantities from both the upper and lower chimneys of about 75 Ci of tritium and about 1,020 Ci of ^{85}Kr were released to the atmosphere. About 178 Ci of tritium and millicurie amounts of cesium-137 and strontium-90 were injected into the Fawn Creek Govt #1 well under a subsurface disposal permit (Colorado Department of Health 1974). Of the total, gas-phase amounts of 52 Ci of tritium and about 776 Ci of ^{85}Kr were from the upper chimney. About 150 Ci of tritium injected into the Fawn Creek Govt #1 well was from the upper chimney. The lower chimney testing removed gas-phase amounts of about 23 Ci of tritium and 244 Ci of ^{85}Kr and about 28 Ci of tritium in the liquid

phase. Table 2 and Table 3 provide estimates of mobile radionuclides remaining in the Rio Blanco chimneys.

2.0 Conceptual and Numerical Model of Flow and Transport within the Mesaverde

The very low permeabilities of the Williams Fork Formation, on the order of microdarcys for the sandstones and even less for the shales, indicate that there is no appreciable flow of gas or liquid within the time frame of concern (hundreds to thousands of years). Non-stimulated wells produce from only a short distance from the wellbore, and for a well to produce enough gas to warrant drilling, formation permeability surrounding the well has to be increased to enhance flow. The nuclear detonations at Rio Blanco and Rulison effectively created a highly stimulated zone with an extremely permeable chimney and a surrounding fractured region of increased permeability. The calculated dimensions of the cavities, chimneys, and nuclear fractured region were based on data from drilling the reentry wells and their production testing. The lack of success in stimulating flow at Rio Blanco relative to Rulison was due the Rio Blanco detonations being located in a gas-bearing interval with a higher water content, which lowers the relative permeability of the gas phase and thereby the overall gas permeability. The deeper section in which the Rulison test was conducted produces less water and is the gas-productive interval targeted by recently drilled wells in both the Rulison and Rio Blanco areas.

Current methods stimulate wells by fracturing the surrounding formation through the injection of fluids with entrained sand under high pressure. There is a limit to the distance from the wellbore that this is effective, and that distance varies with lithology and other factors. In the lower Williams Fork Formation near Rio Blanco and Rulison, it has been shown that stimulated wells recover gas from an area of about 10 acres without influencing adjacent wells. The typical drainage pattern and area has been confirmed by over a hundred wells drilled near the Rulison site. The wells are expected to produce about a billion cubic feet or more of gas on average over a 20−25-year life. Wells near Rio Blanco are currently being located on a 40-acre spacing, though the lithology of the productive interval is essentially the same as that at Rulison. It is assumed, for this study, that wells could eventually be located on a 10-acre spacing near Rio Blanco, without communicating, at least during the initial years of production.

A numerical model is a tool that attempts to quantitatively replicate the site conceptual model and various aspects of the system to allow different scenarios to be tested. At the Rulison site, an important scenario is the minimum distance a producing gas well can be located from the blast cavity without inducing contaminant migration. At Rio Blanco, since wells are not completed in the same section as the detonations, an analogous scenario would be to simulate whether wells could be located below the detonations without inducing downward migration of contaminants. The modeling code was selected based on its ability to simulate the important processes at a site. For instance, the code selected for this study must be able to simulate multiphase flow and transport of a radionuclide (tritium as tritiated water) that is present in both the aqueous and gas phases and to simulate the production of natural gas from wells in the Williams Fork Formation. To improve confidence in the reliability of results, the model was calibrated to site data to test whether it can reproduce what is already known and thus ensure that parameters such as permeability are within reasonable ranges.

The model uses an equivalent porous media approach even though flow is predominantly through a fractured system. The approach is justified in that the fractures through which flow occurs are assumed to be frequent with limited extents in the low-permeability formation, and not rare and extensive, such that they would short-circuit the flow system. The mechanical forces that create the nuclear fractured and hydrofractured regions rubblize the formation to increase permeability.

2.1 Numerical Modeling Code

The TOUGH2_MP code (Transport of Unsaturated Groundwater and Heat_Massively Parallel processing) (Zhang et al. 2008), was selected for the modeling. It is a multiphase, multicomponent, non-isothermal code that allows components to partition between phases depending on thermophysical properties. The equation of state selected was EOS7R, which allows for five components (water, brine, parent radionuclide [RN1], daughter radionuclide [RN2], and air) and two phases (aqueous and gas). The code was modified to calculate a temperature-dependent Henry's law constant based on the vapor pressure. The code was also modified to change the properties of the "air" component to those of methane to better represent the gas reservoirs of the Williams Fork Formation. Simulations were run remotely on a supercomputer at Clemson University. The earlier Rulison and Rio Blanco models used the single processor version of TOUGH2. The versions of the code are essentially the same except for the ability of TOUGH2_MP to handle much larger problems with many more elements in significantly faster simulation times.

3.0 Rio Blanco Model Construction

A number of steps are involved in constructing a numerical model. First, the specific size and location of the area to be modeled has to be selected, and then it has to be discretized into individual elements or cells. The elements have to be populated by material types that represent the domain lithology as closely as data permit. For Rio Blanco, this includes separate types for the detonation zone and hydrofractured regions near wells. The material types are differentiated based on assigned parameters such as permeability, porosity, and capillary properties. Appropriate boundary conditions and initial conditions have to be determined and assigned. Finally, the handling of sources and sinks for simulating extraction of material from the domain must be specified.

3.1 Rio Blanco Model Domain and Discretization

The horizontal dimensions of the main Rio Blanco model domain were the same as those of the Rulison domain, 6,000 ft in the east-west direction and 4,000 ft in the north-south direction (Figure 7, Figure 8, and Figure 9). Vertically, the Rio Blanco domain was extended to include the Ft. Union Formation in addition to the entire Williams Fork Formation (3,800 ft—the gas-productive 2,000 ft thick lower two-thirds of the Williams Fork Formation, 1,000 ft for the non-producing upper third of the Williams Fork, and 800 ft for the Ft. Union [Figure 11]). The three-dimensional model is discretized into elements or cells that are 50 ft (15.24 m) in the horizontal x and y directions (cell centers shown on Figure 8 and Figure 9) and 20 ft (6.1 m) in the vertical z direction, for a total of 1,824,000 cells (120x, 80y, 190z). A subset of the model (Figure 8) was extracted to reduce simulation times for calibrating to the historical post-shot production testing data from the upper chimney.

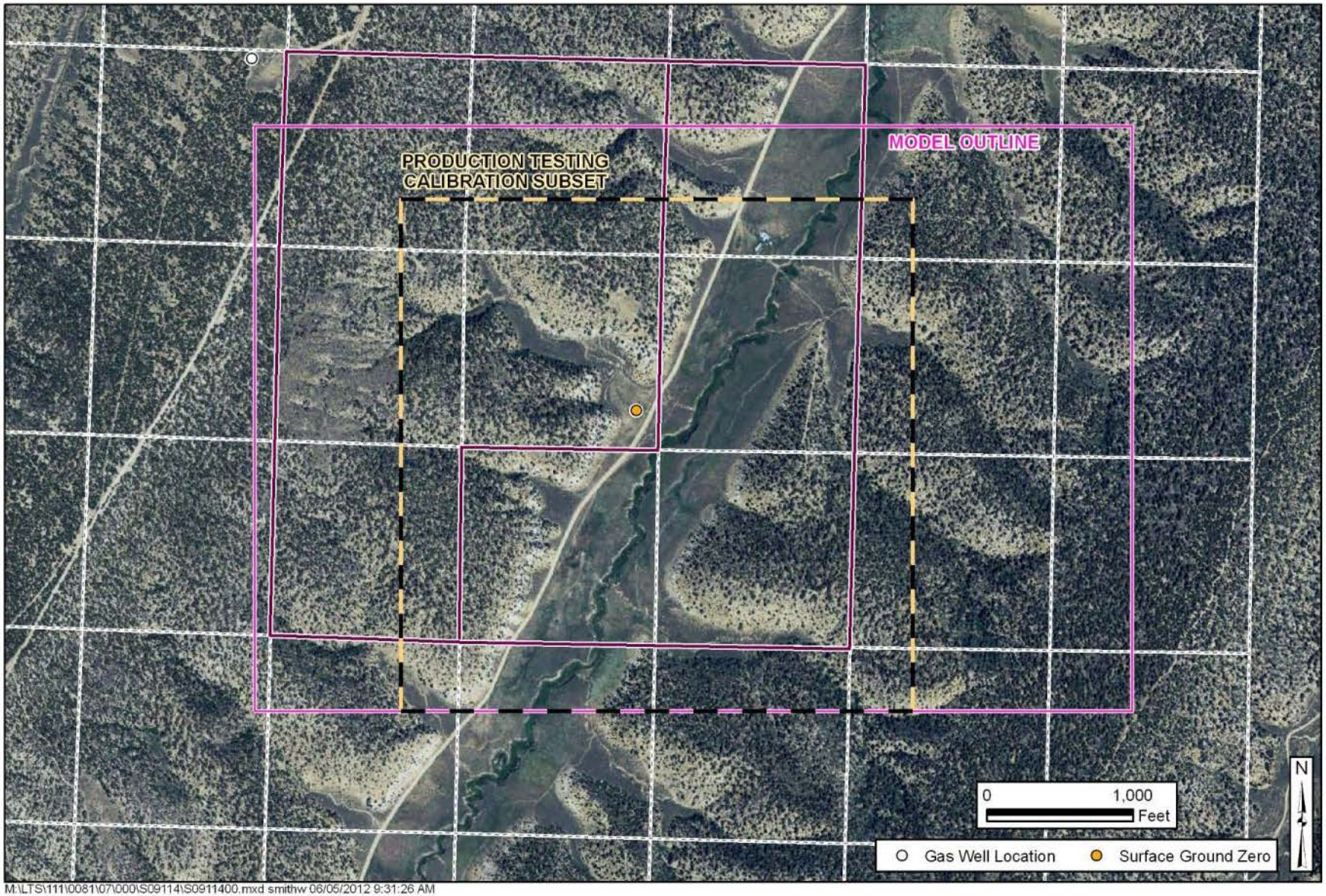

Figure 8. Horizontal Extent of Current Model Domains

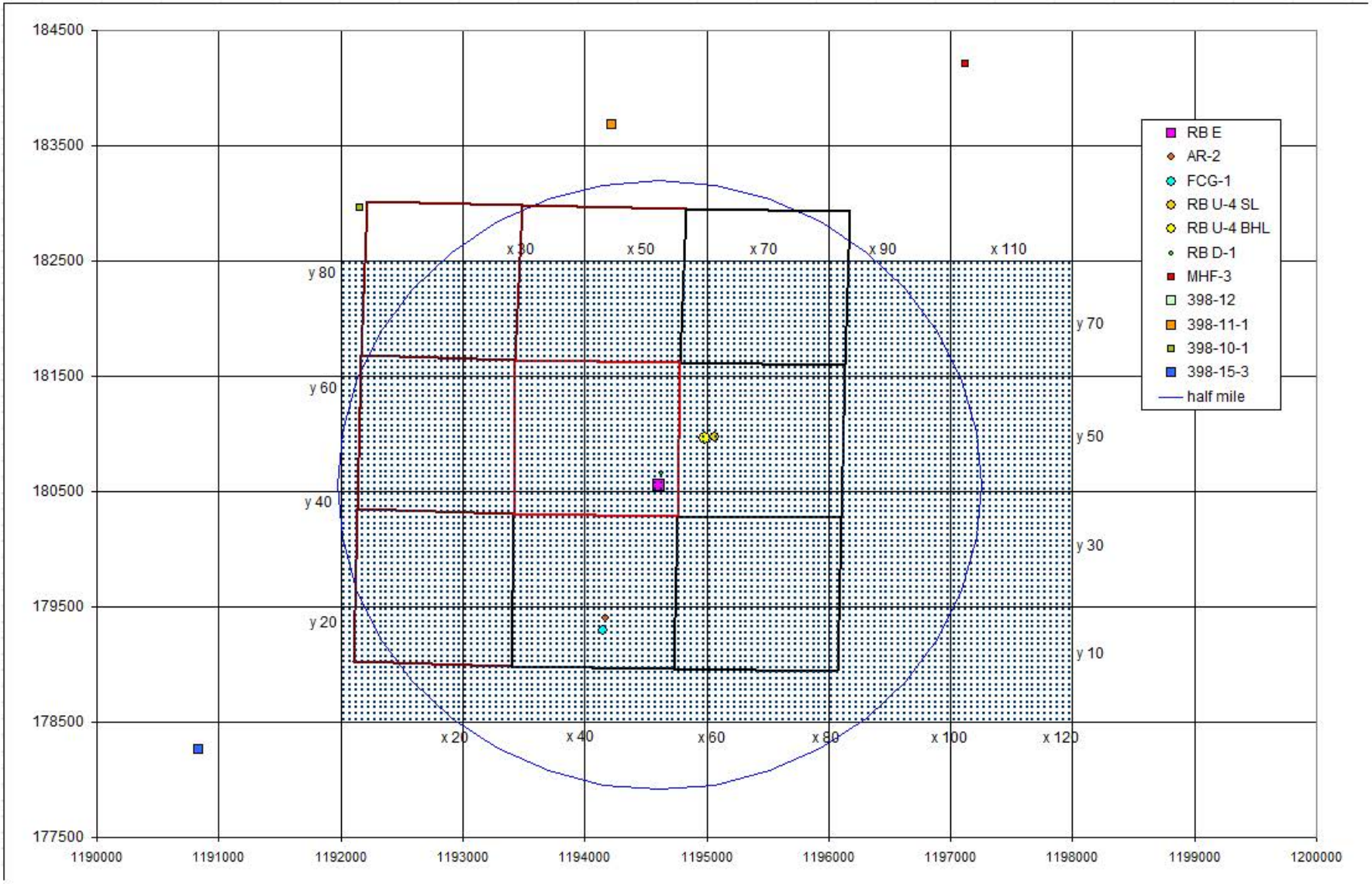

Figure 9. Map of the Rio Blanco Model Area in Real Coordinates (Feet, State Plane Colorado Central, NAD 27), Including Lot Boundaries, Current Wells, and Element Centers (Dark Blue)

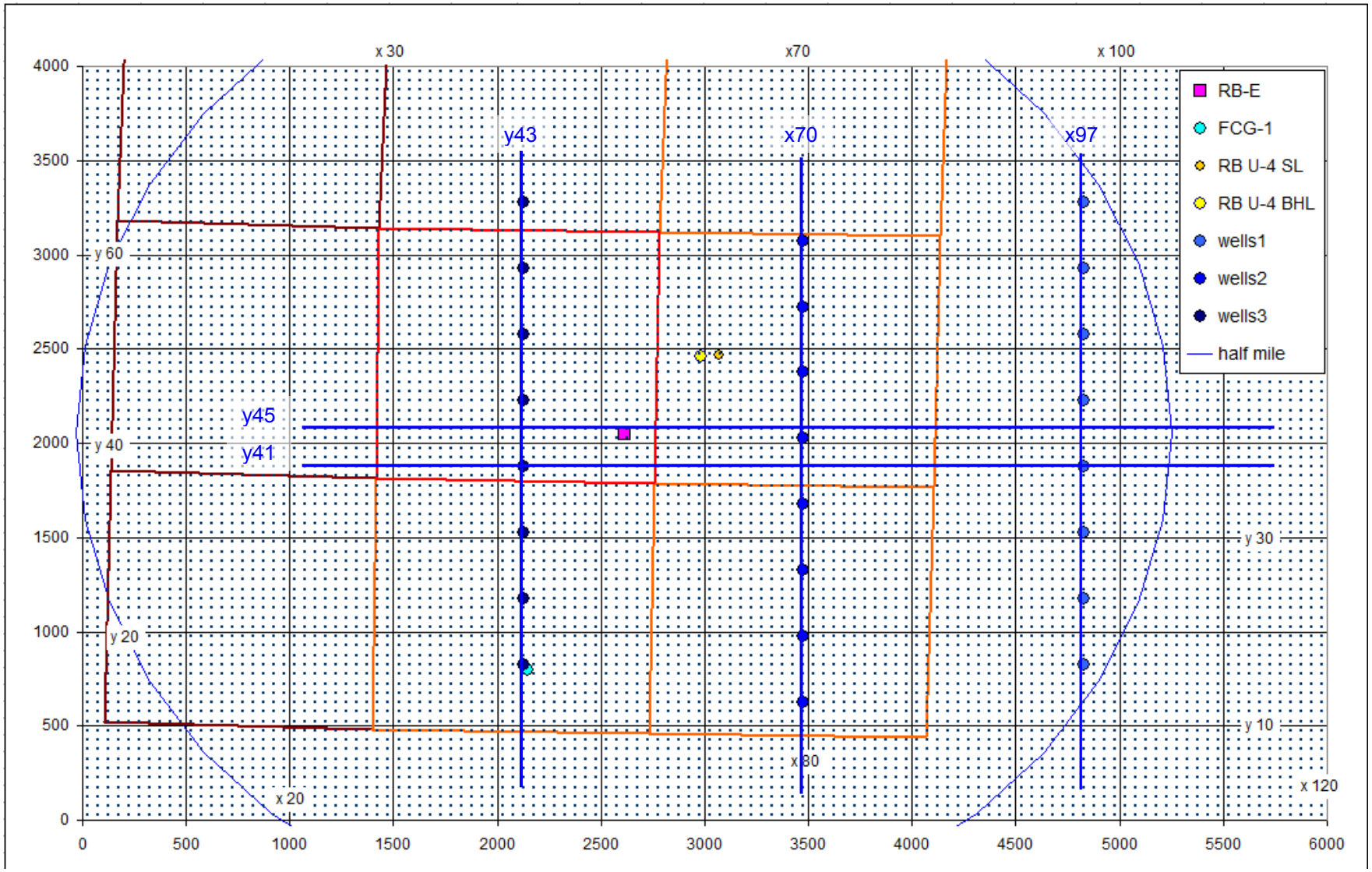

Figure 10. Map of the Rio Blanco Model in Model Coordinates, Including Site Wells, Simulated Hypothetical Wells, and Element Centers
Simulated hypothetical wells are light blue to dark blue; blue lines are reference for Sections 5.1 and 5.3.

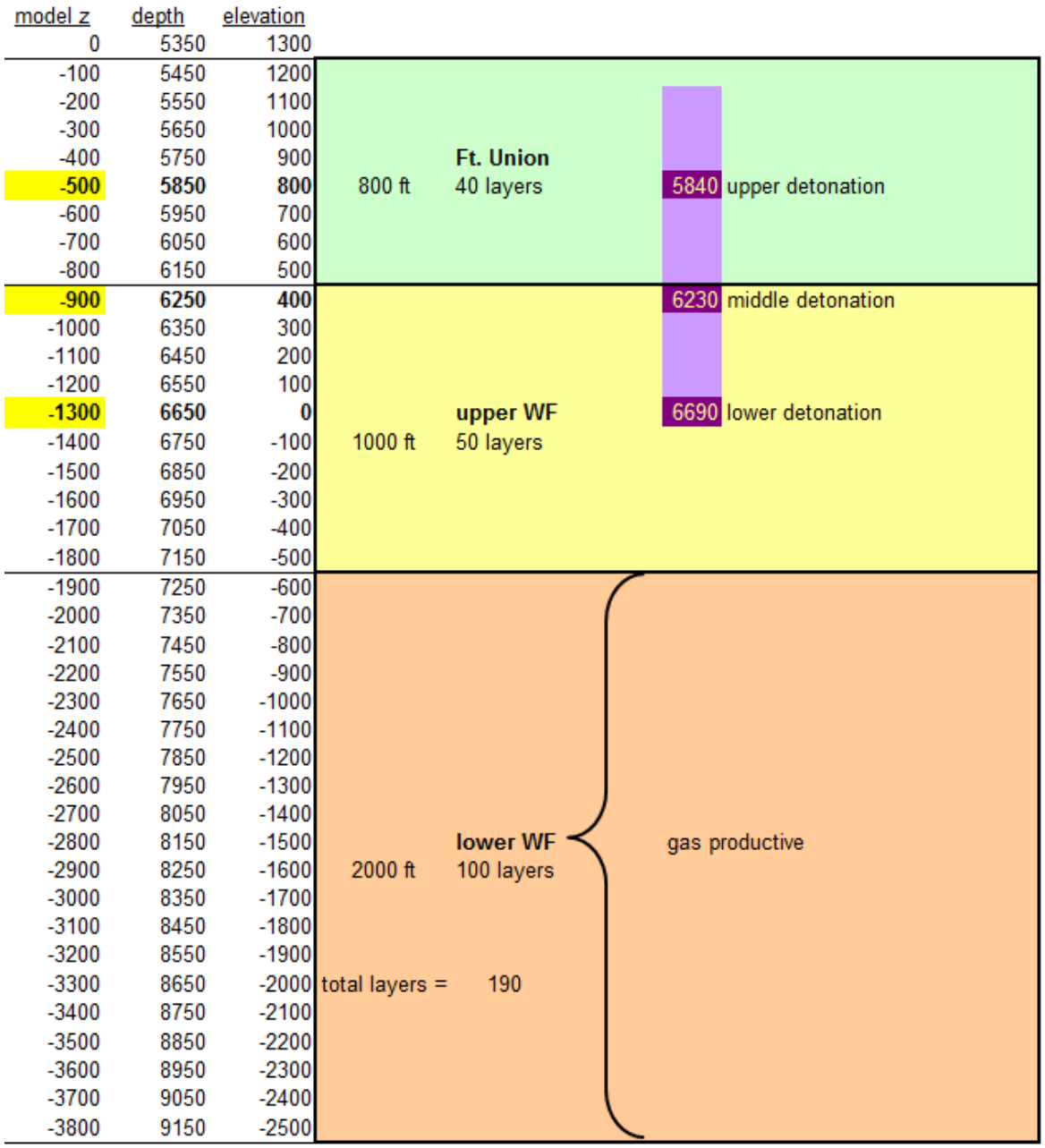

Figure 11. Vertical Extent of the Rulison Model with Model Depth, Elevation, and Vertical Extent of Previous Models

3.2 Formation Lithologic Distribution

Model elements have to be populated with ROCK types that realistically represent the subsurface at the site. ROCK is the keyword in the TOUGH2 input file that identifies the block with information about the different material types. Each ROCK type is assigned a set of parameters (see Section 3.5) that influence flow and transport throughout the model. The productive lower Williams Fork interval is primarily composed of discontinuous interbedded shale and sandstone lenses. The cleaner sandstones are the main candidates for perforating and hydrofracturing. The

detonations at Rio Blanco were in the Ft. Union and upper Williams Fork where the sandstones are more continuous than those in the lower Williams Fork. However, these zones are not targeted because the sandstones are more continuous and have a higher water content that limits gas production while increasing water production. Because of less development in the Rio Blanco area and none within the model domain, the data from near Rulison were used for the Williams Fork Formation. The Rulison data indicate that about 42.5 percent of the targeted Williams Fork section near Rulison can be considered producing sandstones. The remaining 57.5 percent was considered shale for the purposes of the model. Figure 12 shows slices through a sandstone-shale realization with the detonation zones and future potential hydrofractured zones.

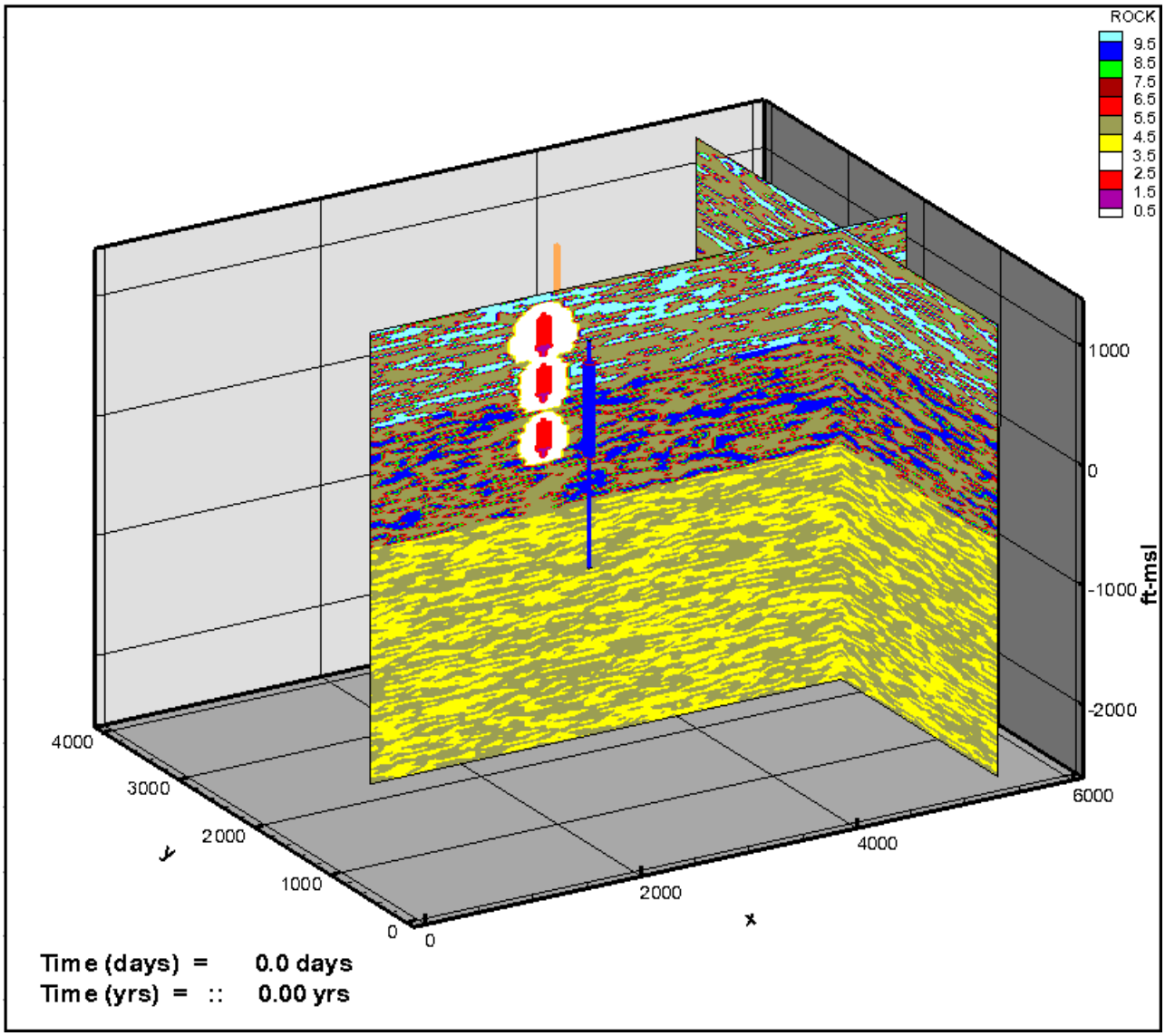

Figure 12. Rio Blanco Model Lithologic Distribution
Includes Well locations for FCG #1 (blue, near) and RB-U4 (orange, far).
ROCK color numbers match with the order of ROCK type in section 3.5, yellow = lower Williams Fork sandstone, olive = shale, white = nuclear fractures, red = chimney, purple = melt glass, blue = upper Williams Fork sandstone, light blue = Ft. Union sandstone

At locations within the model domain where well data are available, the ROCK type is known and assigned based on the well data. These are conditioning points (known values) that do not change for any of the different geostatistical realizations. The remainder of the domain is populated randomly within the constraints of the geostatistics. Log correlations and subsequent geostatistical realizations were generated by DRI (David Gillespie, log correlations; and Yong Zhang, geostatistical distributions) using the same method that was used for previous models. A thorough discussion of the method is provided in Appendix B.

3.3 Rio Blanco Detonation Zones

The cavities were assumed to be essentially spherical, and the subsequent collapse chimneys were assumed to be vertical ellipsoids. For this modeling effort, the nuclear fractured regions were defined as truncated (at depth) ellipsoids with slightly longer east-west axes (aligned with the higher permeability natural fracture trend of the formation). The dimensions of the upper detonation were assigned to be somewhat larger than middle and lower detonations because of the tendency of the fracturing to propagate upward. This was conservative because the lower detonation dimensions used were still slightly larger than the originally calculated dimensions due to model discretization. The equation used to calculate a 3-dimensional ellipsoid is given in Equation 1, and the variable values used to calculate the extents of the chimneys and nuclear fractures are in Table 4.

$$\frac{x^2}{x_r^2} + \frac{y^2}{y_r^2} + \frac{z^2}{z_r^2} = 1 \qquad \text{Equation (1)}$$

Where x, y, z = Distance from an element center to the ellipsoid center in the x,y,z directions,
x_r, y_r, z_r = Ellipsoid radius in the x,y,z directions.

Table 4. Model Coordinates and Ellipsoid Radii of Chimneys and Nuclear Fracture Extents

	x ellipsoid center	y ellipsoid center	z ellipsoid center	x_r ellipsoid radius	y_r ellipsoid radius	z_r, ellipsoid radius	Truncated below
Upper Chimney	2625	2050	−345	80	80	200	−435
Middle chimney	2625	2050	–745	75	70	185	–835
Lower chimney	2625	2050	–1205	75	75	185	−1295
Nuclear fractures (upper)	2625	2050	–385	310	250	310	–540
Nuclear fractures (middle)	2625	2050	–775	250	200	250	–985
Nuclear fractures (lower)	2625	2050	–1245	220	200	250	–1415

When Equation 1 is calculated with a set of element coordinates, if the value is less than 1, the element is within the ellipsoid. The ROCK type for those elements is then changed to the appropriate type. Elements within the nuclear fracture ellipsoid are assigned the ROCK type NFrac, and elements within the chimney ellipsoid are assigned the ROCK types chimn or glass (ROCK type parameters are given in Section 3.5). The truncation depth for the chimney assumes melt glass below that depth within the chimney ellipsoid. The detonation zones were

designed using calculations with Microsoft Excel prior to modifying the TOUGH2 MESH. Side view and top view slices of the model chimneys and nuclear fractured regions are shown in Figure 13 and Figure 14.

	2125	2175	2225	2275	2325	2375	2425	2475	2525	2575	2625	2675	2725	2775	2825	2875	2925	2975	3025	3075	3125
-70	5	5	5	5	5	5	5	5	5	5	5	5	5	5	5	5	5	5	5	5	5
-90	5	5	5	5	5	5	5	5	5	2	2	2	5	5	5	5	5	5	5	5	5
-110	5	5	5	5	5	5	5	5	2	2	2	2	2	5	5	5	5	5	5	5	5
-130	5	5	5	5	5	5	5	2	2	2	2	2	2	2	5	5	5	5	5	5	5
-150	5	5	5	5	5	5	5	2	2	2	2	2	2	2	5	5	5	5	5	5	5
-170	5	5	5	5	5	5	2	2	2	2	1	2	2	2	2	5	5	5	5	5	5
-190	5	5	5	5	5	5	2	2	2	2	1	2	2	2	2	5	5	5	5	5	5
-210	5	5	5	5	5	2	2	2	2	1	1	1	2	2	2	2	5	5	5	5	5
-230	5	5	5	5	5	2	2	2	2	1	1	1	2	2	2	2	5	5	5	5	5
-250	5	5	5	5	5	2	2	2	2	1	1	1	2	2	2	2	5	5	5	5	5
-270	5	5	5	5	5	2	2	2	2	1	1	1	2	2	2	2	5	5	5	5	5
-290	5	5	5	5	5	2	2	2	2	1	1	1	2	2	2	2	5	5	5	5	5
-310	5	5	5	5	5	2	2	2	2	1	1	1	2	2	2	2	5	5	5	5	5
-330	5	5	5	5	2	2	2	2	2	1	1	1	2	2	2	2	2	5	5	5	5
-350	5	5	5	5	2	2	2	2	2	1	1	1	2	2	2	2	2	5	5	5	5
-370	5	5	5	5	2	2	2	2	2	1	1	1	2	2	2	2	2	5	5	5	5
-390	5	5	5	5	2	2	2	2	2	1	1	1	2	2	2	2	2	5	5	5	5
-410	5	5	5	5	2	2	2	2	2	1	1	1	2	2	2	2	2	5	5	5	5
-430	5	5	5	5	2	2	2	2	2	1	1	1	2	2	2	2	2	5	5	5	5
-450	5	5	5	5	2	2	2	2	2	0	0	0	2	2	2	2	2	5	5	5	5
-470	5	5	5	5	5	2	2	2	2	0	0	0	2	2	2	2	5	5	5	5	5
-490	5	5	5	5	5	2	2	2	2	0	0	0	2	2	2	2	5	5	5	5	5
-510	5	5	5	5	5	2	2	2	2	2	0	2	2	2	2	2	5	5	5	5	5
-530	5	5	5	5	5	2	2	2	2	2	2	2	2	2	2	2	5	5	5	5	5
-550	5	5	5	5	5	5	5	5	2	2	2	2	2	5	5	5	5	5	5	5	5
-570	5	5	5	5	5	5	5	5	2	2	2	2	2	5	5	5	5	5	5	5	5
-590	5	5	5	5	5	5	5	2	2	2	1	2	2	2	5	5	5	5	5	5	5
-610	5	5	5	5	5	5	5	2	2	2	1	2	2	2	5	5	5	5	5	5	5
-630	5	5	5	5	5	5	2	2	2	1	1	1	2	2	2	5	5	5	5	5	5
-650	5	5	5	5	5	5	2	2	2	1	1	1	2	2	2	5	5	5	5	5	5
-670	5	5	5	5	5	5	2	2	2	1	1	1	2	2	2	5	5	5	5	5	5
-690	5	5	5	5	5	5	2	2	2	1	1	1	2	2	2	5	5	5	5	5	5
-710	5	5	5	5	5	5	2	2	2	1	1	1	2	2	2	5	5	5	5	5	5
-730	5	5	5	5	5	5	2	2	2	1	1	1	2	2	2	5	5	5	5	5	5
-750	5	5	5	5	5	5	2	2	2	1	1	1	2	2	2	5	5	5	5	5	5
-770	5	5	5	5	5	5	2	2	2	1	1	1	2	2	2	5	5	5	5	5	5
-790	5	5	5	5	5	5	2	2	2	1	1	1	2	2	2	5	5	5	5	5	5
-810	5	5	5	5	5	5	2	2	2	1	1	1	2	2	2	5	5	5	5	5	5
-830	5	5	5	5	5	5	2	2	2	1	1	1	2	2	2	5	5	5	5	5	5
-850	5	5	5	5	5	5	2	2	2	0	0	0	2	2	2	5	5	5	5	5	5
-870	5	5	5	5	5	5	2	2	2	2	0	2	2	2	2	5	5	5	5	5	5
-890	5	5	5	5	5	5	2	2	2	2	0	2	2	2	2	5	5	5	5	5	5
-910	5	5	5	5	5	5	2	2	2	2	0	2	2	2	2	5	5	5	5	5	5
-930	5	5	5	5	5	5	5	2	2	2	2	2	2	2	5	5	5	5	5	5	5
-950	5	5	5	5	5	5	5	2	2	2	2	2	2	2	5	5	5	5	5	5	5
-970	5	5	5	5	5	5	5	2	2	2	2	2	2	2	5	5	5	5	5	5	5
-990	5	5	5	5	5	5	5	5	5	5	5	5	5	5	5	5	5	5	5	5	5
-1010	5	5	5	5	5	5	5	5	5	2	2	2	5	5	5	5	5	5	5	5	5
-1030	5	5	5	5	5	5	5	5	2	2	2	2	2	5	5	5	5	5	5	5	5
-1050	5	5	5	5	5	5	5	5	2	2	1	2	2	5	5	5	5	5	5	5	5
-1070	5	5	5	5	5	5	5	2	2	2	1	2	2	2	5	5	5	5	5	5	5
-1090	5	5	5	5	5	5	5	2	2	1	1	1	2	2	5	5	5	5	5	5	5
-1110	5	5	5	5	5	5	5	2	2	1	1	1	2	2	5	5	5	5	5	5	5
-1130	5	5	5	5	5	5	5	2	2	1	1	1	2	2	5	5	5	5	5	5	5
-1150	5	5	5	5	5	5	2	2	2	1	1	1	2	2	2	5	5	5	5	5	5
-1170	5	5	5	5	5	5	2	2	2	1	1	1	2	2	2	5	5	5	5	5	5
-1190	5	5	5	5	5	5	2	2	2	1	1	1	2	2	2	5	5	5	5	5	5
-1210	5	5	5	5	5	5	2	2	2	1	1	1	2	2	2	5	5	5	5	5	5
-1230	5	5	5	5	5	5	2	2	2	1	1	1	2	2	2	5	5	5	5	5	5
-1250	5	5	5	5	5	5	2	2	2	1	1	1	2	2	2	5	5	5	5	5	5
-1270	5	5	5	5	5	5	2	2	2	1	1	1	2	2	2	5	5	5	5	5	5
-1290	5	5	5	5	5	5	2	2	2	1	1	1	2	2	2	5	5	5	5	5	5
-1310	5	5	5	5	5	5	2	2	2	0	0	0	2	2	2	5	5	5	5	5	5
-1330	5	5	5	5	5	5	2	2	2	2	0	2	2	2	2	5	5	5	5	5	5
-1350	5	5	5	5	5	5	5	2	2	2	0	2	2	2	5	5	5	5	5	5	5
-1370	5	5	5	5	5	5	5	2	2	2	0	2	2	2	5	5	5	5	5	5	5
-1390	5	5	5	5	5	5	5	2	2	2	2	2	2	2	5	5	5	5	5	5	5
-1410	5	5	5	5	5	5	5	2	2	2	2	2	2	2	5	5	5	5	5	5	5
-1430	5	5	5	5	5	5	5	5	5	5	5	5	5	5	5	5	5	5	5	5	5
-1450	5	5	5	5	5	5	5	5	5	5	5	5	5	5	5	5	5	5	5	5	5
-1470	5	5	5	5	5	5	5	5	5	5	5	5	5	5	5	5	5	5	5	5	5

Figure 13. Vertical (Side View) Slice of the Model Chimneys and Nuclear Fractured Regions (y = 1,825 ft; purple represents melt glass, red represents the chimney, and white represents the nuclear fractured region.)

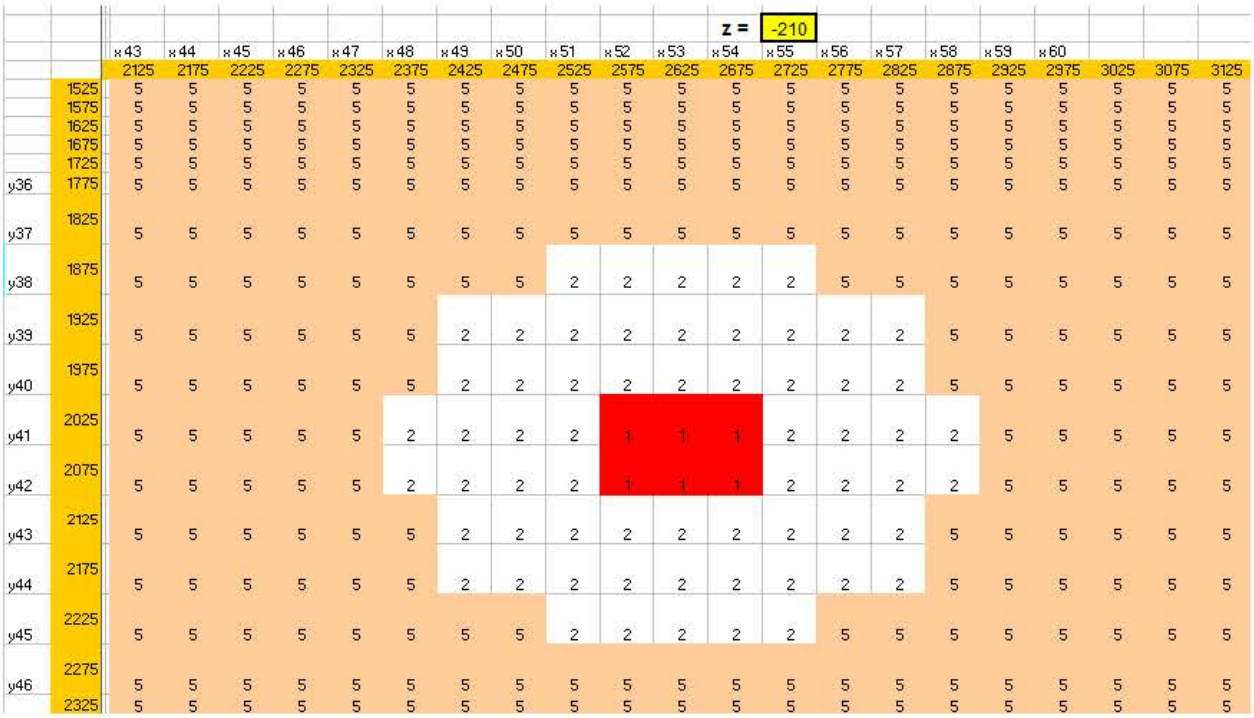

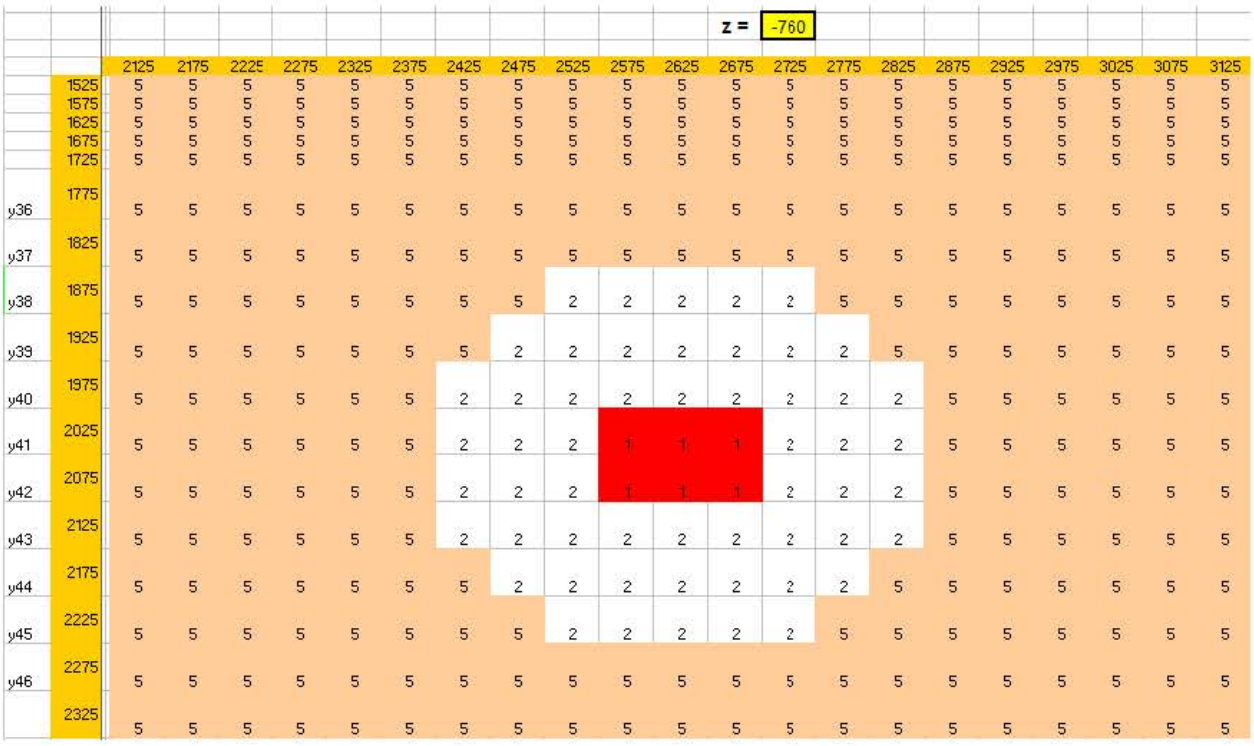

Figure 14. Horizontal (Top View) Slices of the Model Chimneys and Nuclear Fractured Regions That Resulted from the Upper and Middle Detonations
The horizontal slice through the lower chimney is identical to the middle chimney;
"z" is the model depth of the slices (–210 ft and –760 ft); red represents the chimney, and white represents the nuclear fractured region.

3.4 Hydrofracturing of Wells

There are no current production wells within the model domain. Potential future wells (blue circles in Figure 10) were simulated as being completed in the lower Williams Fork Formation, the primary interval targeted by gas companies in the area. The wells were also positioned on a 10-acre spacing interval, like that being applied near Rulison, but as of yet, not being applied near Rio Blanco. Intervals within the producing section were selected for perforating and hydrofracturing based on sandstone thickness. Sandstones within the lower Williams Fork that were 40 ft or more in thickness (model layers are 20 ft thick, so two or more consecutive elements in the vertical column at each well) were simulated as being hydrofractured. Much like an actual well, no information about how laterally extensive the sandstone was away from the wellbore was used to decide which interval would be hydrofractured. And, like an actual well, the horizontal distance that hydrofracturing extended from the wellbore was to a degree controlled by the lithology surrounding the wellbore. Hydrofractures were assumed to extend farther in sandstones than in shales, and it was assumed that hydrofracturing would be more effective in the sandstones. The extent of hydrofracturing was determined using two nested ellipsoids to calculate a near and a far hydrofracture extent. Elements within the near ellipsoid, both sandstones and shales, were hydrofractured. Sandstone elements were changed to hydrofractured near sandstone (`HFnsd`), and shale elements were changed to hydrofractured shales (`HFshl`). The permeability of `HFnsd` elements was set at 40× the permeability of lower Williams Fork sandstones (`LWFsd`), and the permeability of the shale initially increased 4×. Outside the inner ellipsoid but within the far ellipsoid, only the sandstone elements were hydrofractured. They were changed from sandstone to hydrofractured far sandstone elements (`HFfsd`) with a permeability increase of 4× that of the previous `LWFsd` elements. The permeability and permeability increases for hydrofracture elements (constrained to the lower Williams Fork) were those determined from the Rulison model, which was calibrated to production data from gas wells within its domain. The axes of the ellipsoids were elongated east-west in the direction of the natural fracture trend of the formation.

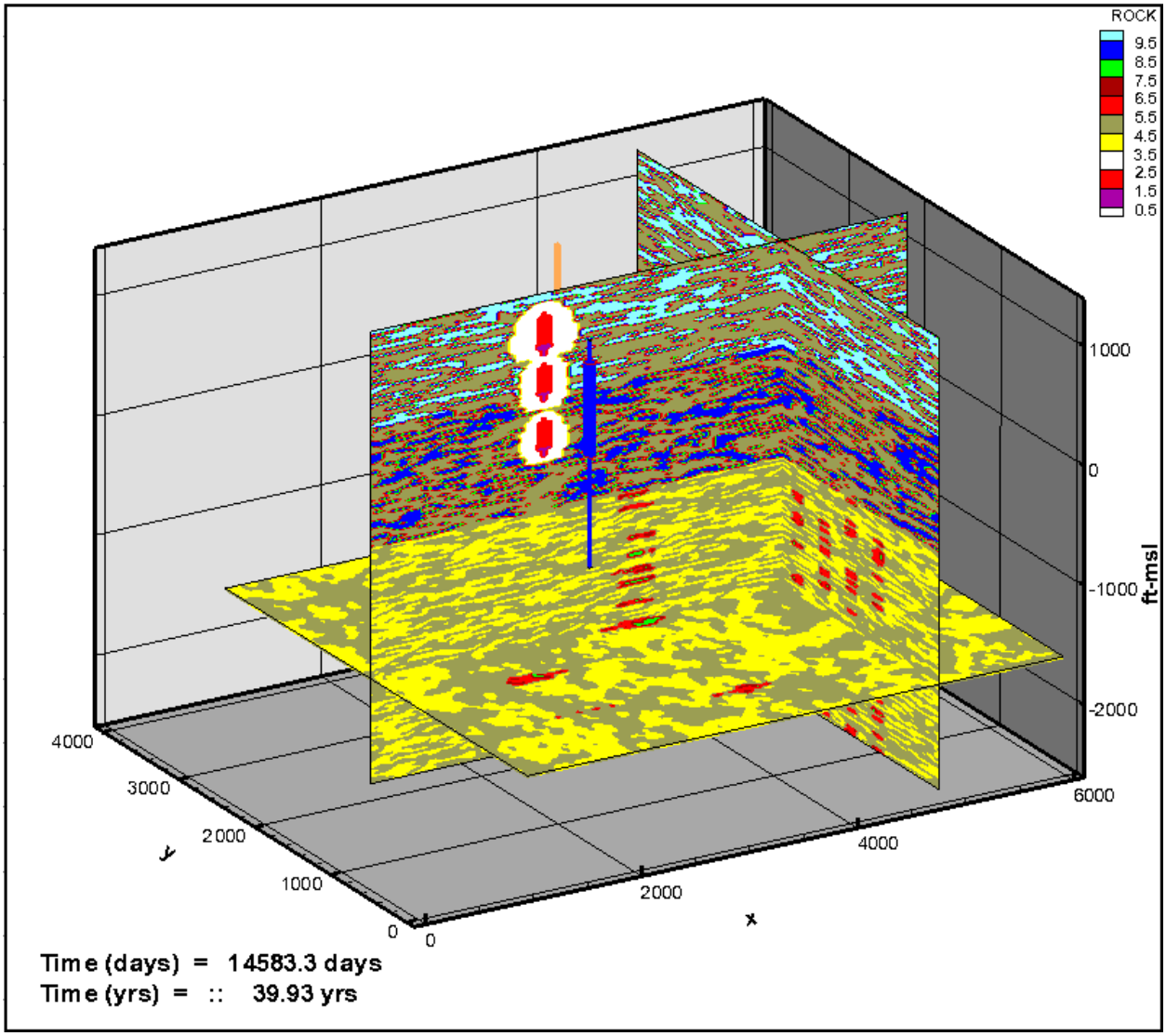

Figure 15. Sliced Model Domain Showing Several Hydrofractured Wells (Simulated Potential Future) and Detonation Zones
(yellow = lower Williams Fork sandstone, olive = shale, white = nuclear fractures, red = chimney or HFnsd, dark red = HFfsd, green = HFshl, dark blue = upper Williams Fork sandstone, light blue = Ft. Union sandstone)

3.5 ROCK (Material) Parameters

Porosity, permeability (for the *x*, *y*, and *z* directions), capillary pressure curves, and relative permeability curves are specified for each material or ROCK type (Table 5). ROCK type names are limited to five characters.

Table 5. ROCK types used in the Rulison and Rio Blanco Models

Order	ROCK Type	Description
1	glass	Melt glass, allows constant heat source at base of chimney
2	chimn	High-permeability and high-porosity chimney
3	NFrac	Nuclear fractured
4	LWFsd	Lower Williams Fork sandstone, gas reservoirs
5	shale	Shale, any formation in the section
6	HFnsd	Hydrofractured sandstone near a well, max permeability increase
7	HFfsd	Hydrofractured far sandstone, less permeability increase
8	HFshl	Hydrofractured shale, restricted to the near region (as HFnsd)
9	UWFsd	upper Williams Fork sandstone, gas-bearing but nonproductive
10	FtUsd	Ft. Union sandstone, gas-bearing but nonproductive (Rio Blanco)

3.5.1 Permeability and Porosity

Reasonable ranges of permeability and porosity values for the ROCK types were determined by calibrating the Rio Blanco model to production and pressure data from the reentry well into the upper chimney. The Rio Blanco detonations were in the Ft. Union Formation and the upper Williams Fork Formation. Calibrating the Rio Blanco model to the reentry well data determined reasonable parameters for the permeability and porosity of the chimneys, nuclear fractured region, and the Ft. Union sandstones. The permeability and porosity of the lower Williams Fork sandstones (below the detonations) were ported from the Rulison model, which was calibrated to reentry well and gas well production within this interval. A discussion of the model calibration is in Section 4.0.

3.5.2 Capillary Pressure and Relative Permeability

Capillary pressure and relative permeability values for each ROCK type were based on published information about the Mesaverde in Byrnes and Cluff (2009). Charts (modified from Byrnes and Cluff [2009]) of capillary pressure and relative permeability curves for Mesaverde rocks of different permeabilities are shown in Figure 16 and Figure 17 The capillary pressure curves assigned to different ROCK types in the models are based on the TRUST capillary function (Narasimhan et al. 1978) and are overlain on the chart in Figure 16. The relative permeability curves assigned to different ROCK types in the models are based on Corey (1954), except the curve for shale, which is based the van Genuchten-Mualem model (Mualem 1976; van Genuchten 1980) and are overlain on the chart in Figure 17. Values for unique ROCK types in the model (chimn, NFrac, HFnsd, HFfsd, and HFshl) were estimated considering the effects that hydrofracturing would have on the unfractured rock (tend to increase relative gas permeability and decrease capillary pressure relative to the published Mesaverde values).

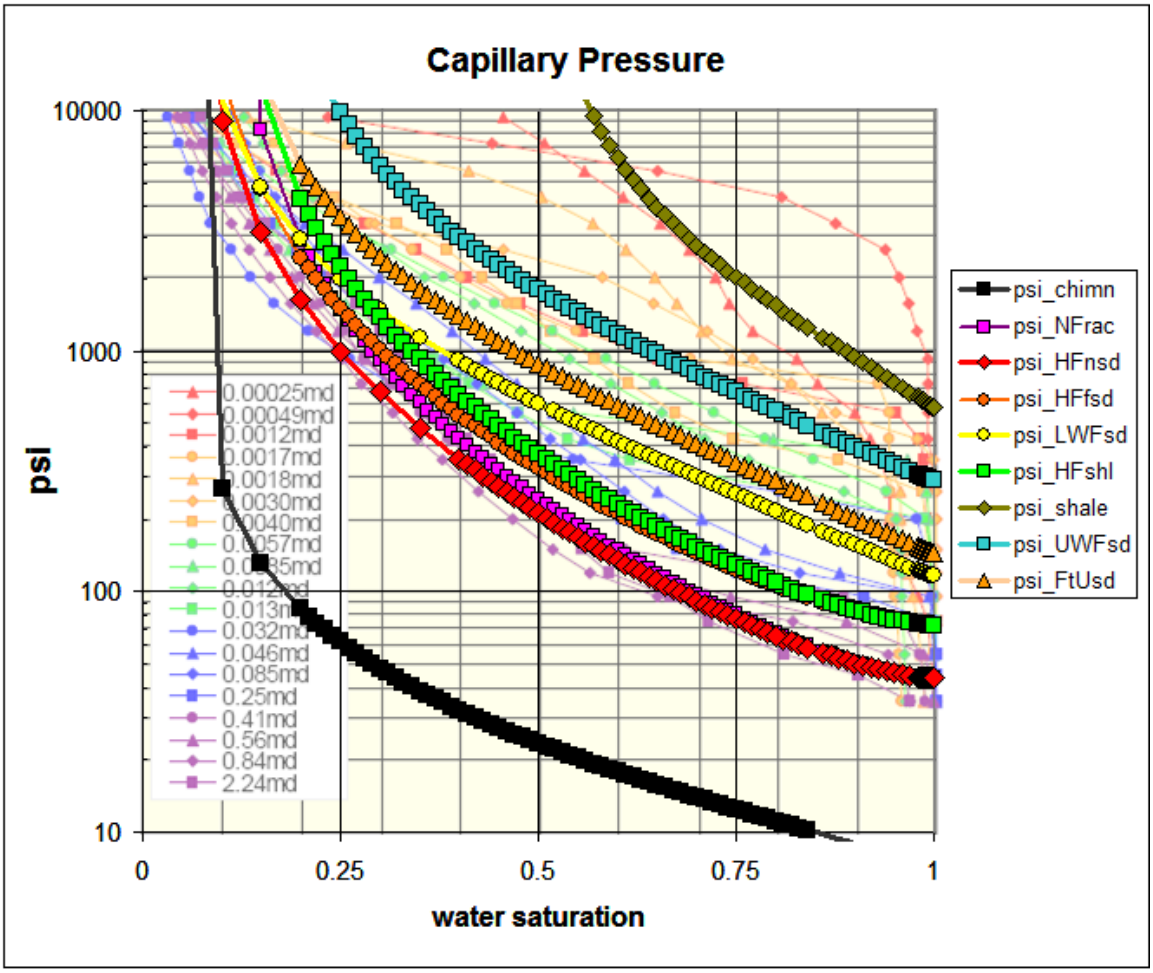

Source: Byrnes and Cluff 2009

Figure 16. Capillary Pressure Curves for the Modeled ROCK Types

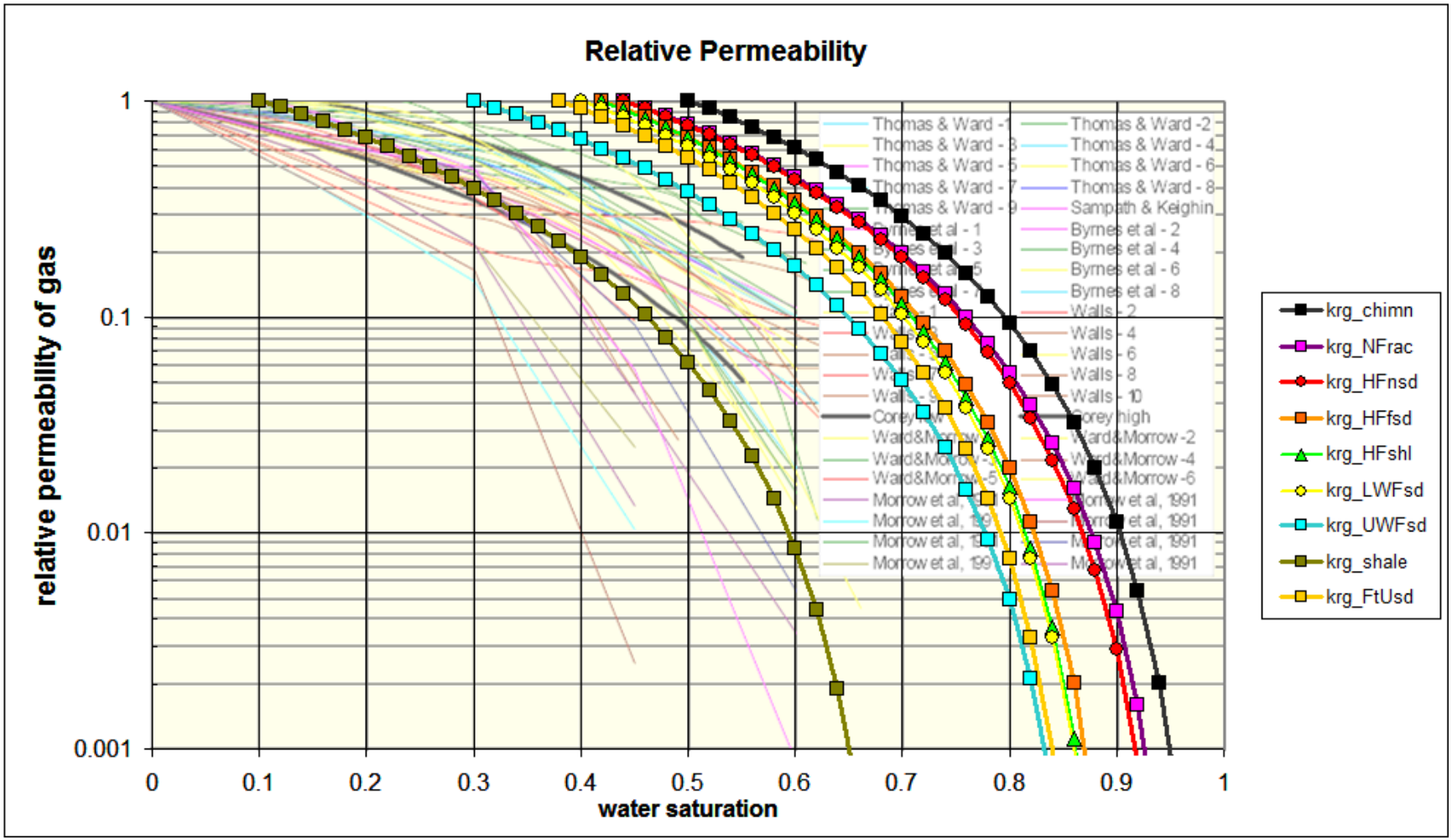

Source: Byrnes and Cluff 2009

Figure 17. Gas Relative Permeability Curves for the Modeled ROCK Types

Capillary pressure and relative permeability can significantly affect the movement of fluids in a multiphase system. For partially saturated gas reservoirs, the presence of a wetting phase (water) impedes the movement of the nonwetting (gas) phase because the gas must overcome the capillary pressure of the water. For example, at a water saturation of 50 percent, gas in the nonproductive upper Williams Fork sandstones would require nearly 2,000 pounds per square inch (psi) to displace water from capillary forces alone (Figure 16). Additionally, the presence of water partially blocks openings, reducing the area through which gas can flow, reducing the permeability of the gas phase. For example, at a water saturation of 50 percent, the permeability of the nonproductive upper Williams Fork sandstones would have a gas permeability of about 40 percent of the native formation permeability due to the presence of water (Figure 17). A good contrast is the capillary pressure and gas permeability of the shale (gas is essentially immobile) to that of the chimney, where gas can move freely (Figure 17). Note that the relative permeability curves were selected at the high-permeability range to be conservative.

3.6 Boundary Conditions

The size of the model domain in combination with the very low native permeabilities of the formations allows for no-flow boundaries on all sides without significantly altering the flow field, even for wells near boundaries. The majority of flow within the model domain is from regions that have been fractured to allow flow, the nuclear fractured region or hydraulically fractured regions surrounding gas wells. These regions are separated from boundaries by the very low permeability formation, and any significant interaction with boundaries over the time frame of the simulations would in itself indicate that the model is not calibrated to observed real-world conditions. This is also a conservative formulation in that any well–boundary interaction would increase the pressure decline at the well, increase the pressure gradient, and increase the potential for transport of radionuclides from the detonation.

3.7 Initial Concentration and Partitioning of Tritiated Water (THO) Between Gas and Aqueous Phases

The Henry's Law constant is used to describe the partitioning of a compound between the gas and aqueous phases. A common example is the group of compounds known as VOCs (volatile organic compounds). For instance, the air above a container of water that contains dissolved benzene (the aqueous phase) will have a detectable odor from the benzene vapor and humidity from the water vapor (the gas phase) because of their tendency to evaporate, which is quantified by their vapor pressure. This partitioning provides a method to calculate the mass fraction of THO in the gas phase using the vapor pressure of water, assuming that THO is in molecular equilibrium with the gas and liquid phases. This is not precise, but within a few percent, because the THO molecule is heavier than regular H_2O (20 vs. 18 grams per mole [g/mol]), causing it to be slightly under-represented in the real system relative to the simulations. The Henry's Law constant used to calculate the partitioning of THO between the two phases is simply the water vapor pressure.

The water vapor pressure is directly related to temperature (Figure 18), and the code was modified to calculate a temperature-dependent Henry's Law constant based on the vapor pressure (enacted in the code as the inverse of the vapor pressure, HCRN1 [Henry's Constant Radionuclide 1]). The inverse pressure form of the Henry's Law constant is developed in Equation 2 and was used to reproduce published values (Smiles et al. 1995) for confirmation.

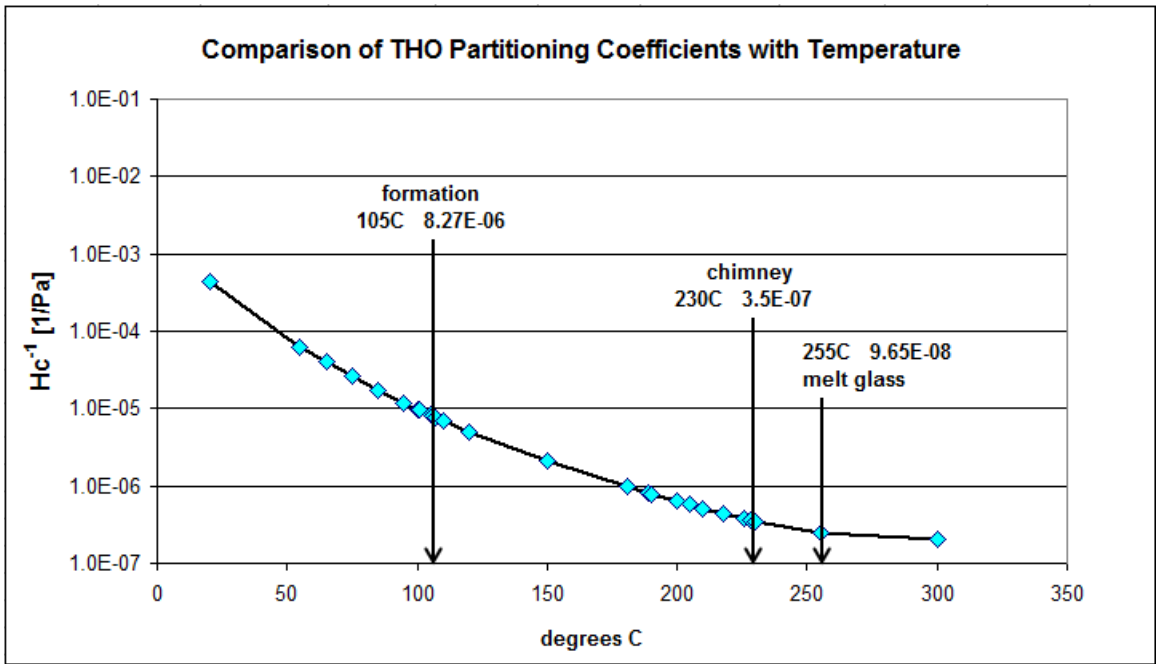

Figure 18. Inverse Vapor Pressure of Water Relative to Temperature

Inverse Henry's Law constant: $HCRN1 = \frac{\chi_l^{THO}}{P_g^{THO}}$ Equation (2)

Where:

χ_l^{THO} = mole fraction of tritiated water in the aqueous phase,

P_g^{THO} = partial pressure of tritiated water vapor in the gas phase.

Gas and aqueous phases should have same ratio of molecules:

$$\frac{P_g^{THO}}{P_g^{H_2O}} = \chi_g^{THO} = \chi_l^{THO}$$

Substitute to get HCRN1, same pressure units (pascals [Pa]) as TOUGH2 EOS7R (1/Pa)

$$HCRN1 = \frac{\chi_l^{THO}}{P_g^{THO}} = \frac{\frac{P_g^{THO}}{P_g^{H_2O}}}{P_g^{THO}} = \frac{1}{P_g^{H_2O}}$$

Much of the remaining tritium at the Rio Blanco site is present in water as THO and within crystals in the melt rock (up to 40 percent [Toman 1974]). Most of the tritiated methane created by the upper blast was removed by the production testing. Only a portion of the tritiated methane and ^{85}Kr was removed from the lower chimney due to the abbreviated testing. No tritiated methane or ^{85}Kr was removed from the middle chimney, which was not reentered. The Rio Blanco model followed the process of the Rulison model and assumed that all remaining tritium was present as THO. This is justified for ^{85}Kr because it is not retained in the body, which limits its exposure, and uptake would require immersion in a cloud of gas that would far more harmful

than any ^{85}Kr present in the gas. However, simulations of tritiated methane migration in a follow-up study would be justified. Tritiated methane migrates more conservatively with produced gas than tritiated water vapor (little to no partitioning into the liquid phase, which retards tritiated water migration, discussed below) and when burned, it is converted to carbon dioxide (CO_2) and tritiated water ($CH_3T + 2O_2 >$ heat $+ CO_2 + H_2O + THO$), providing a potential uptake mechanism. Carbon-14 is much longer-lived (5,730-year half-life) than tritium (12.3-year half-life) and will therefore persist far longer, with over 99 percent of what was produced, and not removed by production testing, remaining in the year 2050. Much less ^{14}C was produced by the detonations, and it was found in CO_2, not methane, which would limit its potential uptake.

The initial concentration was assigned to chimney elements (1.0×10^{-10} for Rio Blanco) as a mass fraction of THO in the aqueous phase (a primary variable). This is a conservatively high estimate, though less than that used for the Rulison model because the Rio Blanco devices were designed to produce significantly less tritium. The gas-phase mass fraction of THO (a secondary variable) is calculated (partitioned) with the first time-step of the simulations based on the initial thermophysical properties for the chimney elements. The code was also modified to replace air with methane. This was necessary to get the initial partitioning correct because the molecular weight of air (29 g/mol) is greater than that of methane (16 g/mol). The mass fraction of THO in the gas phase will be higher if it partitions into a less-dense gas phase (methane rather than air). Figure 19 shows the effects of molecular weight and temperature on the initial partitioning of THO from the aqueous phase to the gas phase. Two additional molecular weights (35 and 23 g/mol) are shown in addition to those for air and for methane to better show the effects of molecular weight on the initial partitioning.

Partitioning of THO between the aqueous and gas phases is important beyond the initial partitioning. In order for THO in the gas phase to migrate an appreciable distance from the detonation zone (higher temperature than the formation), it will have to pass through the surrounding relatively cooler formation. The water saturation in the formation is about 0.50, and any tritiated water vapor that comes into contact with the liquid water will be depleted in THO due to the preferential partitioning of THO at lower temperatures into the aqueous phase. Considering that the relative permeability of liquid in the formation is orders of magnitude less than that of gas, this partitioning acts as an effective retarding mechanism to THO migration. Tritium does not exchange between water and methane molecules except at very high temperatures. In experiments, no exchange was observed at temperatures up to 300 °C (Frick et al. 1971).

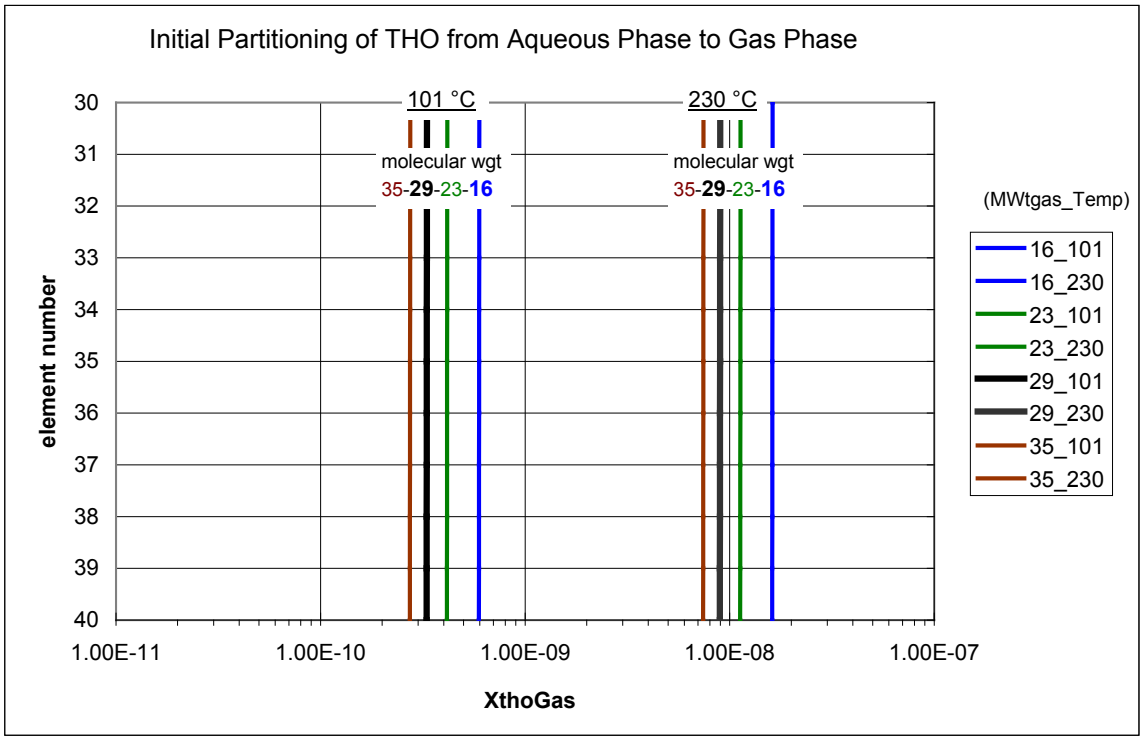

Figure 19. Effects of Molecular Weight and Temperature on the Initial Partitioning of THO from the Aqueous Phase to the Gas Phase

3.8 Initial Conditions

A set of initial conditions has to be supplied for every model element prior to running simulations. Ideally, they represent the undisturbed natural conditions of the system. Initial conditions are specified for each element in TOUGH2 as a set of primary variables (in the file INCON) from which all secondary variables can be calculated. For the EOS7R equation of state, the primary variables for two-phase conditions are gas-phase pressure, brine mass fraction, mass fraction of THO, mass fraction of helium-3, gas saturation, and temperature. The gravity capillary equilibrium initial conditions were calculated analytically using the TRUST capillary function (Narasimhan et al. 1978). Initial conditions were first calculated for the entire MESH with no detonation zone. Elements in the MESH located in the detonation zones were converted to the `ROCK` types `NFrac`, `chimn`, and `glass` to simulate the detonation area properties. Initial conditions for those elements were changed to be more representative of the new `ROCK` types, which have significantly different parameters than either sandstone or shale. Tests of varying the initial condition of hydrofractured elements by increasing their water content (due to remnant injected water from the hydrofracturing process) indicated that the water content quickly dropped in the simulations and was not significant beyond the initiation of production, so the step was not included. This is consistent with actual initial production period in wells which is designed to remove the water introduced during the hydrofracturing process.

3.8.1 Formation

The initial pressure at the bottom of the Rio Blanco domain was specified as 16.83 megapascals (MPa) and resulted in an initial pressure range of 13.9 to 16.83 MPa (about 2,000 to 2,440 psi) from the top to the bottom of the domain. This range allowed the initial pressure to match the shut-in pressure of the reentry well to the upper chimney of 14.1 MPa (2,050 psi) (Toman 1974). Water saturations are about 0.50 in the productive sandstones and about 0.65 in the shales. Reported formation temperatures are about 90 °C (Toman 1974) at the detonation depth as compared to 105 °C at Rulison, which was deeper in the section and below more overburden. The Rio Blanco model spans a larger vertical section than Rulison and was initialized with a gradational temperature range to accommodate the higher temperatures at the production interval (103.5 °C at the base of the Rio Blanco domain) and lower temperatures at the detonation depths (90 °C for the upper chimney depth).

3.8.2 Detonation Zones

The detonations created three separate chimneys (cavities and subsequent rubble-filled collapse chimneys) with properties significantly different from those of the native formation and surrounded by a fractured zone of increased permeability. A different water saturation distribution was assigned to each chimney, allowing its influence to be compared in the same simulation. The lower chimney was mostly dry, the lower half of the middle chimney was saturated, and the upper chimney was mostly saturated. The initial water content of nuclear fracture elements was not changed from that of the original sandstone or shale. This approach will overestimate the amount of tritium created by assuming more liquid but will not alter the source concentration (activity). Figure 20 shows the initial liquid saturation distribution.

The chimney elements were assigned an initial temperature of 260 °C (the same as the Rulison model), and the nuclear fracture elements were assigned a temperature of 155 °C (assumed to be 50 °C hotter than the formation to reduce THO partitioning from the gas phase to the much less mobile aqueous phase). The melt glass elements at the base of the chimneys were assigned a temperature of 255 °C (491 °F) and given very low permeability and porosity to act as a constant heat source. The initial pressure in the chimneys was increased above initial formation pressures (from 14.1 to 15 MPa) to create an outward pressure gradient to assist diffusion prior to reentry testing. Figure 21 shows the initial temperature distribution.

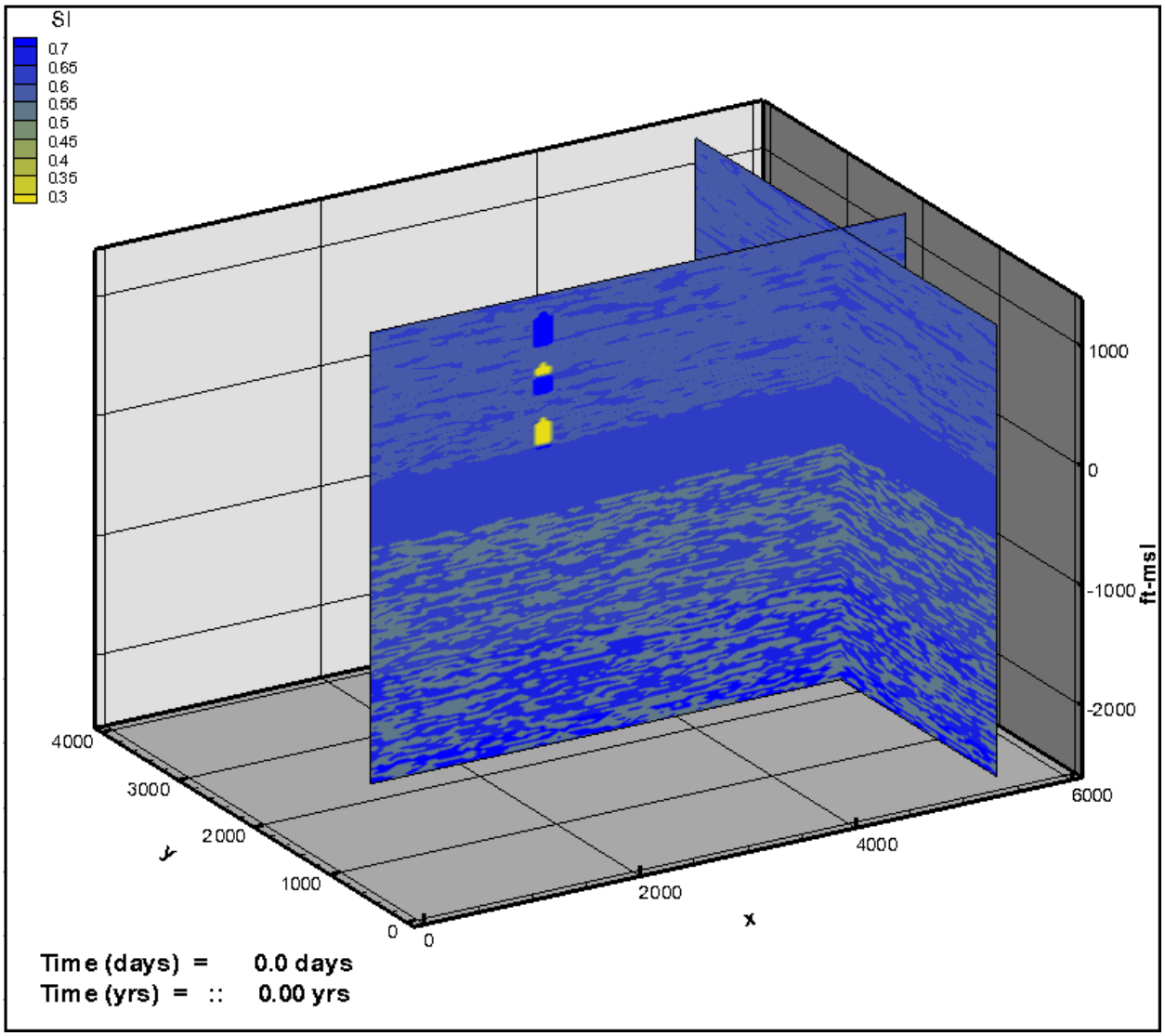

Figure 20. Initial Liquid Saturation Conditions (Flood)
Lower water saturation in the chimney (yellow), sandstone (tan), higher water saturation in the shale (blue), and highest saturation in the upper chimney which was considered saturated, the upper part of the middle chimney and the lower chimney (yellow) were considered the least saturated

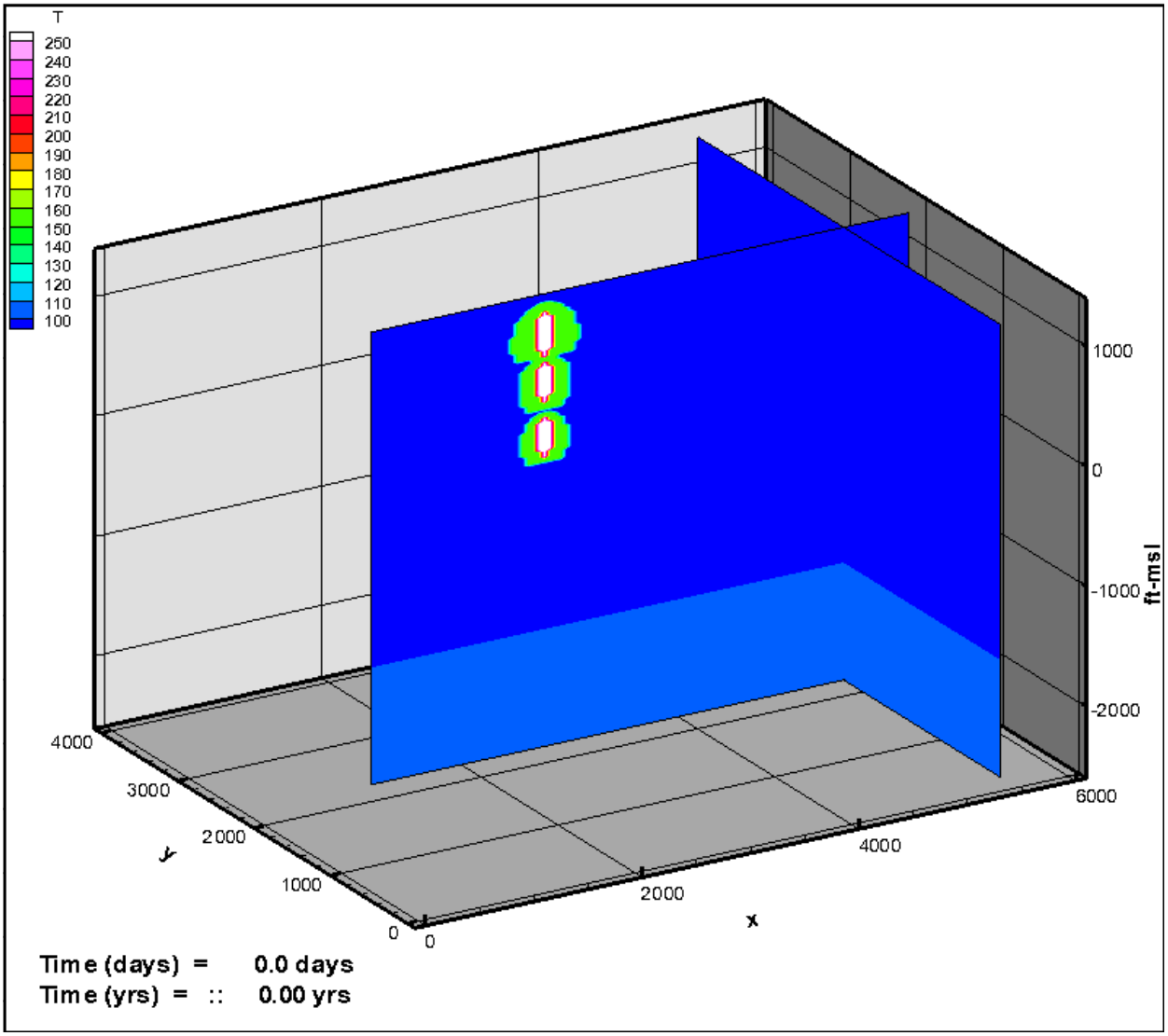

Figure 21. Initial Temperature Distribution

3.9 Decay and Diffusion

The majority of the tritium produced by the detonation has been removed from the subsurface through the decay of tritium to stable helium-3. The half-life of tritium is 12.32 years, or 4,500 days (Lucas and Unterweger 2000). An easy way to visualize the effect of tritium decay is that for every 40-year period, the amount of tritium decreases by an order of magnitude. For instance, the approximately 1,000 Ci of tritium remaining in the middle chimney at Rio Blanco after 1973 (no reentry well) will have decayed to about 100 Ci in 2013 and to 10 Ci in 2053. The decay rate for ^{85}Kr is even faster; with a half-life of 10.76 years, only 7 percent remains after 40 years. The daughter product of ^{85}Kr is the stable isotope rubidium-85.

Diffusion, and the associated parameter tortuosity, was carried out using a constant diffusivity model for these simulations. This method was adopted for the 2009 Rulison Model Addendum

(Cooper et al. 2009) as a more conservative approach (favors more diffusive transport) and was used in all subsequent modeling at Rulison.

3.10 Well Treatment (Sources and Sinks)

Several different methods are available in TOUGH2 to simulate wells (sinks), and the one that is chosen depends not only on what is to be produced but also on the available data about production. Sinks and sources are specified in the `GENER` block of the input file.

3.10.1 Reentry Wells

Production from the reentry wells was simulated using a `MASS` extraction (Pruess et al. 1999) rate in kilograms per second of combined of gas and water based on the historical data that recorded both the amount of gas and water extracted over time and the resulting pressure decline. Production testing on the upper chimney (from well AR-1) took place over 25 days (ignoring earlier brief rate tests) in two separate tests that produced 97.7 MMCF of dry gas and 13,343 barrels of water. The first test ran from November 15 to November 21, 1973. The second test lasted from January 29 till February 15, 1974 (Figure 22). Production testing on the lower chimney (from well AR-2) took place over 7 days from December 11 to December 17, 1974, and produced 26.9 MMCF of dry gas and 1,967 barrels of water (Figure 23).

The observed data of million cubic feet of gas plus barrels of water was converted to a kilogram per second rate for model input. The gas volume and water volume were converted to kilograms using the ideal gas law ($PV = nRT$) for the gas. A single element in the upper part of the chimney was selected as the reentry well extraction location. Drilling in the reentry wells ceased after loss of circulation fluids in the high-permeability chimney or in adjacent fractures. The `MASS` production option (kilograms per second combined gas and water) was used in the model to simulate the production tests and the declining production rates (Figure 24).

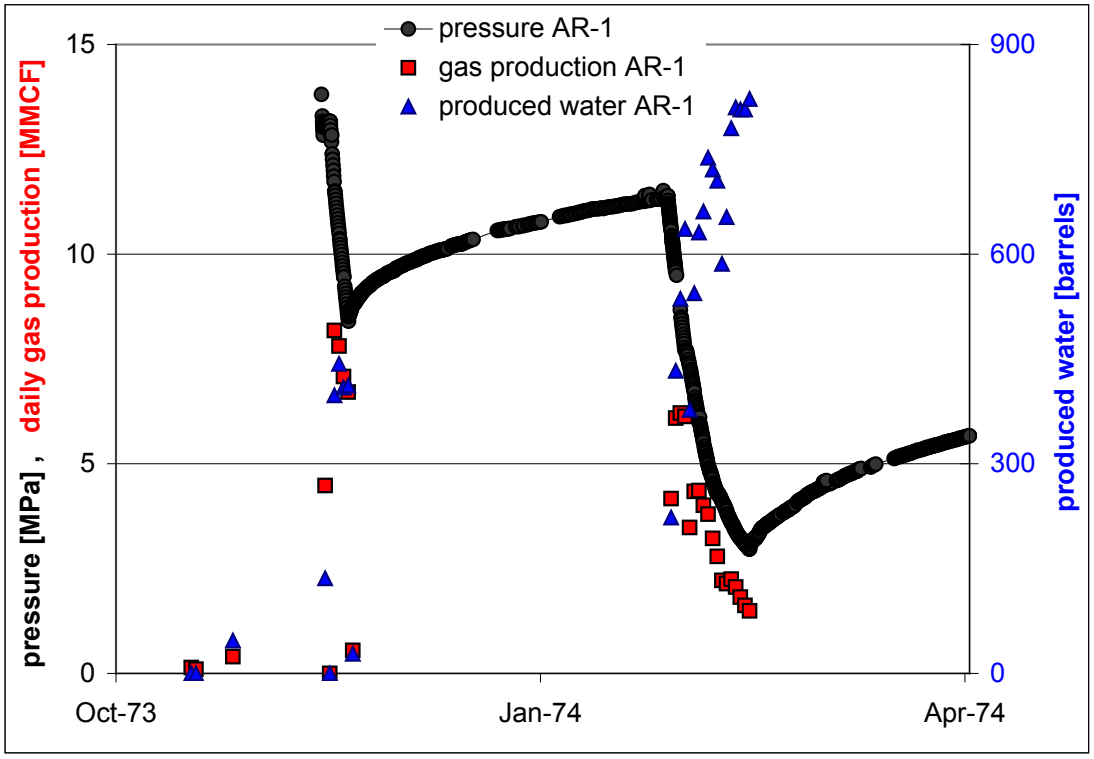

Source: Toman 1974

Figure 22. Pressure Decline Curve for the Upper Chimney Reentry Well Production

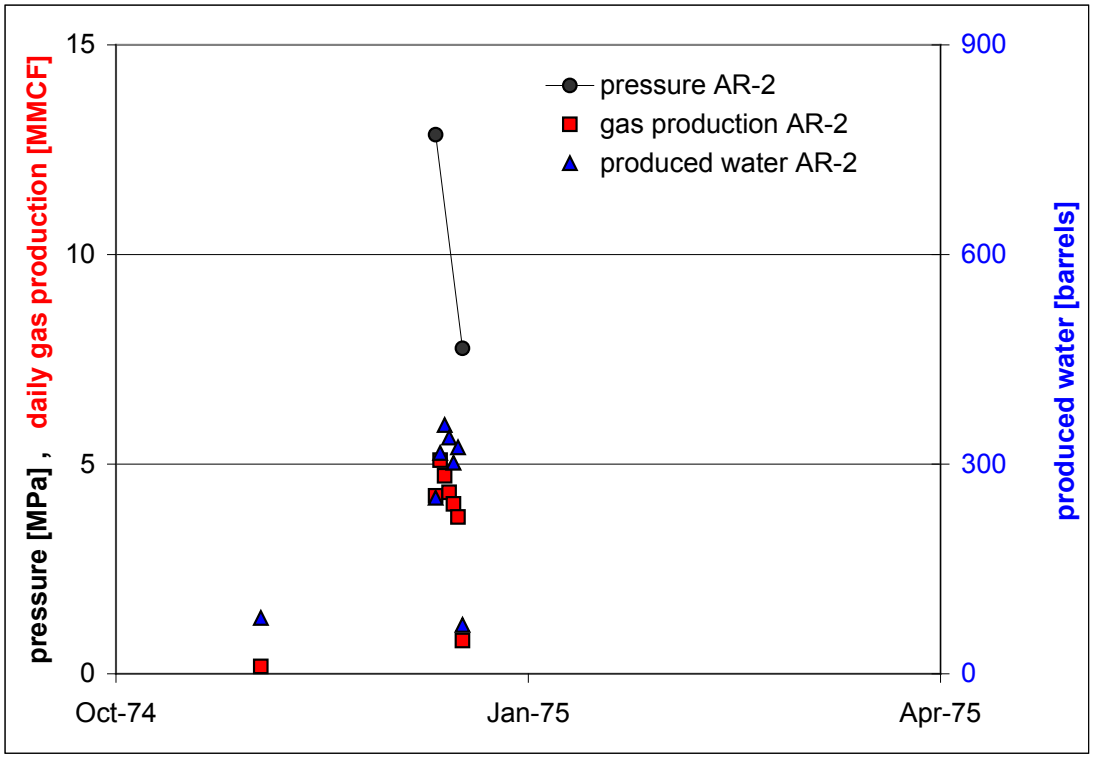

Source: CER 1975

Figure 23. Pressure Decline Curve for the Lower Chimney Reentry Well Production

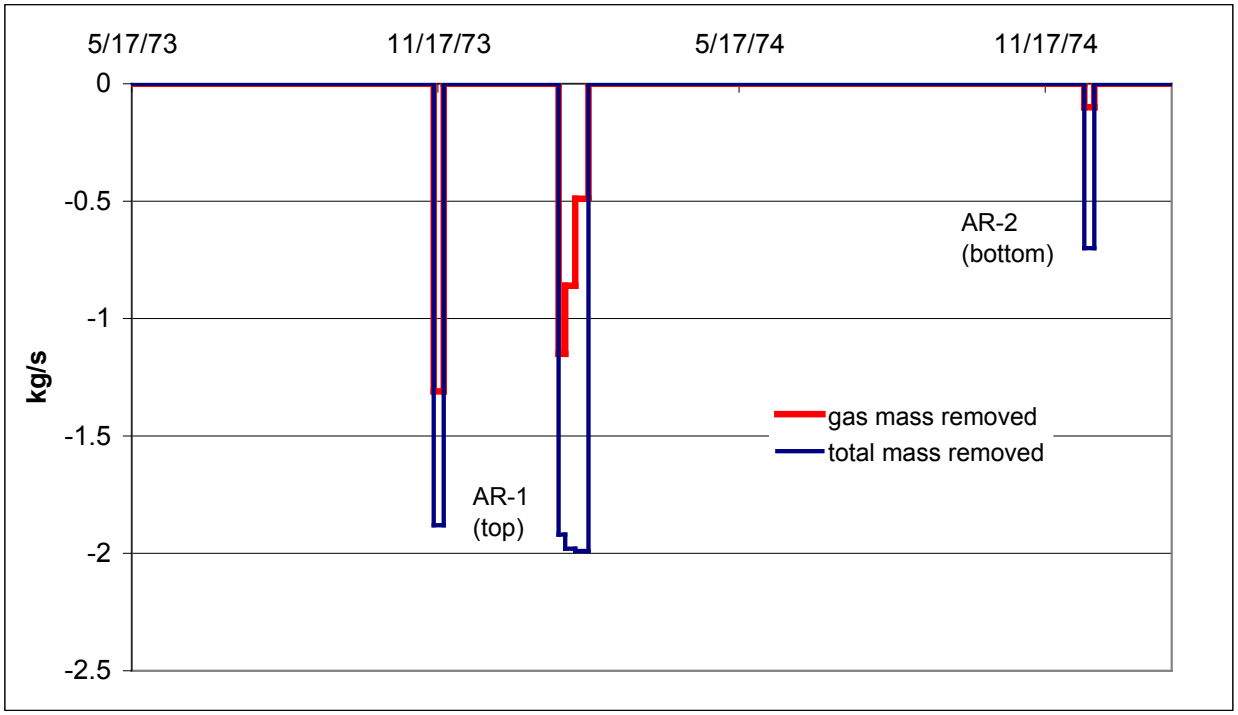

Note: kg/s = kilograms per second

Figure 24. Simulated Mass Rate Removed

3.10.2 Gas Wells

Production from future gas wells was simulated as production against a specified wellbore pressure (well on deliverability, Pruess et al. 1999). A pressure of 600 psi (estimated down-hole pressure at the perforated interval) was used based on discussions with Noble Energy engineers (operator of gas wells within the Rulison model domain, since there are currently no gas wells within the Rio Blanco model domain). The specified pressure was assigned to perforated well elements using the `DELV` option in the model, and fluids flowed into the well due to the pressure differential. The pressure difference (about 1,800 psi; 2,400 − 600) and production rate are highest when a well begins production and then declines over time as fluids (primarily gas) are depleted.

4.0 Model Calibration

Simulations were initially run with model parameters from previous modeling efforts at Rulison to test how well the model could reproduce the pressure data from the historical reentry well production testing. Parameter values were adjusted to achieve the best match with the new model. The specific parameter values arrived at during the calibration process should be considered in a general context or as a limited range and not taken as absolutes. The parameters that achieve the best match will change slightly depending on the sand/shale realization and even more so with changes to the conceptual model, like the size and elongation of the nuclear fractured region.

4.1 Upper Chimney Reentry Well Calibration

The calibration of model parameters for the detonation zone and the Ft. Union Formation was based on the historical reentry well data into the upper chimney (Figure 22). The calibration simulations were conducted on a subset of the model domain from the vicinity of the detonation (490,000 elements) to reduce computation time to allow for the numerous simulations required for calibration. Parameters adjusted during the calibration process were the permeability and porosity of the chimney, nuclear fractured region, and Ft. Union sandstone. The best fit achieved (simulation 19) is shown on Figure 25, and the fit parameters are given in Table 6. The permeability of the Ft. Union sandstone in the horizontal direction of the natural fracture trend (k*x*) was assumed to be 10× that of the permeability normal to the trend (k*y*) and that of the vertical permeability (k*z*). This anisotropy ratio was constant for all simulations. One significant difference of the Rio Blanco simulations from the Rulison simulations, is the low effective porosity (0.015 vs 0.06) based on calibration of the nuclear fractures (though the value is within a reasonable range). This is likely due to the higher water content of the Ft. Union Formation (formation of the upper Rio Blanco detonation) relative to the lower Williams Fork Formation (Rulison detonation).

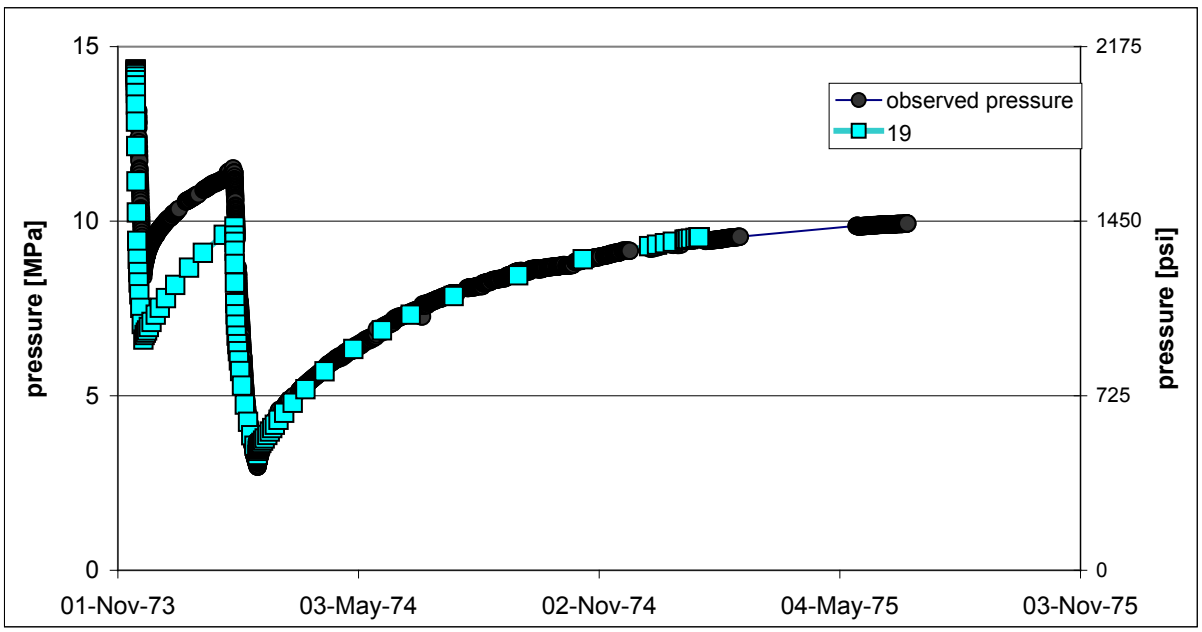

Figure 25. Overlay of Calibrated Simulated Pressure Curve with Observed Pressure

Table 6. Parameters from Calibration That Provided the Best Fit for One Realization

Unit	Permeability[b] (k*x*)	Permeability (k*y*, k*z*)	Porosity
chimn	0.1×10^{-11}	0.1×10^{-11}	0.30
NFrac	0.1×10^{-16}	0.1×10^{-16}	0.015
FTusd	0.1×10^{-18}	0.1×10^{-19}	0.03
shale [a]	0.1×10^{-19}	0.1×10^{-19}	0.06

[a] shale properties provided for comparison (not adjusted for calibration)
[b] for comparison, a darcy is about 0.1×10^{-11} (1.0×10^{-12})

The latter series of simulations, 8 through 21 (Figure 26), that were run to achieve the good-fit case demonstrate how the results vary with different calibration parameters (Table 7). The tendency during the calibration process (especially the earlier simulations based initially on Rulison parameters that are not shown) was to under-predict the overall observed pressure drop (the first and second production tests combined) and to under-predict the pressure recovery of the first test alone. This is due to the lower permeability and gas relative permeability of the Ft. Union sandstones in comparison to those of the lower Williams Fork, and the effect that had on the detonation zone properties.

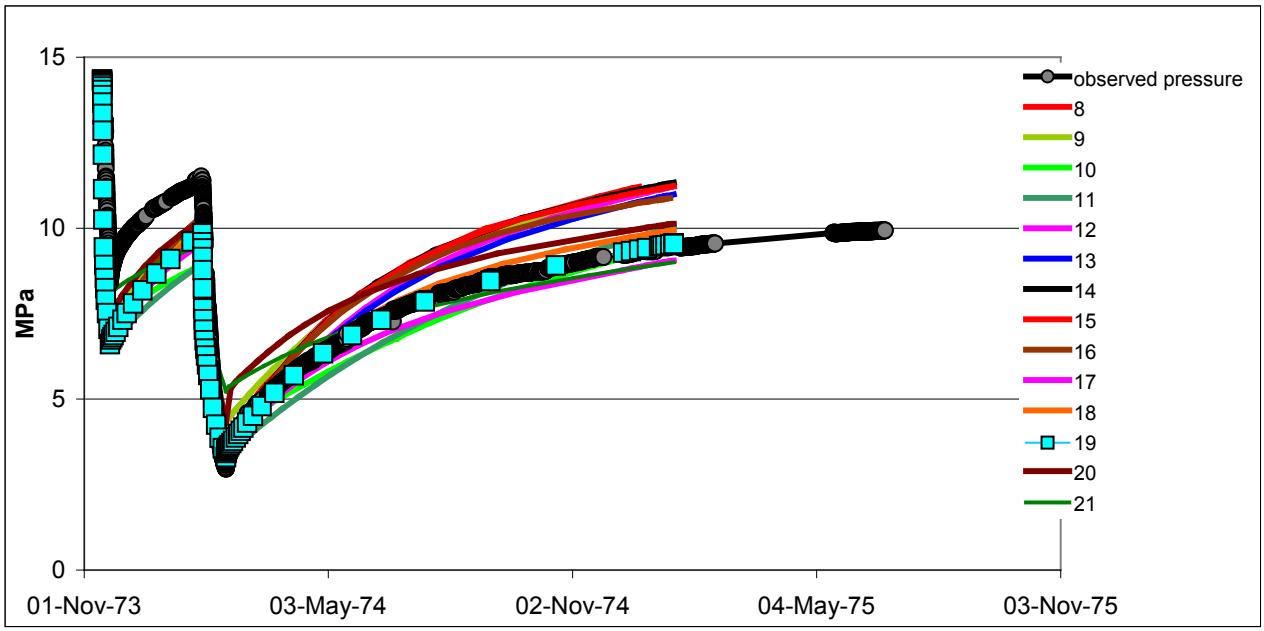

Figure 26. Plot of Results of Parameter Calibration Simulations

Table 7. Range of Parameters Used in the Sensitivity Runs

Unit	kx (low)	kx (high)	Porosity (low)	Porosity (high)
chimn	0.1×10^{-12}	0.1×10^{-11}	0.30	0.70
NFrac	0.5×10^{-17}	0.1×10^{-16}	0.03	0.03
FTusd	0.1×10^{-18}	0.5×10^{-17}	0.015	0.04

4.2 Other Significant Well Data Considered for Calibration

Production testing of the lower chimney (well AR-2 was tested for only 7 days) did not provide sufficient data to be used for calibration. The lower chimney is in the upper Williams Fork Formation and nearer (vertically) to the gas-producing interval in the area. Well RB-U4 was drilled after the detonations (about 600 ft NE of surface ground zero [SGZ], shown on Figures 4, 9, 10, and 12) to test the native formation permeability away from the detonation zone because of the poor production of the Rio Blanco test relative to the Rulison test. RB-U4 produced only about 0.375 MMCF of gas and 6,668 barrels of water from the Ft. Union over a 3 week period in early 1975. It was recompleted at a later date in the upper Williams Fork where the permeability

was too low to test, even after hydraulic fracturing. Prior to this testing, it was not known that a primary problem with limited production from the Rio Blanco test was that the relative permeability of the gas phase was reduced by the higher water contents of the formations where the detonations occurred. Hydraulic fracturing, which increases the permeability by fracturing the formation, also introduces large amounts of water into the formation, which reduces the relative permeability of the gas phase. The high permeability of the Ft. Union Formation in the calibration process, listed in Table 7, was used for the upper Williams Fork in the full-scale simulations to maintain a conservative bias.

5.0 Rio Blanco Simulation Results

The primary benefit of a numerical model is that past, current, and future scenarios can be tested. The Rio Blanco model was initialized to conditions following the detonations and used to simulate the reentry well production testing, the subsequent pressure recovery after testing ended, and the migration of contamination from the detonation zones to its current extent (primarily by diffusion). The Rulison Path Forward document (DOE 2010) puts forth a logical approach to future gas development in the vicinity of the Rulison test, and the Rulison model was used to simulate the enactment of the Path Forward drilling plan. A similar approach was used to simulate the potential future development of gas reserves near Rio Blanco. A series of model runs simulate three sets of wells approaching the site from the east. The first wells are just inside a half-mile, the second set is less than a quarter-mile east, and the third set is about 500 ft west of SGZ (Figure 8).

The Rio Blanco model utilized a large subset of the domain, which excludes the west 1,000 ft, for the approaching series of wells from the east (1,520,000 elements). The simulations are a composite of two separate primary simulations, which are in turn composed of separate simulations as needed to improve use of computation time and assignment of well production rates. The first step after model construction was to simulate the post-detonation events up until potential future gas wells begin to be installed (2015). The second step simulates production from the staged additions of future gas wells for over the next 20 years and then for another 20 years until production ends for the last wells installed (2055).

5.1 Simulations from Post-Detonation to 2015 Conditions

The initial modeling simulated conditions from post-detonation, May 17, 1973, up until future gas wells begin simulated production, January 1, 2015 (Table 8). Figure 27 through Figure 34 (designated X for plot of mass fraction THO gas, P for pressure) are vertical sections (y41 on Figure 10) that show the progression of conditions throughout the simulation. Pressure is shown on the concentration plots as black contours to reference with the color pressure plots.

Table 8. Key Steps in Simulating Post-detonation to 2015

Date	Days Since Detonation	Process	Figure
05/17/1973	0	Initial diffusion after the detonation	27
11/15/1973	182	Begin reentry well testing AR-1, test 1	28
11/21/1973	188	Production test 1 ends	29
12/11/1974	257	Production test 2 begins	30
12/17/1974	274	Production test 2 ends	31
12/11/1974	447	Production test AR-2 begins	32
12/17/1974	466	Production test AR-2 ends	33
06/24/1975	768	Last pressure reading, AR-1	
01/01/2015		Simulation ended	

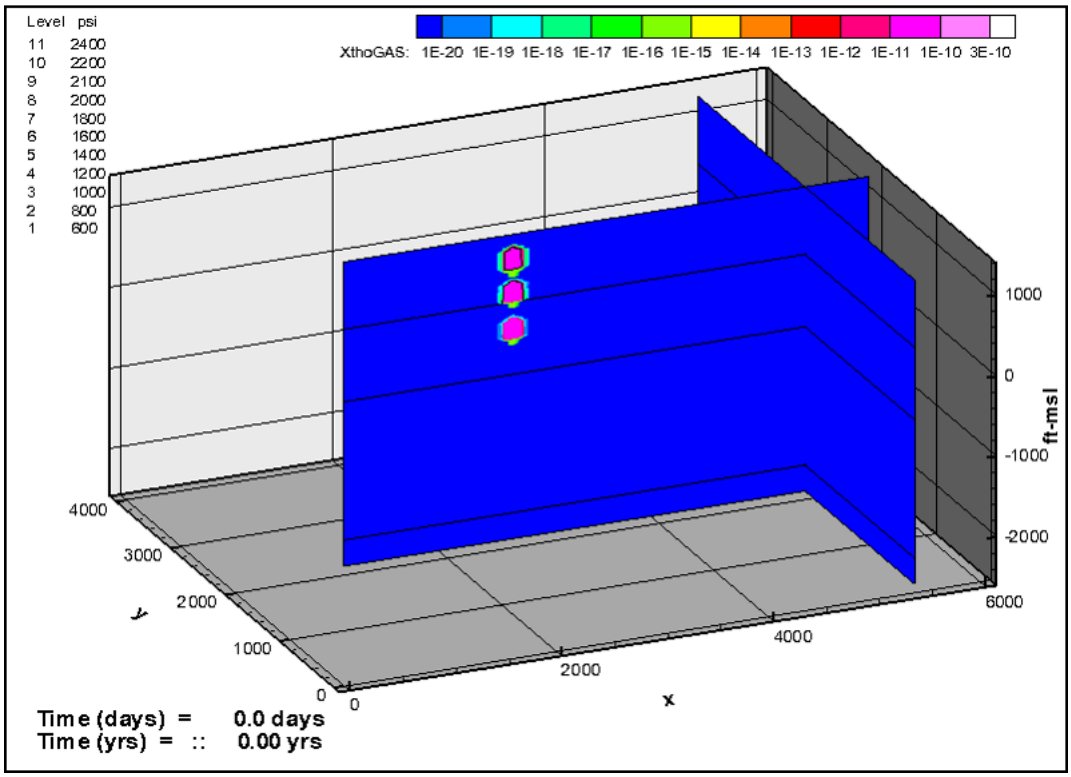

Figure 27X. Initialized Mass Fraction of THO in the Gas Phase (Xthogas) After the Detonation

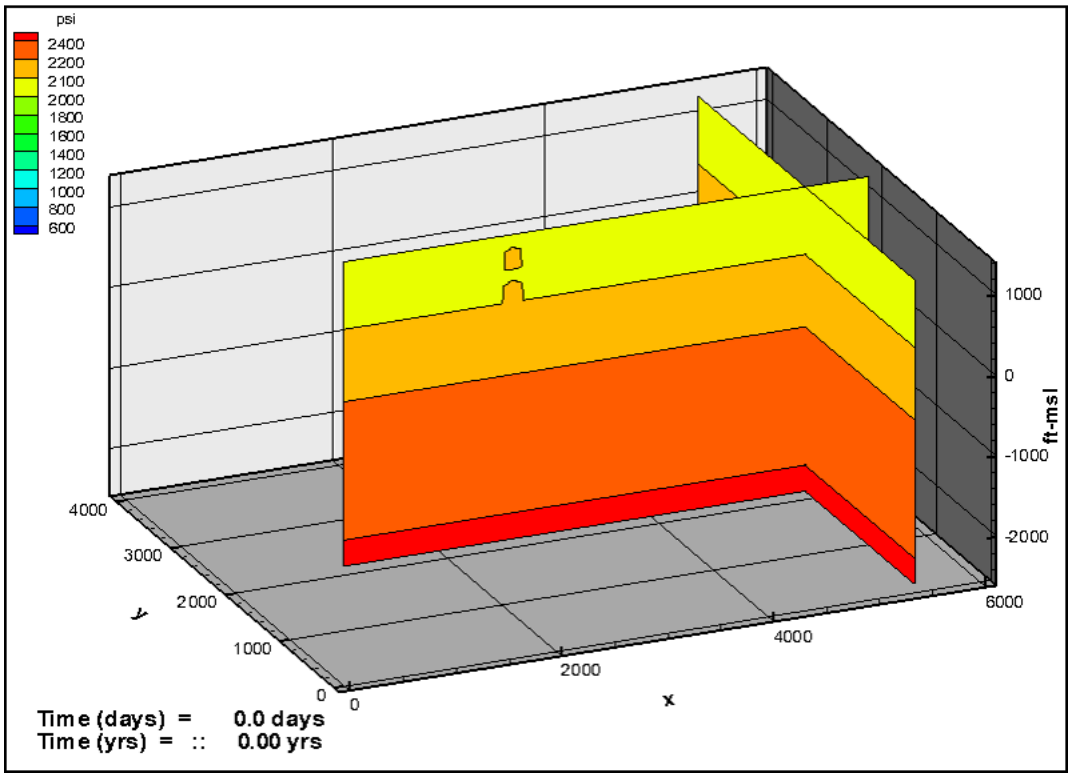

Figure 27P. Initialized Pressure Distribution After the Detonation

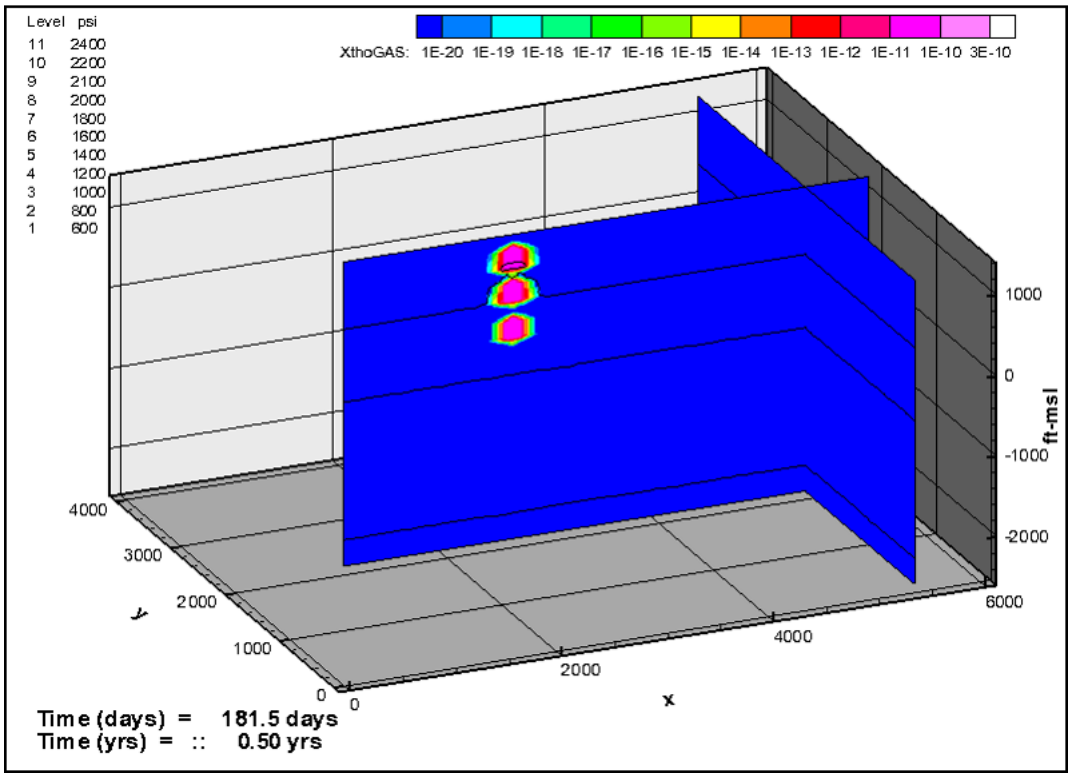

Figure 28X. Mass Fraction of THO Gas Beginning of Production Testing

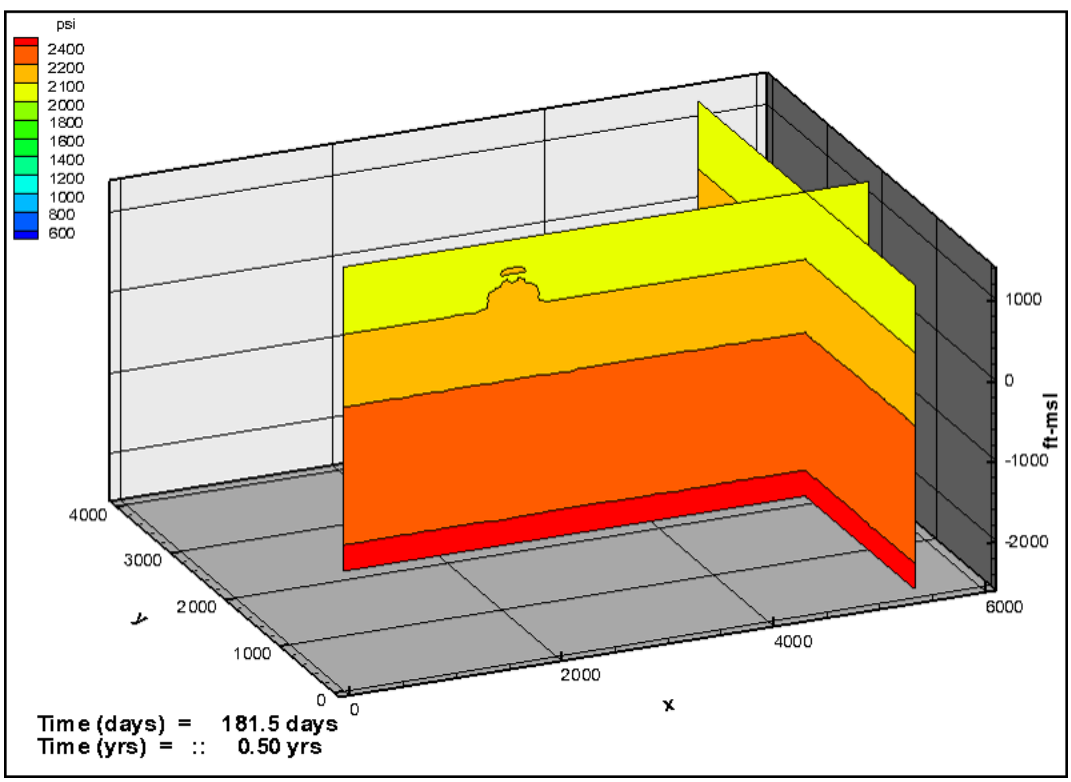

Figure 28P. Pressure Distribution at Beginning of Production Testing

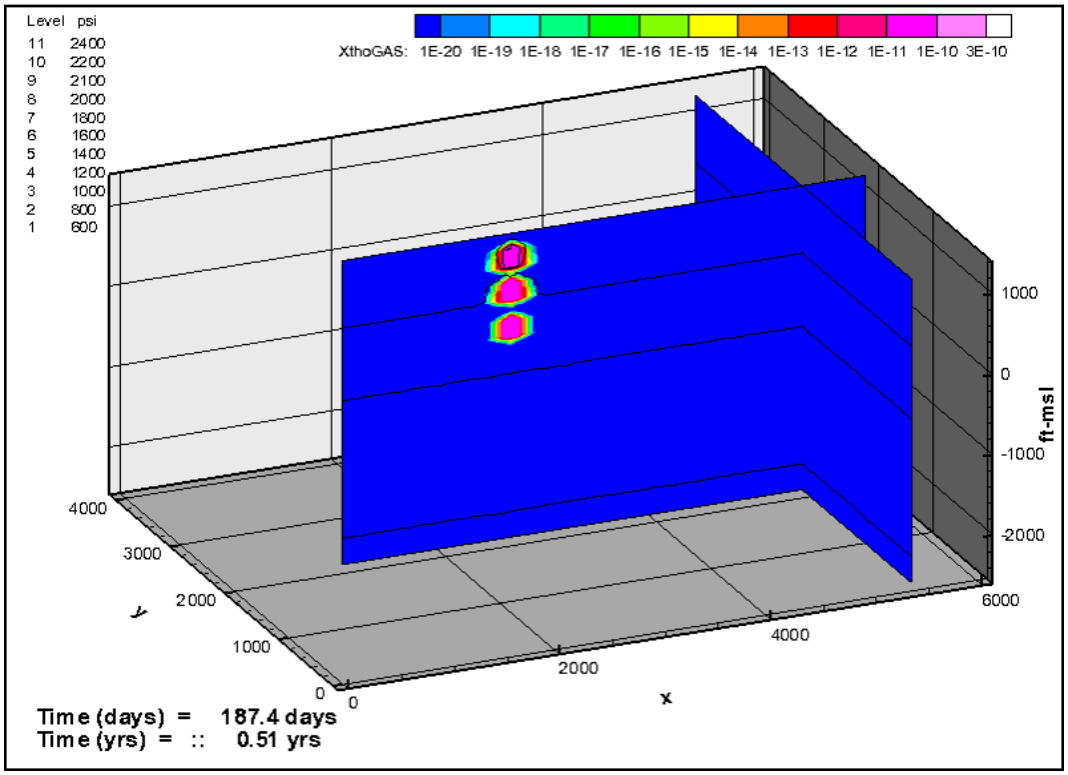

Figure 29X. Mass Fraction of THO After First Production Test, AR-1

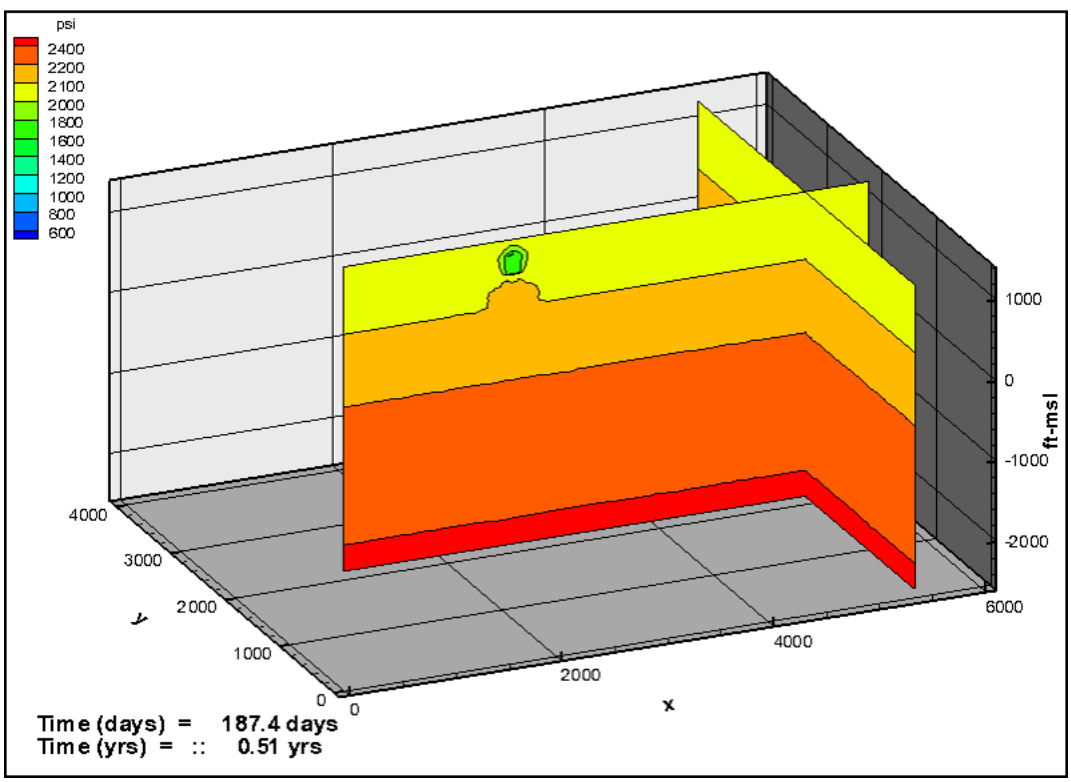

Figure 29P. Pressure Distribution After First Production Test, AR-1

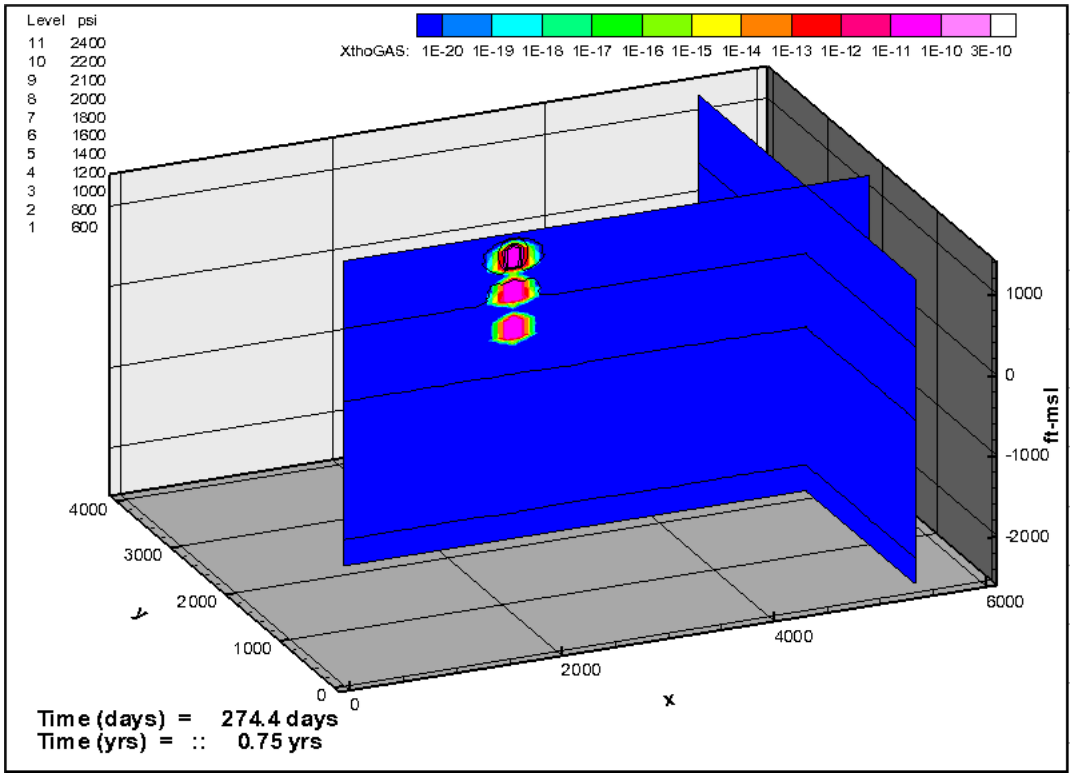

Figure 30X. Mass Fraction of THO After Second Production Test, AR-1

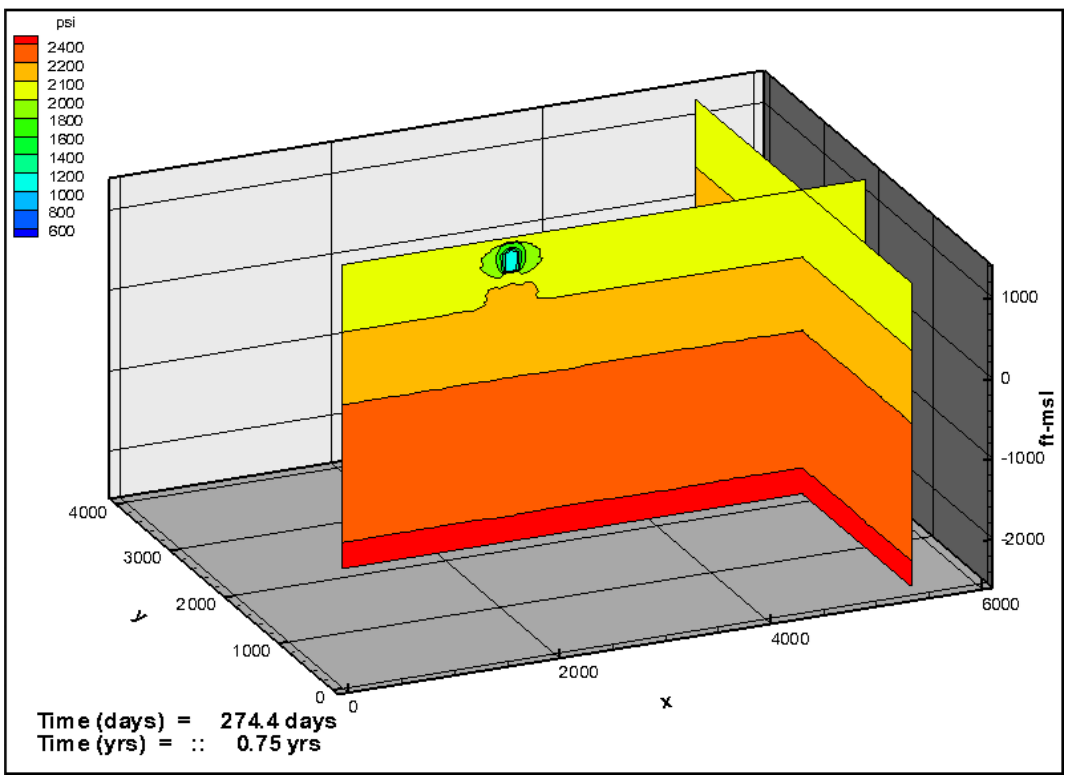

Figure 30P. Pressure Distribution After Second Production Test, AR-1

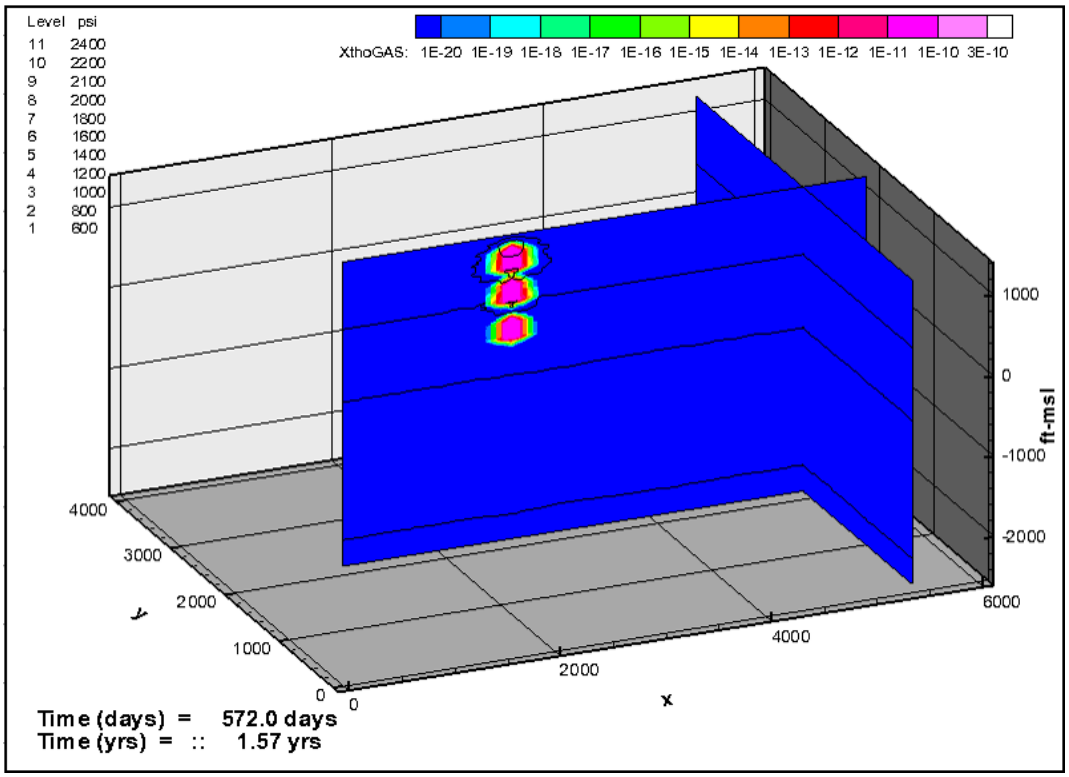

Figure 31X. Mass Fraction of THO Beginning AR-2 Testing

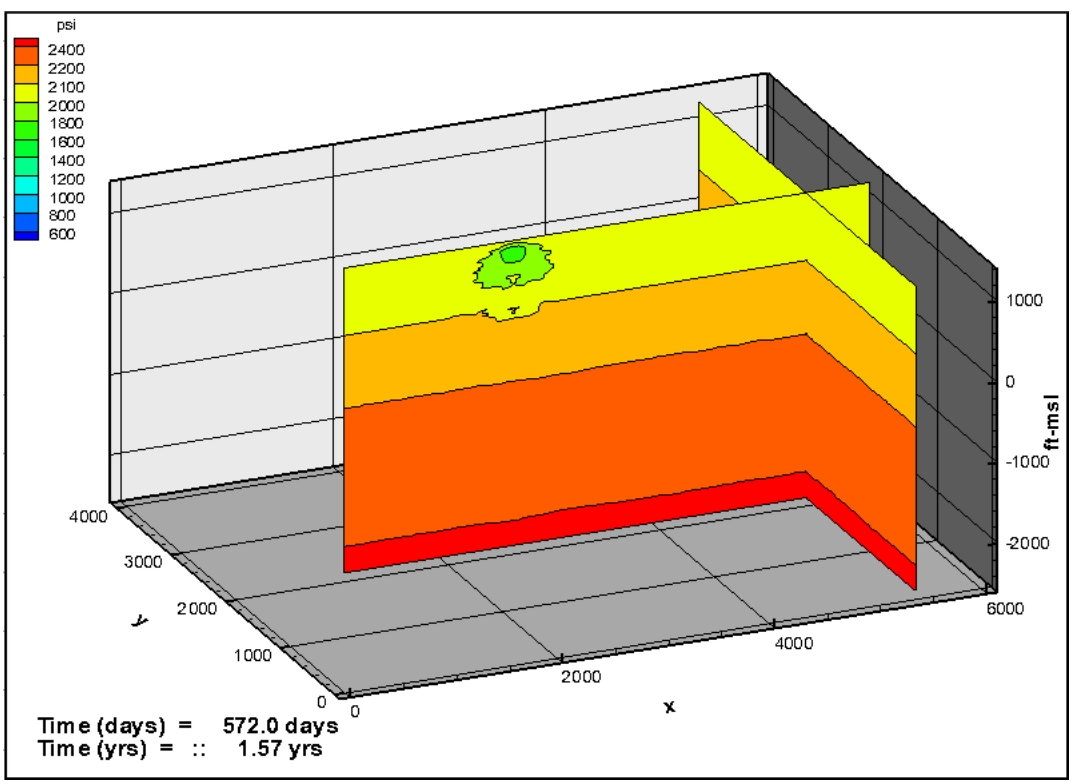

Figure 31P. Pressure Distribution Beginning AR-2 Testing

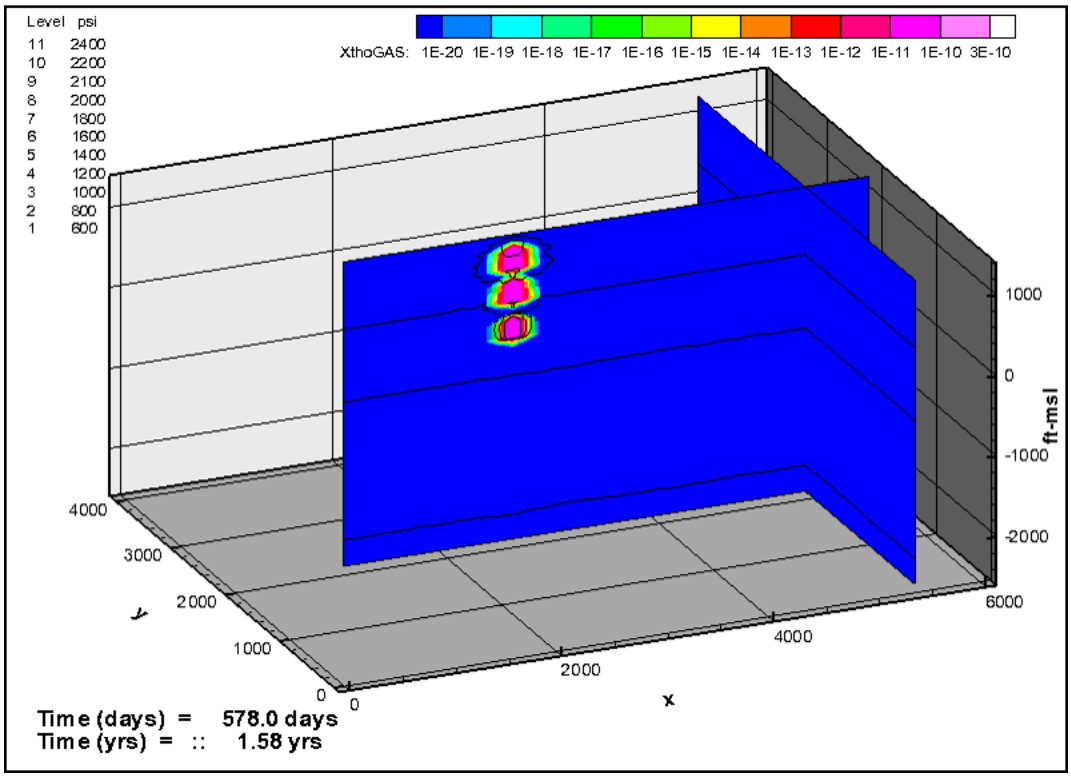

Figure 32X. Mass Fraction of THO End of AR-2 Testing

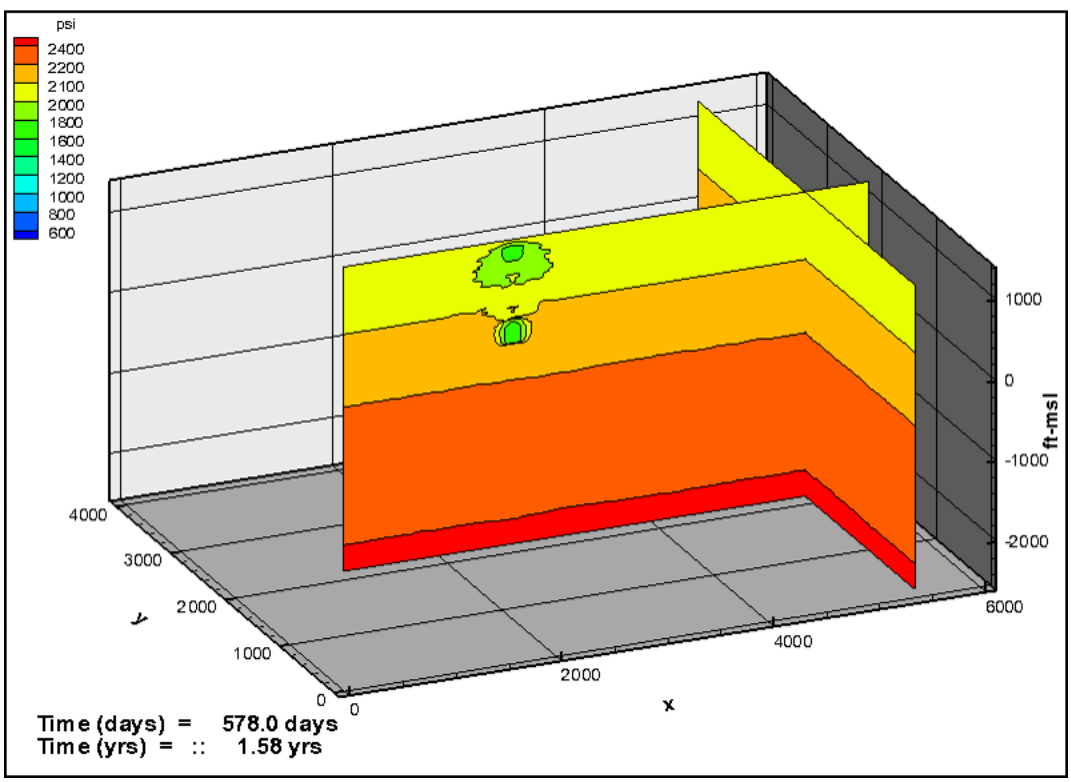

Figure 32P. Pressure Distribution End of AR-2 Testing

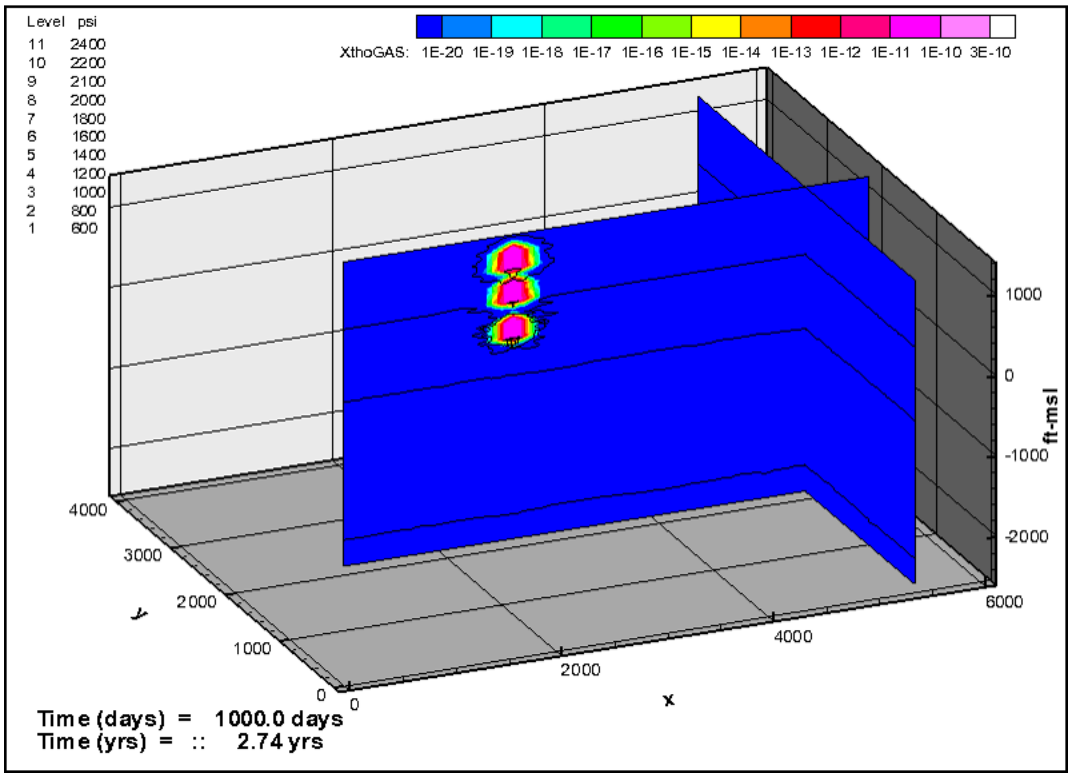

Figure 33X. Mass Fraction of THO 1000 days After Detonations

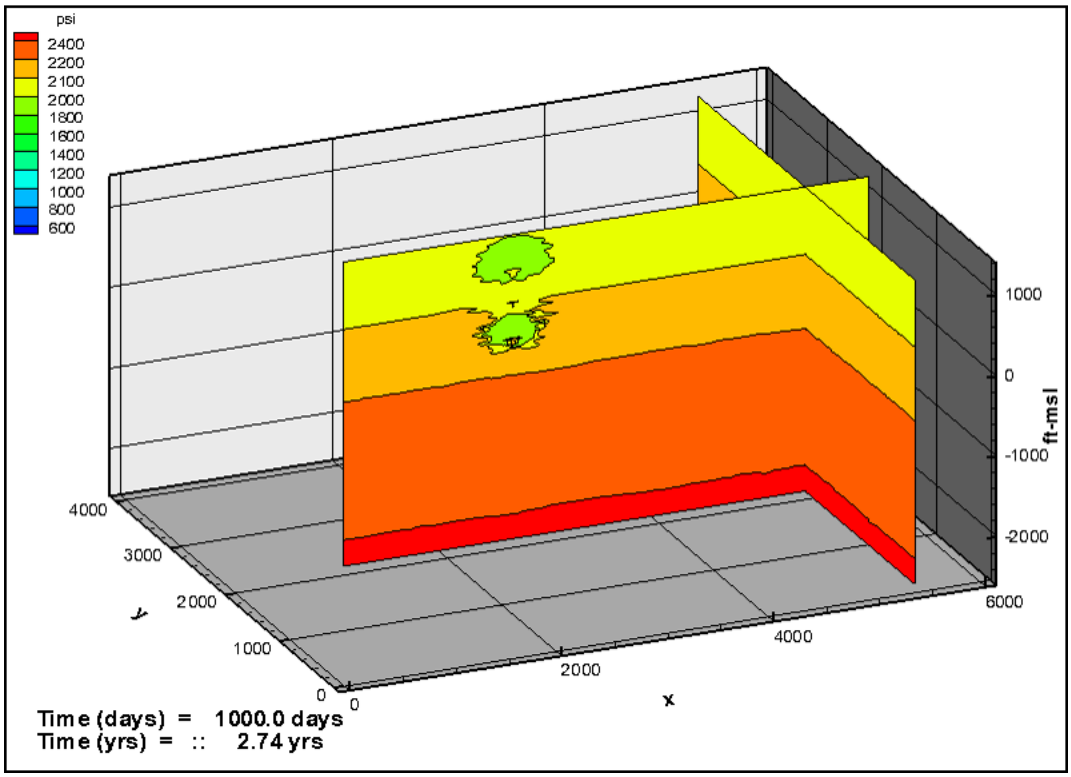

Figure 33P. Pressure Distribution 422 days After End of Production Testing of AR-2

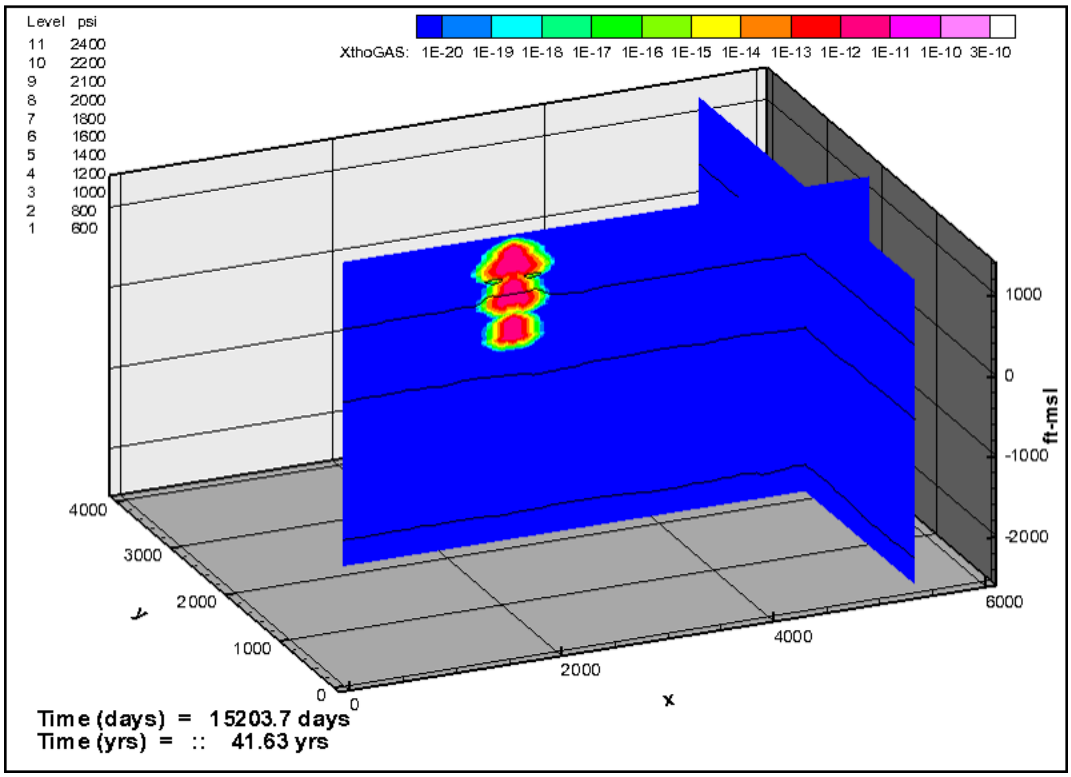

Figure 34X. Mass Fraction of THO in 2015

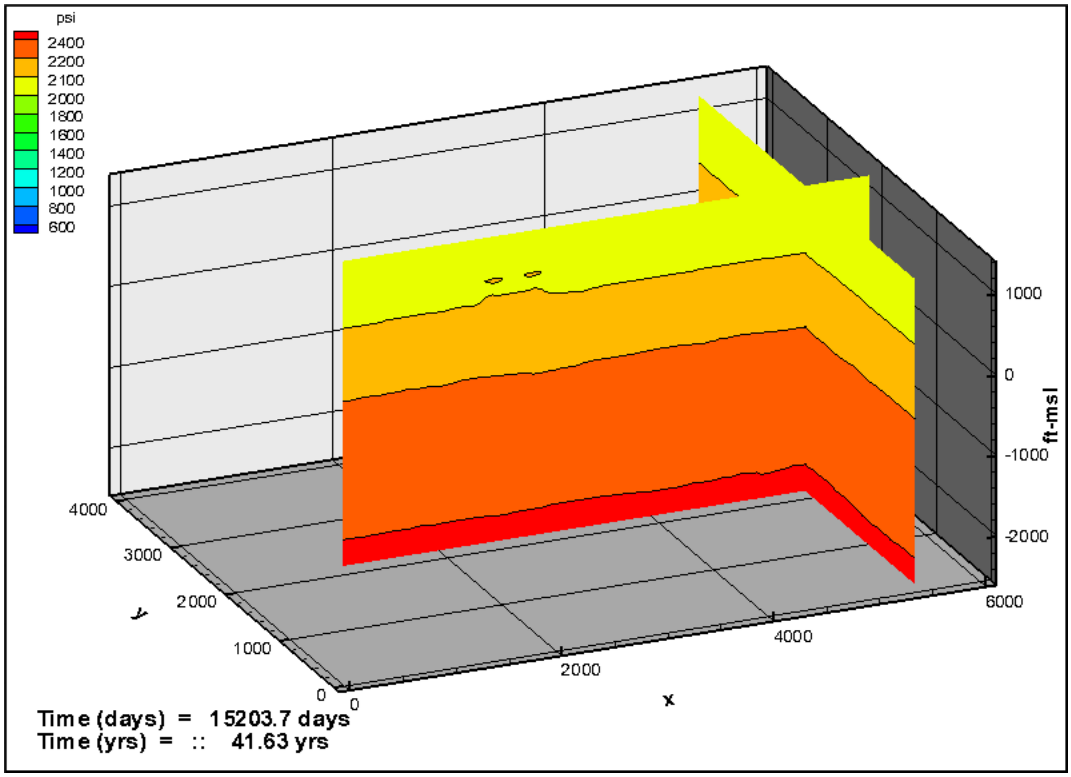

Figure 34P. Pressure Distribution in 2015

The Figure 27 montage shows the concentration of tritium as mass fraction of THO in the gas phase and the pressure distribution moments into the initial simulations.

Figure 28 shows the simulated conditions just before production begins. Key points are the migration of THO from the chimneys into the nuclear fractured region, aided by the higher pressure that was initialized in the chimney, and that the initialized pressure has not yet equilibrated with the formation pressure, unlike at the Rulison site, where production testing began over a year after the detonation.

Figure 29 shows the simulated conditions after the first of two production tests on well AR-1. Production reduced pressures to about 1,220 psi (8.4 MPa) in the detonation zone, creating an inward pressure gradient. The inward gradient did not reverse the migration due to diffusion.

Figure 30 shows the simulated conditions after the second and last production test on AR-1. Production reduced pressures to about 430 psi (3.0 MPa) in the chimney and to less than 1,500 psi in the nuclear fractured region of the upper chimney. The inward pressure gradient caused the concentration in the gas phase (Figure 30X) to contract slightly in the upper chimney. Much of the tritium that diffuses outward as tritiated water vapor, partitions into the low mobility aqueous phase in the formation surrounding the detonation zone. The liquid and vapor have the same mole fraction of tritiated water, but the liquid contains far more molecules and therefore most of the tritium. This tritium is difficult to remove by gas extraction only and in an environment where the liquid is much less mobile than the gas, it acts as a persistent source in the same way that the tritiated liquid water in the detonation zone is a persistent source.

Figure 31 shows the simulated conditions at the beginning of testing on well AR-2, which reentered the lower chimney. Pressures in the upper chimney have recovered to about 1,600 psi as the pressure drop extended into the sandstones adjacent to the upper detonation zone and into the middle detonation zone.

Figure 32 shows the simulated conditions at the end of production testing on AR-2. Pressures in the lower chimney dropped below 1,200 psi. The concentration distribution in the lower chimney was not noticeably altered by the limited production testing on AR-2.

Figure 33 shows the simulated conditions 1,000 days after the detonation or 422 days after production testing ended. Pressures in both the upper and lower chimneys and nuclear fractured regions are still below 2,000 psi.

Figure 34 shows the simulated conditions 42 years after the detonations (2015). The extent of the contamination has continued to spread and is controlled by the extent of the nuclear fractures. The spread away from the upper chimney, with a more extensive simulated nuclear fracture region, is more than that from the lower and middle detonations. The different water saturation applied to each chimney does not appear to significantly influence contaminant migration. Pressures in the detonation zones have essentially recovered to those of the formation prior to the production testing. The key finding from the initial set of simulations is that even with an elongated nuclear fracture region and a constant heat source, contamination remains relatively near the detonation zone. Another observation is that, unlike at the Rulison test, temperatures remain high throughout each chimney during the testing and only slightly spread over time (Figures 35 and 36). Temperatures at Rulison were affected by a more extensive production testing period.

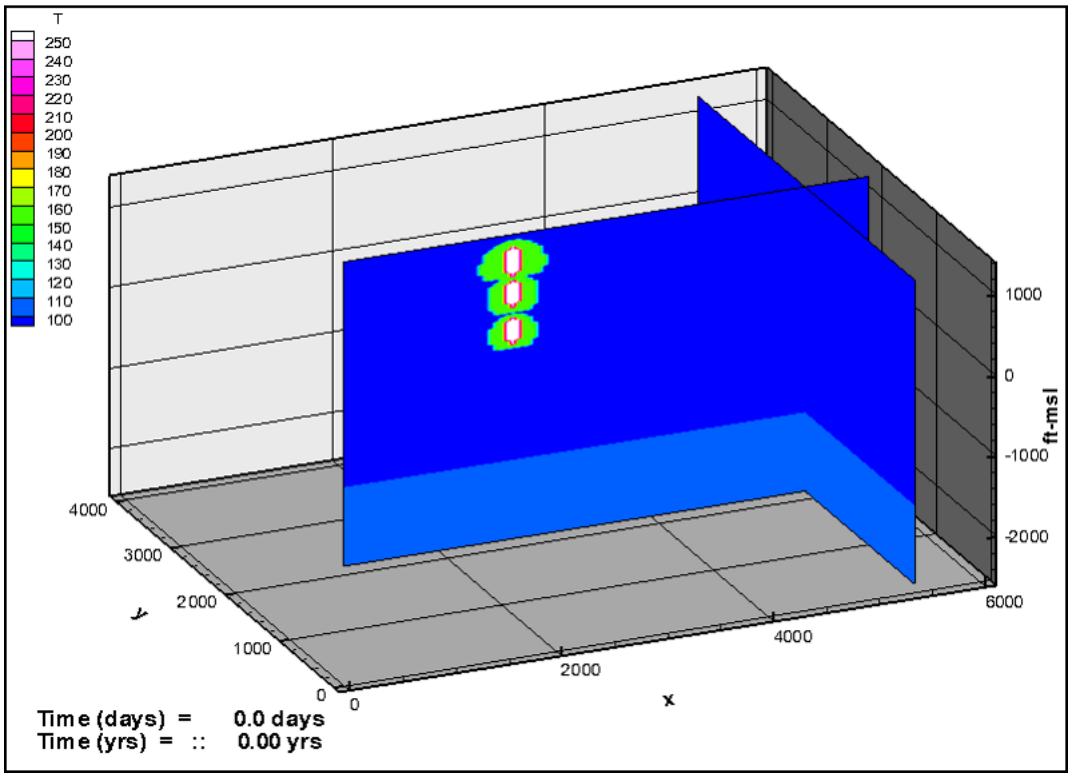

Figure 35. Initial Temperature Distribution

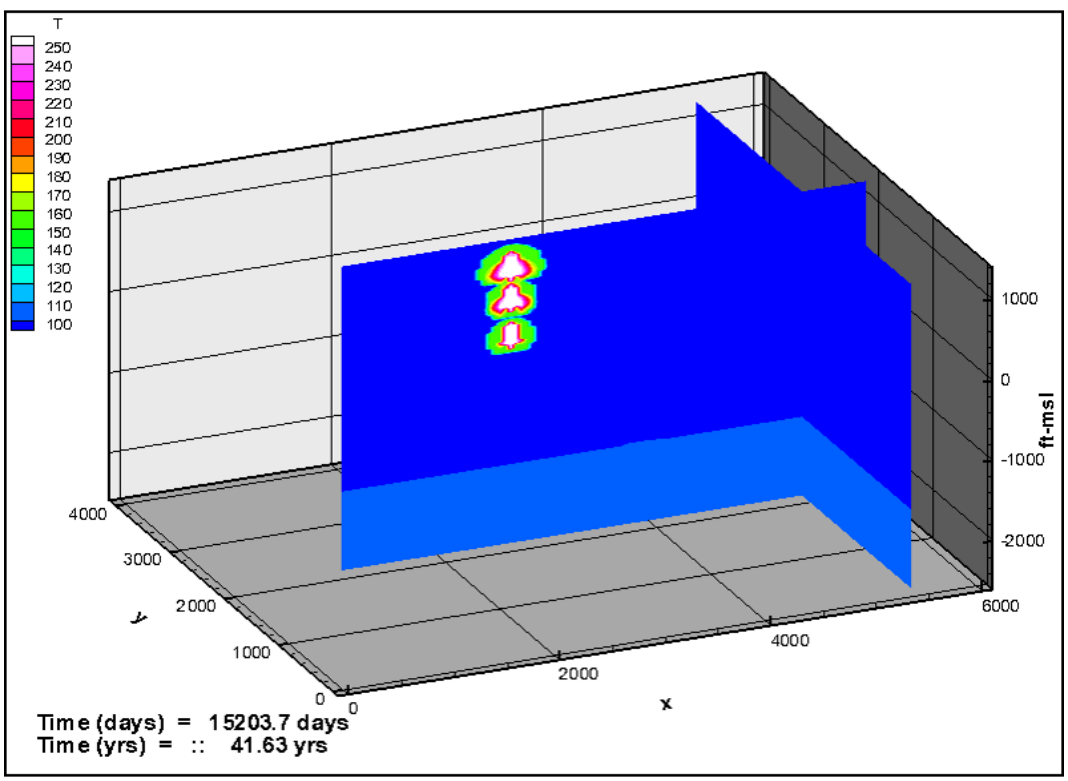

Figure 36. Temperature Distribution in 2015

5.2 Consideration of Recompleting Well RB-U4

Well RB-U4 was recently considered for recompletion as a monitoring well to confirm the presence or absence of radionuclides near the detonation zone. This well would provide a safe entry to within 600 ft of the detonations without having to drill through formation that would create handling issues for drill cuttings considering the proximity to the detonations. Unfortunately, a section of casing was removed in preparation for using the well for reentry into the middle chimney, which never occurred, making reentry and recompletion of the well risky from a drilling perspective. Figure 387 shows simulated concentrations at well RB-U4 in 2015. The "as is" diagram for RB-U4 (Figure 378) shows that it is cased from several thousand feet above the upper detonation (5,840 ft) to below the lower detonation (6,690 ft).

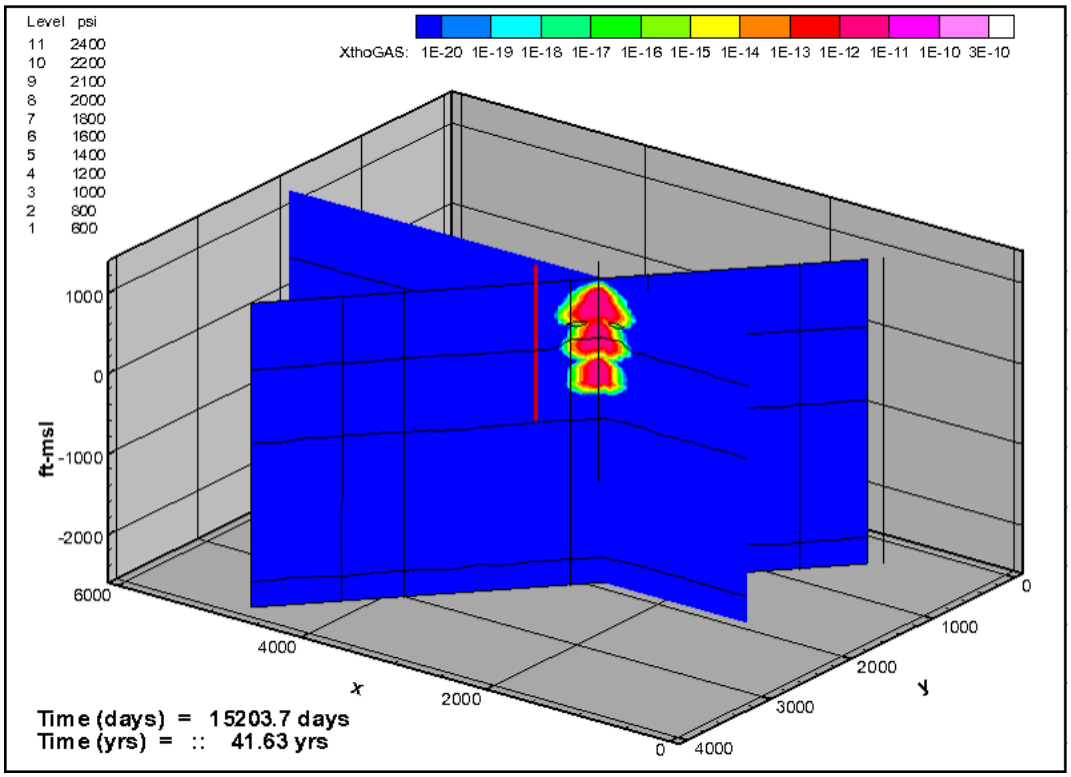

Figure 37. Simulated Concentration Distribution Relative to Well RB-U4 in 2015

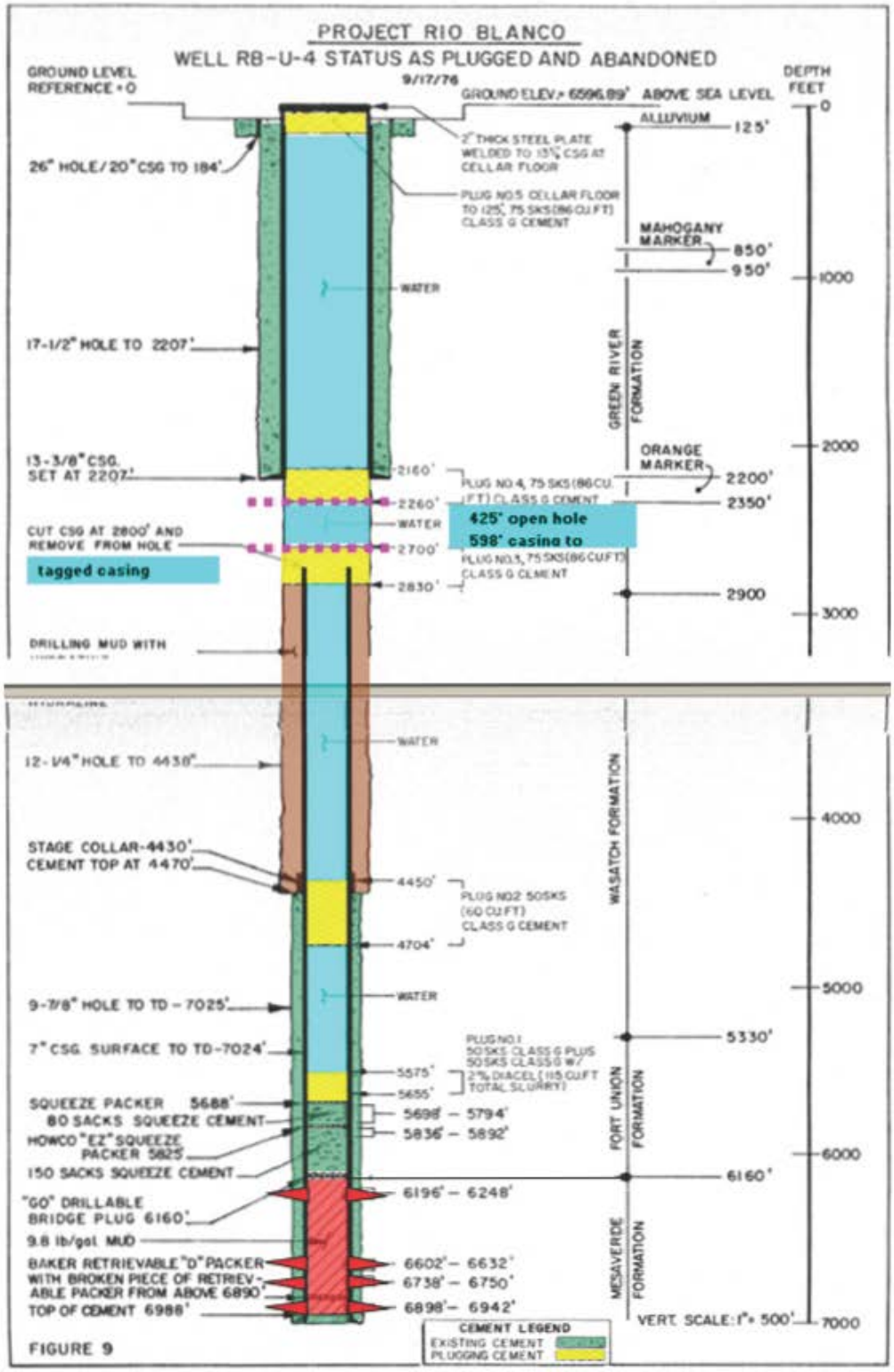

Source: ERDA 1975

Figure 38. "As Is" Diagram of Well RB-U4

5.3 Simulation of Future Drilling near Rio Blanco

The Rulison Path Forward document (DOE 2010) recommends that wells encroaching on the site be drilled in a conservative, staged approach to minimize the risk of encountering contamination. Drill a set of wells, monitor, drill the next set closer, and so forth. This approach was used for modeling the future drilling near Rio Blanco by simulating one potential well installation timeline (Table 9) to evaluate potential effects on the contamination and institutional control boundary. It was also decided to position the Rio Blanco simulated wells on a 10-acre spacing, as at Rulison, even though current practice is for 40-acre spacing in this area. This accounts for the possibility of closer positioned wells in the future while adopting a more conservative approach that increases the pressure decline in the producing formation. The simulation continues from the 2015 condition simulation (Section 5.1) and begins with the installation of eight production wells within a half-mile east of SGZ. The second set of eight wells are within the surface footprint of the institutional control boundary and less than a quarter mile from SGZ. One of the third and final set of wells is within about 500 ft of SGZ, and one of the wells is almost coincident (in the *x* and *y* location but not vertically) with well FCG #1, the tritium disposal injection well. Note that many wells (as many as 20 would not be unusual for 10-acre spacing) are drilled directionally from a single drill pad.

Figure 39 through Figure 43 (designated X for color flood of mass fraction THO gas with pressure contours, P for color flood of pressure with mass fraction contours) are vertical sections through the model (locations on Figure 10). The figures show multiple sections to highlight effects that cannot be seen on a single plane. All views are looking NNE except as noted in captions.

Table 9. Milestones in the Rio Blanco Simulation

Date	Years Since Gas Production	Process	Figure
2015	0	1st set of wells (wells1) begin production	34
2016	1	1 year into wells1 production	39
2020	5	2nd set of wells (wells2) begin production	40
2035	20	3rd set of wells (wells3) begin production Wells1 off production	41
2040	25	Wells2 off production	42, 44
2055	40	Wells3 off production	43, 45

Figure 44 shows the pressure distribution in 2035 (contours for mass fraction THO gas phase) with well RB-U4. Figure 45 shows the pressure distribution in 2055 with well FCG #1 (the thicker part of the well is the injection interval). Note that native pressures near RB-U4 and FCG #1 are unaffected by the reduced pressures in the underlying producing interval.

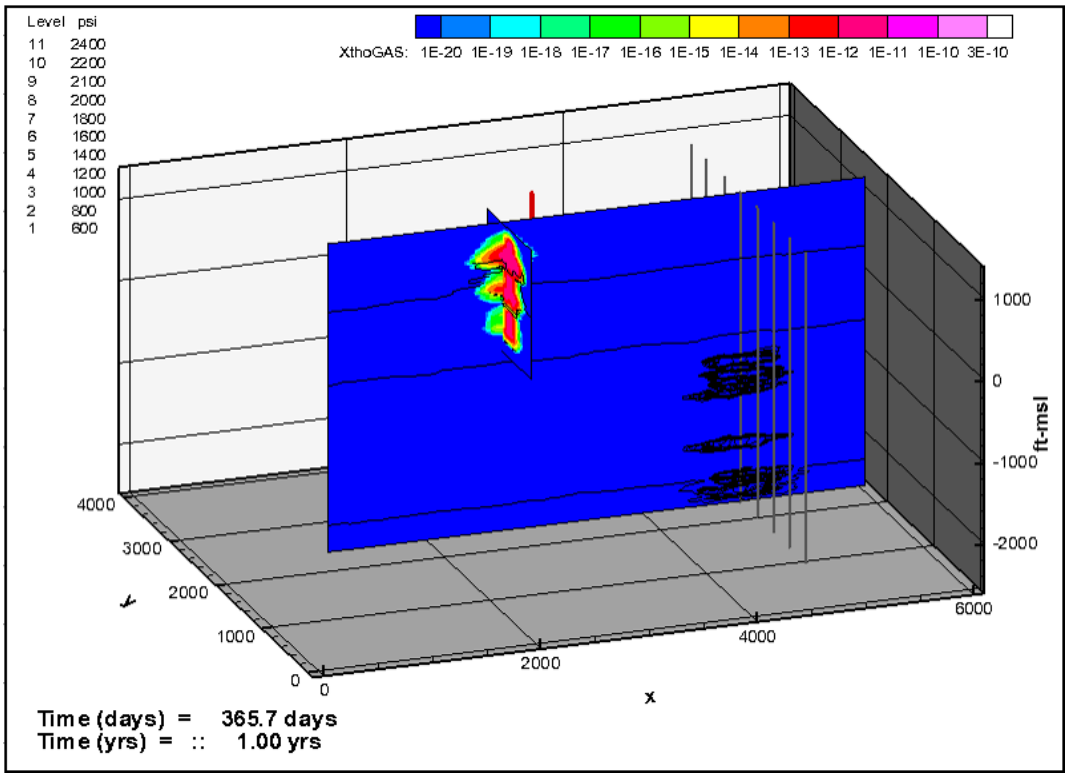

Figure 39X. Mass Fraction of THO in 2016 (y45)

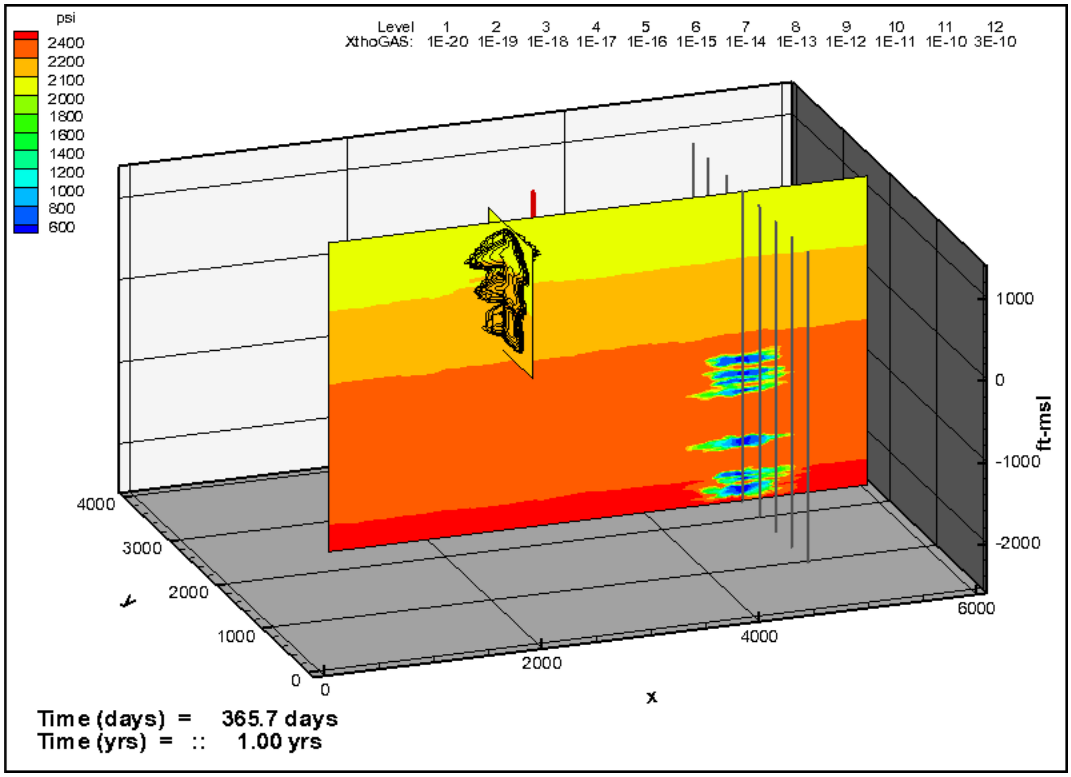

Figure 39P. Pressure Distribution in 2016

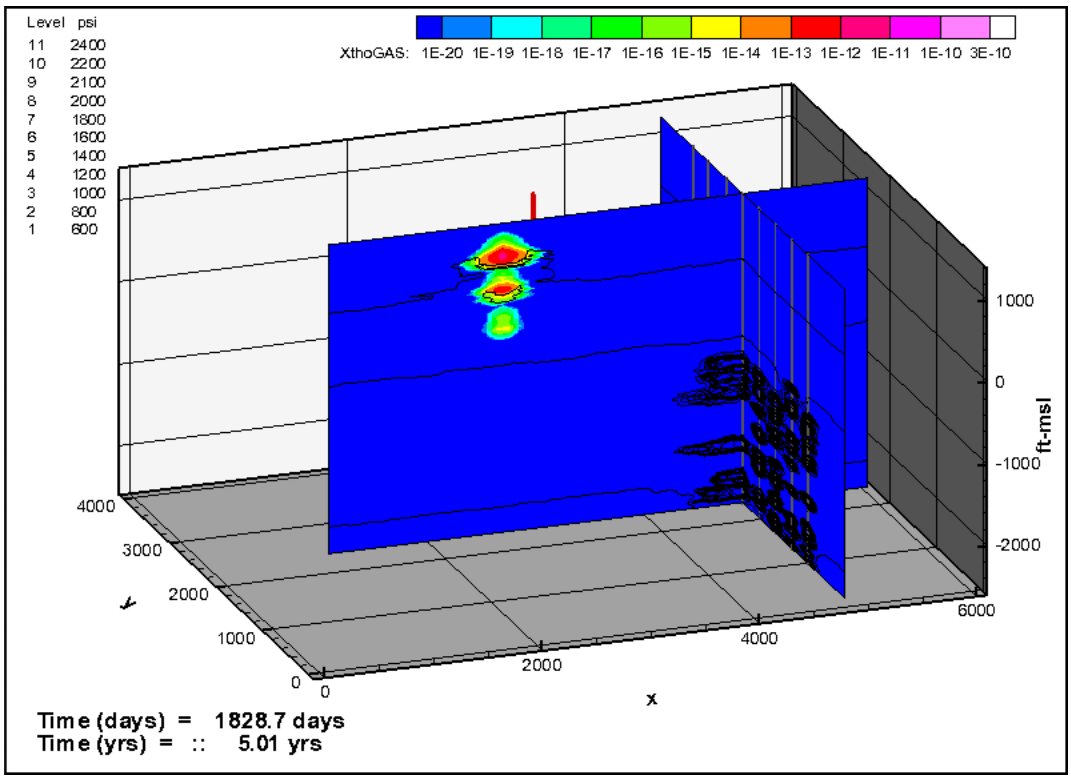

Figure 40X. Mass Fraction of THO in 2020 (y45, x97)

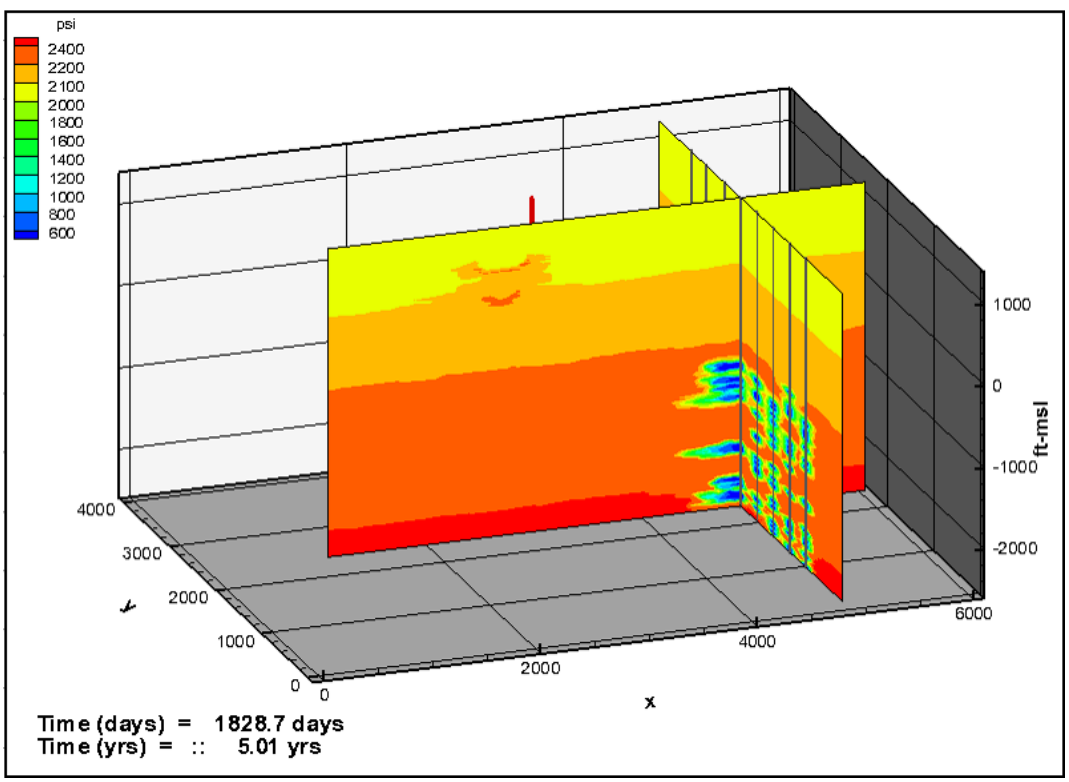

Figure 40P. Pressure Distribution in 2020

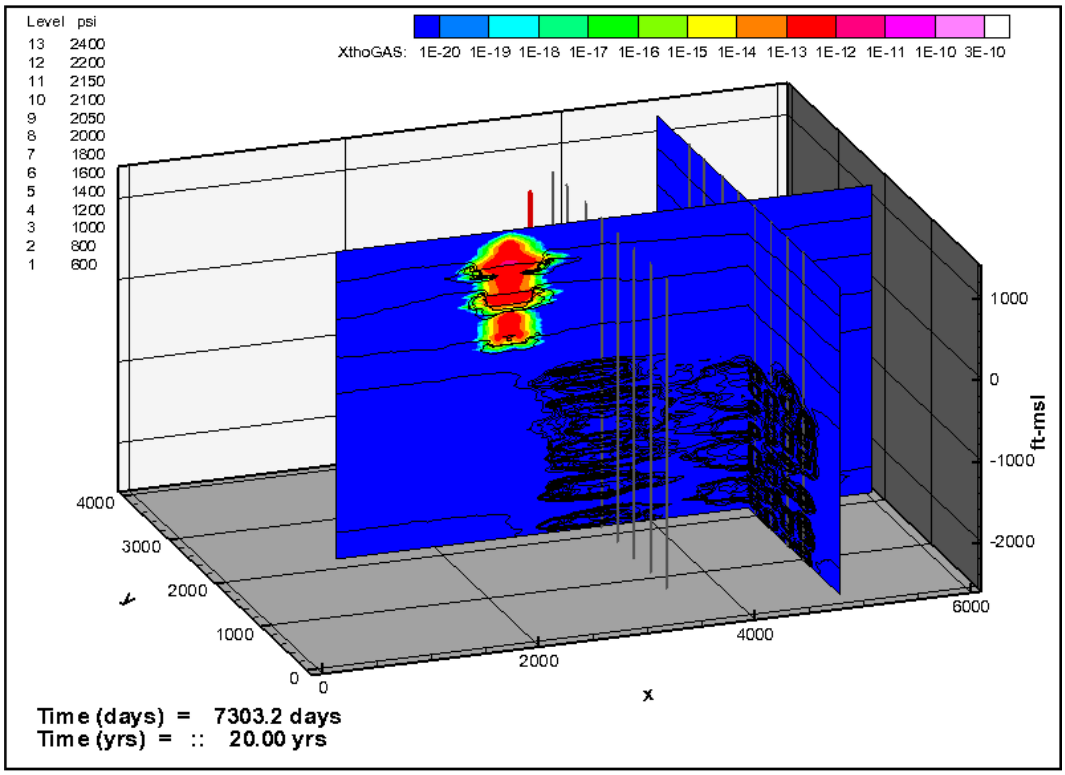

Figure 41X. Mass Fraction of THO in 2035 (y41, x97)

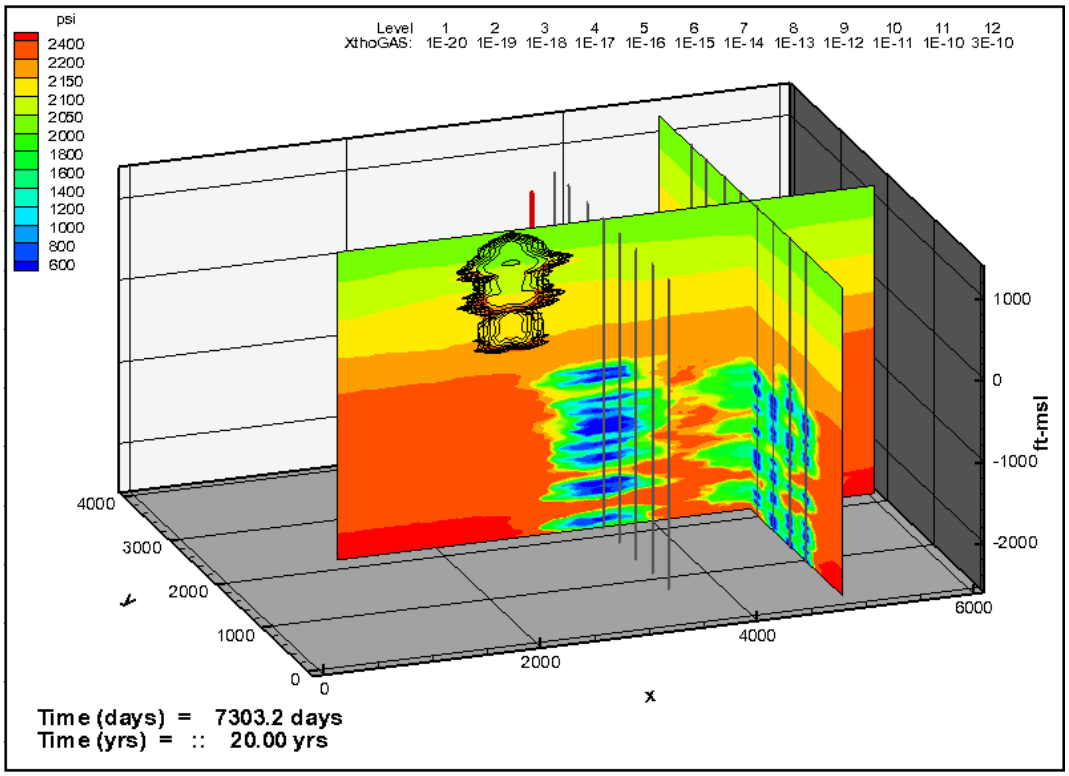

Figure 41P. Pressure Distribution in 2035

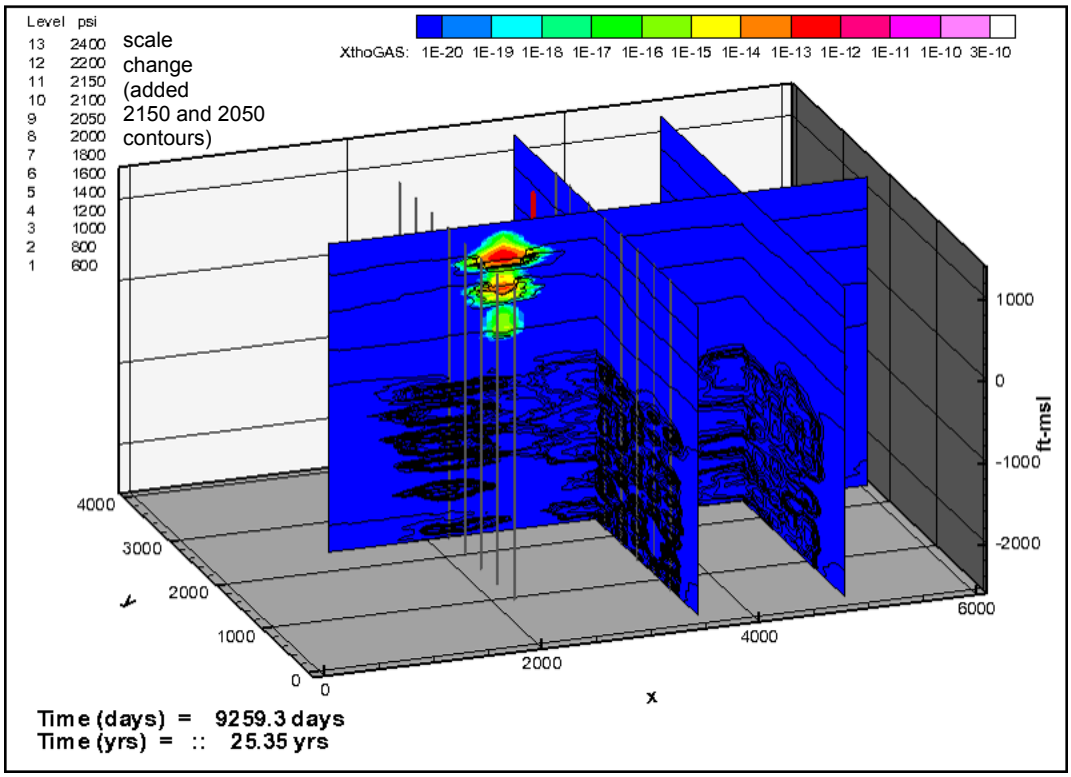

Figure 42X. Mass Fraction of THO in 2040 (y45, x70, x97)

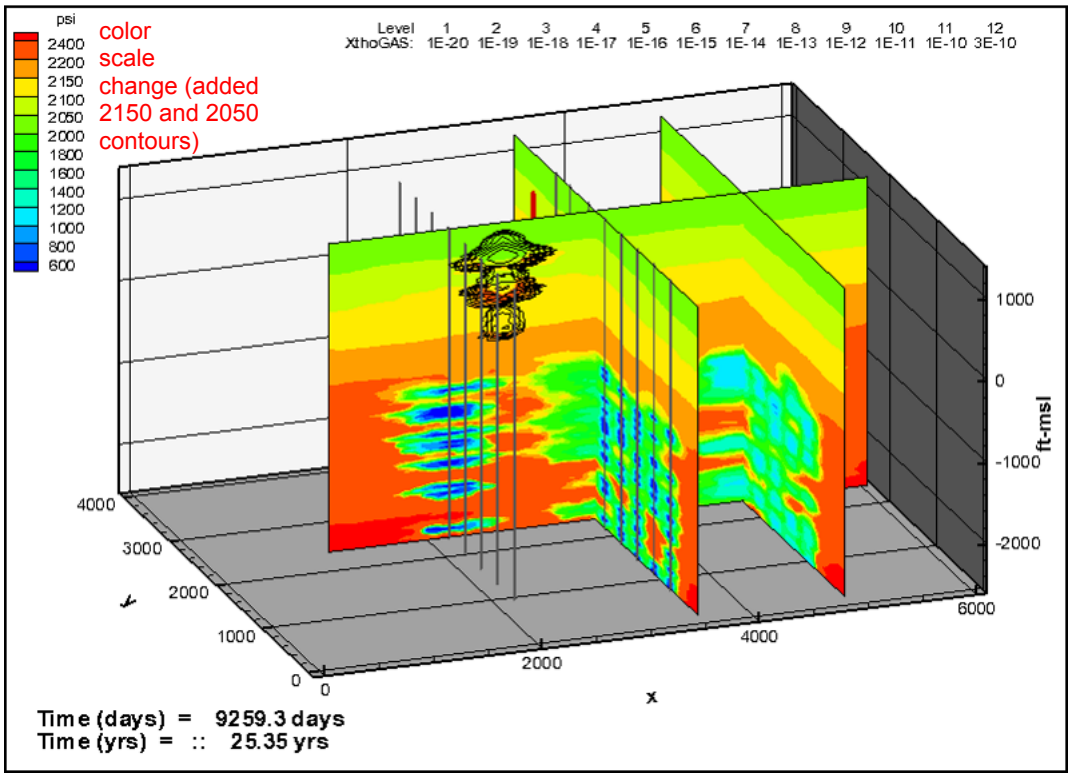

Figure 42P. Pressure Distribution in 2040

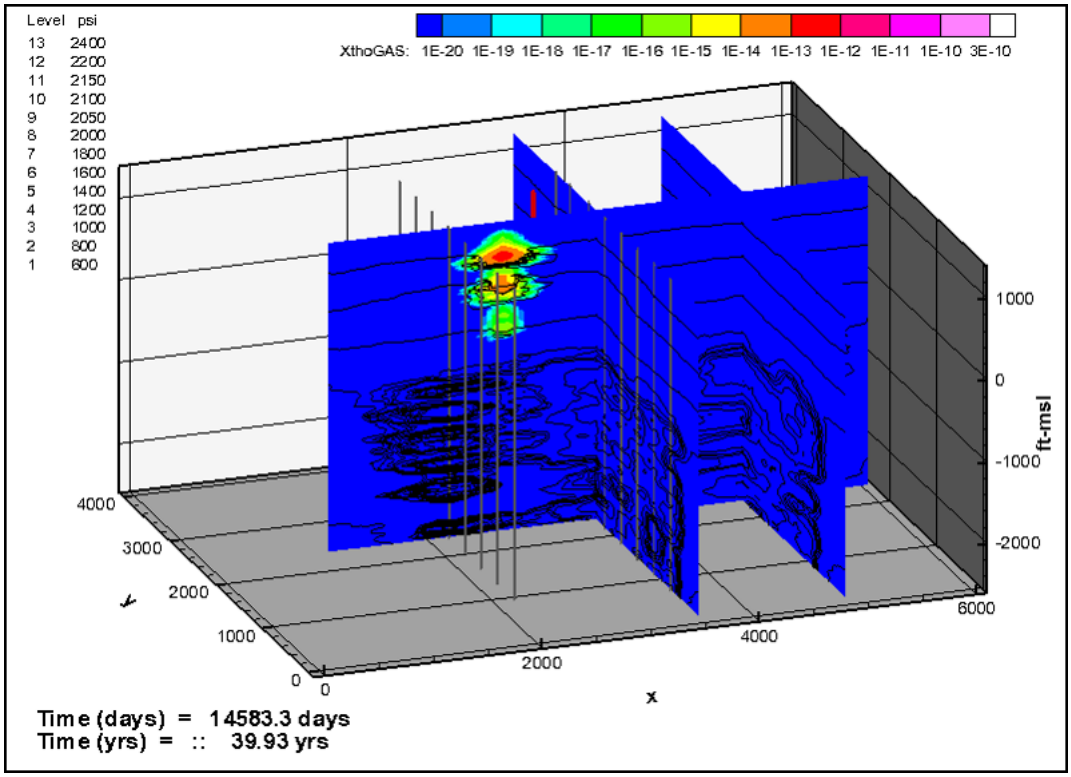

Figure 43X. Mass Fraction of THO in 2055 (y45, x70, x97)

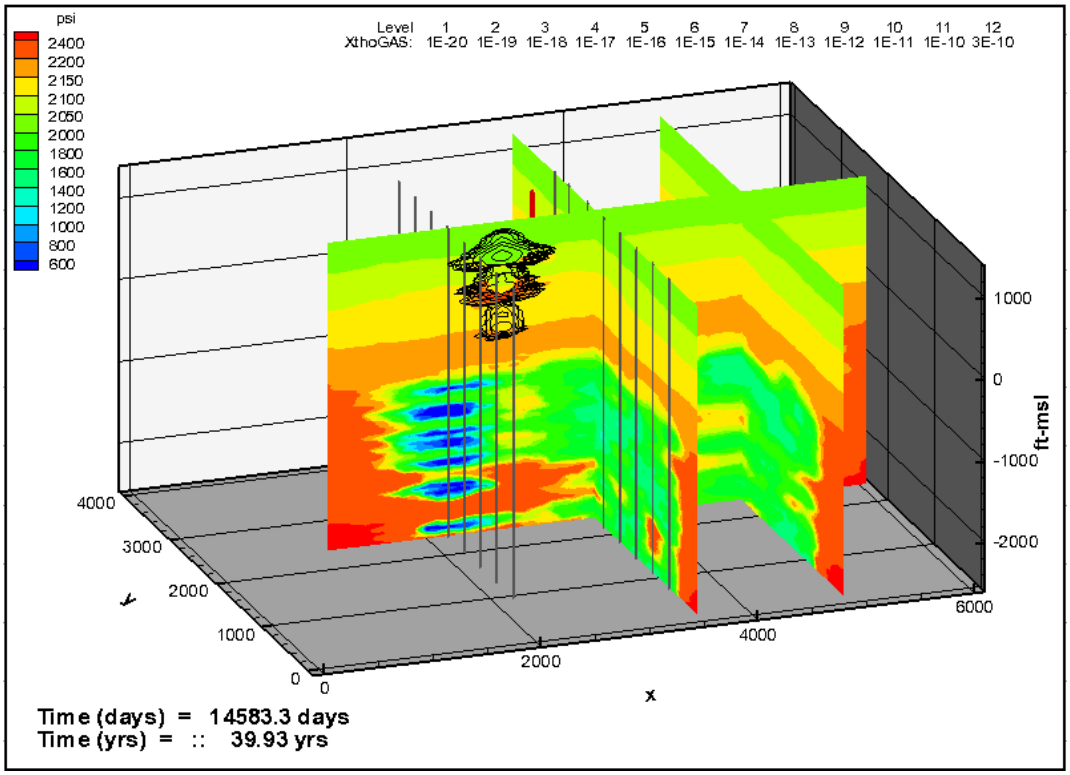

Figure 43P. Pressure Distribution in 2055

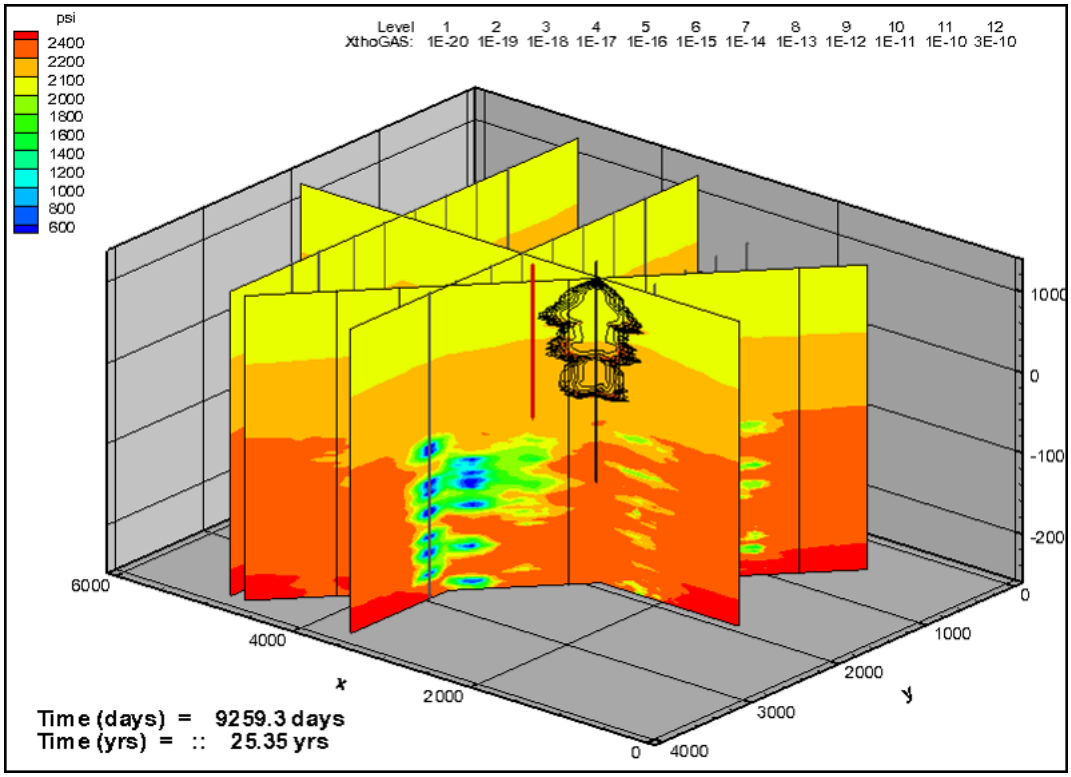

Figure 44. Pressure Distribution in 2040 with Well RB-U4 (looking SE)

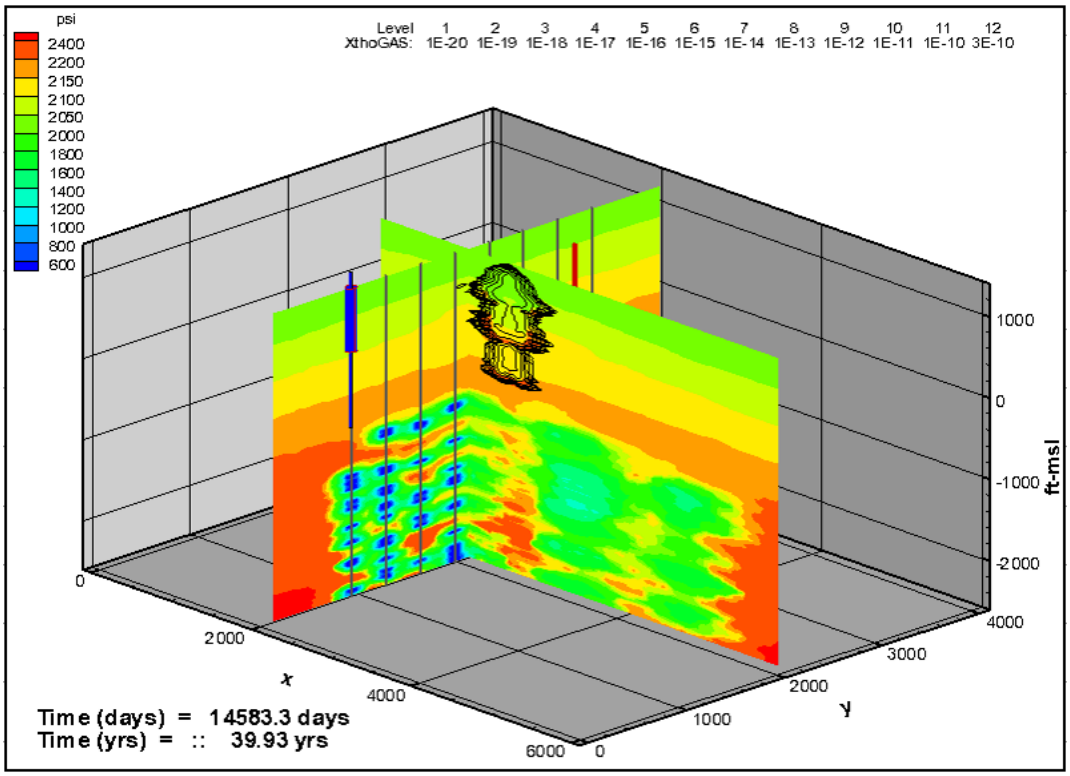

Figure 45. Pressure Distribution in 2055 With Well FCG #1 (looking NW)

The Figure 39 montage shows the concentration of tritium as mass fraction of THO in the gas phase and the pressure distribution 1 year after production in the first set of simulated gas wells (2016). The concentration distribution is not noticeably different from the distribution of 1 year earlier (Figure 34X), as would be expected in that the producing wells are 2,200 ft from the detonation zone and in a deeper section. The y45 panel is about 200 ft north of the center of the detonation zone. The effects of production on the pressure distribution around the wells are as expected. The effects of only one well (multiple hydrofracture intervals) can be seen.

Figure 40 shows the simulated conditions 5 years into production of the first set of wells (2020), just before the second set of wells, located 900 ft east of the site (wells2), begin production. An additional panel (x97) is shown to provide a perpendicular view through the model to allow the effects of more than one well to be seen. It shows that the simulated extent of the pressure effects are primarily east-west and limited north-south, as is observed in actual wells. The concentration distribution is little changed since 2015, though in order to see the full effects of the wells, the panel shown is y45 (200 ft north of y41, which goes through the center of the detonation). Wells east and west of each other are typically offset to limit inter-well communication in the direction of the natural fracture trend. This plot clearly shows the larger volume that was adopted for the upper detonation zone.

Figure 41 shows the simulated conditions in 2035, 20 years after production of the initial wells began (and now ends) and 15 years into production of the second set of wells. The theoretical wells 500 ft west of the site begin production at this time (no results yet). The highest concentration in the chimney has decreased nearly a second order of magnitude since the detonation.

Figure 42 shows the simulated conditions in 2040, 5 years after wells1 went off production, 20 years into production of wells2 (and now ends), and 5 years into production of wells3. Three slices are shown (y45 [not in line with wells2 or the detonation by 200 ft], x70, and x97) to see the effects of multiple wells on the pressure distribution. At this point, all simulated wells in the domain have been on production for at least 5 years. Two additional contours were added to the pressure plots to better see any small pressure gradient that may develop between the detonations and the producing interval.

Figure 43 shows the simulated conditions in 2055 (end of the simulation), 20 years after production from wells1 ended, 15 years after production from wells2 ended, and 20 years after production from wells3 began (and now ends). Three panels are shown (y45, x70, and x97) to see the effects of multiple wells on the pressure distribution (wells 1, wells3, and the detonation are out of the plane). The highest concentration in the chimney continues to decline, and low concentration continues to spread laterally. It is important to note that no obvious connection exists between the pressure drawdown in the producing interval and the detonation zones (Figure 43P), even with two additional contours (2,150 and 2,050 psi) being added to highlight this effect.

A plot of the temperature distribution (Figure 44) at the end of the simulation (2055) shows that the temperature within the detonation zones has changed somewhat since the gas well simulations began (Figure 36). The constant temperature source of the melt glass prevented a more significant decrease in temperature. The slight temperature decrease at production wells, in

response to the lower pressures during production, show up as dark blue at the produced hydrofracture zones.

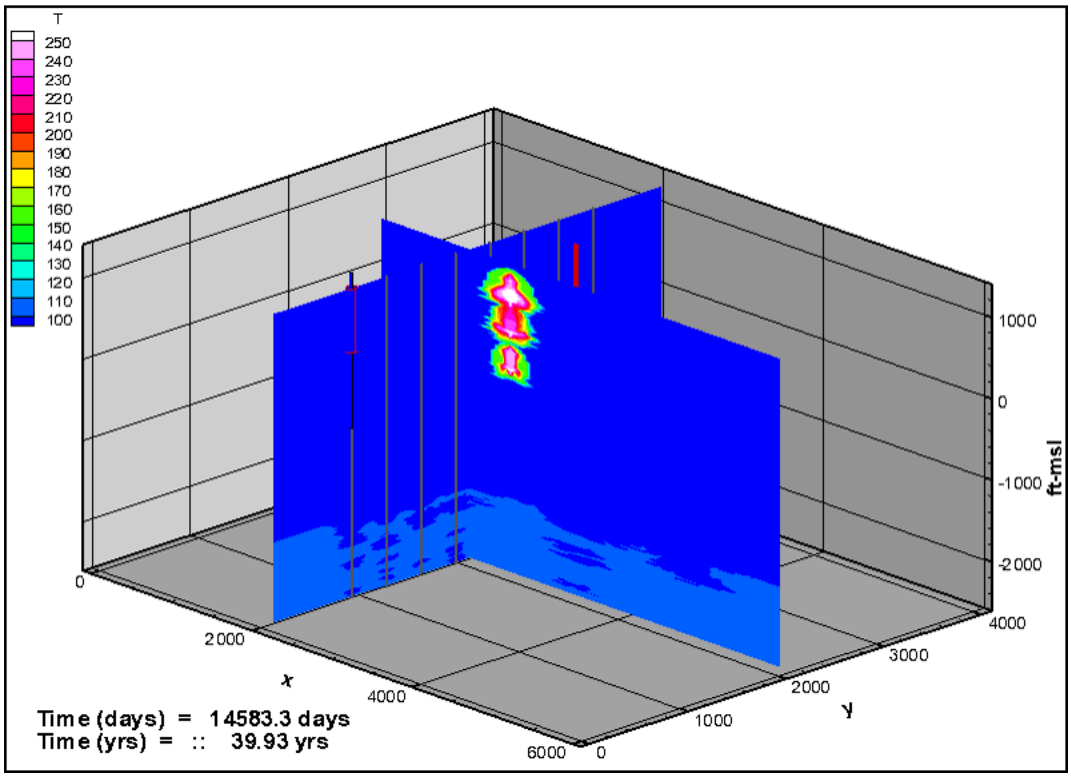

Figure 46. Simulated Temperature Distribution in 2055

6.0 Summary and Conclusions

The primary objectives of this study were to simulate the current extent of contamination near the Project Rio Blanco detonations and to determine how closely gas development wells could be drilled without encountering contamination. The model simulated the production from theoretical future wells installed in a staged approach (beginning in 2015) based on the Rulison Path Forward document (DOE 2010). The model was calibrated to the historical production and pressure data from the reentry well into the upper chimney. Attempts were made to be conservative by elongating the detonation zone (both the chimney and surrounding nuclear fractured region) in the direction of the natural fracture trend in the area.

This study confirmed the results of the previous Rio Blanco (Cooper et al. 2005) modeling in that it predicts that contamination, in the form of tritiated water, does not migrate far from the detonation zone. These results are based on a conceptual model that assumes the fractured formation can be simulated using an equivalent porous media approach. The frequency, connectivity, and limited permeability extent of individual fractures perform as a pore matrix within a representative elementary volume the size of the individual model elements. The finding that THO did not migrate from the detonation zone was fully expected, considering the retarding effects of THO vapor coming into contact with liquid water. The simulated results also indicate that it is unlikely that production from gas wells in the underlying lower Williams Fork

Formation will reduce pressure in the producing interval enough to create a pressure gradient with the detonation zone, even for wells beneath the detonation within the institutional control boundary. The lack of an induced pressure gradient suggests that simulations of even more conservative but less prevalent contaminants such as tritiated methane, ^{85}Kr, and ^{14}C (as part of the CO_2 molecule) that were not removed by production testing would not migrate to wells in the underlying producing interval.

The figures in this text and animations on the accompanying DVD provide simulation results that simplify the concept of the three simultaneous detonations at Rio Blanco and their relationship to gas production in the Piceance Basin.

7.0 References

Many of the documents are available on the LM website:
http://www.lm.doe.gov/Rio_Blanco/Documents.aspx

AEC (U.S. Atomic Energy Commission), 1973. *Project Rulison: Managers Report*, NVO-71, PNE-R-63, Nevada Operations Office, Las Vegas, Nevada.

AEC (U.S. Atomic Energy Commission and Continental Oil), 1974. *Project Rio Blanco Data Report: Production Testing (RB-E-01) November 1973 and January-February 1974,* NVO-148, Industrial Applications Division, Nevada Operations Office, Las Vegas, Nevada.

Bowen, S.M., D.L. Finnegan, J.L. Thompson, C.M. Miller, P.L. Baca, L.F. Olivas, C.G. Geoffrion, D.K. Smith, W. Goishi, B.K. Esser, J.W. Meadows, N. Namboodiri, and J.F. Wild, 2001. *Nevada Test Site Radionuclide Inventory, 1951–1992*, LA-13859-MS, Los Alamos National Laboratory, Los Alamos, New Mexico, September.

Byrnes, A.P., and R.M. Cluff, 2009. *Analysis of Critical Permeability, Capillary Pressure and Electrical Properties for Mesaverde Tight Gas Sandstones from Western U.S. Basins*, U.S. DOE Contract Number DE-PS26-04NT42072.

CER (CER Geonuclear), 1975. *Project Rio Blanco Radioactivity and the Environment: RB-AR-2 Addendum*, PNE-RB-63 Addendum, October 1975.

Colorado Department of Health, Water Quality Control Division, *Permit for Subsurface Disposal*, November 9, 1973, with Amendments 1 and 2 dated November 8, 1974, and December 6, 1974.

Cooper, C.A., M. Ye, J. Chapman, and C. Shirley 2005. *Radionuclide Migration the Rio Blanco Site, a Nuclear-Stimulated Low-Permeability Natural Gas Reservoir*, Desert Research Institute Report No. 45215.

Cooper, C.A., M. Ye, and J. Chapman, 2007. *Tritium Transport at the Rulison Site, a Nuclear-Stimulated Low-Permeability Natural Gas Reservoir*, Desert Research Institute Report No. 45224.

Cooper, C.A., M. Ye, J. Chapman, and R. Hodges, 2009. *Addendum: Tritium Transport at the Rulison Site, a Nuclear-stimulated Low-permeability Natural Gas Reservoir*, Desert Research Institute.

Cooper, C.A., J. Chapman, and R. Hodges, 2010. *Update of Tritium Transport Calculations for the Rulison Site: Report of Activities and Results During 2009–2010*, Desert Research Institute Letter Report.

Corey, A.T., 1954. "The Interrelation Between Gas and Oil Relative Permeabilities," NNA.19900720.0036, *Producers Monthly*, 38–41, November.

DOE (U.S. Department of Energy), 2010. *Final Rulison Path Forward*, LMS/RUL/SO4617, Office of Legacy Management, Grand Junction, Colorado, June.

ERDA (U.S. Energy Research and Development Administration), 1975. *Project Rio Blanco Formation Evaluation Well (RB-U-4) Drilling, Completion and Initial Testing Report*, NVO-168.

Frick, R.O., and J.A. Wethington, Jr., 1971. "Tritium Exchange Between Hydrocarbons and Steam," *Transactions of the American Nuclear Society*, 12(2): 467–468, October.

Green, G.N., 1996. *The Digital Geologic Map of Colorado in ARC/INFO Format,* USGS Open File Report 92-0507, U.S. Geological Survey.

Lucas, L.L., and M.P. Unterweger, 2000. "Comprehensive Review and Critical Evaluation of the Half-Life of Tritium," *Journal of Research of the National Institute of Standards and Technology*, 105(4), July-August.

Mualem, Y., 1976. "A New Model for Predicting the Hydraulic Conductivity of Unsaturated Porous Media", *Water Resour. Res.*, 12(3): 513–522.

Narasimhan, T.N., P.A. Witherspoon, and A.L. Edwards, 1978. "Numerical Model for Saturated-Unsaturated Flow in Deformable Porous media, Part 2: The Algorithm," *Water Resour. Res.*, 14(2): 255–261.

Pruess, K., C. Oldenburg, and G. Moridis, 1999. *TOUGH2 User's Guide, Version 2.0*, LBNL-43134.

Smiles, D.E., W.R. Gardner, and R.K. Shulz, 1995. "Diffusion of Tritium in Arid Disposal Sites," *Water Resour. Res.*, 31(6): 1483–1488.

Sokol, D., 1970. *Ground Water Safety Evaluation—Project Gasbuggy*, PNE-1009, prepared by Teledyne Isotopes, Palo Alto, California, for the U.S. Atomic Energy Commission, Nevada Operations Office, Las Vegas, Nevada, September.

Toman, J., 1974. *Project Rio Blanco: Project Scientist's Summary Report of Production Test Data and Preliminary Analysis of Top Chimney/Cavity*, UCRL-76280, Lawrence Livermore Laboratory, Livermore, California.

Van Genuchten, M.Th., 1980. “A Closed-Form Equation for Predicting the Hydraulic Conductivity of Unsaturated Soils,” NNA.19911009.0008, *Soil Sci. Soc.*, 44: 892–898.

Yurewicz, D.A., K.M. Bohacs, J.D. Yeakel, and K. Kronmueller, 2003. “Source Rock Analysis and Hydrocarbon Generation, Mesaverde Group and Mancos Shale, Northern Piceance Basin, Colorado,” in Peterson, K.M., T.M. Olson, and D.S. Anderson, eds., *Piceance Basin 2003 Guidebook: Rocky Mountain Association of Geologists*, pp 130–153.

Zhang, K., Y.S. Wu, and K. Pruess, 2008. *User's Guide for TOUGH2-MP—A Massively Parallel Version of the TOUGH2 Code*, LBNL-315E.

Appendix A

Summary Reports on Projects Rio Blanco and Rulison from 2001 Through 2010

This page intentionally left blank

The U.S. Department of Energy (DOE) and its predecessor agencies conducted a program in the 1960s and 1970s that evaluated technology for the nuclear stimulation of low-permeability natural gas reservoirs. The objective of the program was to produce natural gas from formations not conducive to production by convention means such as hydraulic fracturing. As a result, all of the tests were conducted in low-permeability formations contained within oil and gas reservoirs. These conditions precluded contact of the test radionuclides with mobile, potable water, and hence the risk of human exposure was considered very low to non-existent. At the conclusion of each project in the late 1960s and early 1970s, surface facilities were removed, wells were plugged and abandoned, and drilling restrictions were instituted for the subsurface region immediately around the nuclear cavities.

In the 1990s, DOE began a thorough environmental restoration program to remediate and close facilities that supported nuclear testing. The three gas-stimulation test sites are included in the program now under the direction of the Office of Legacy Management. Although the land surfaces at the sites had previously been cleaned and closed, additional testing and analysis is being conducted to assure that the closures meet current environmental standards. Similarly, the disposition of the subsurface regions impacted by the tests is being re-evaluated. Of particular concern for the subsurface is an assessment of the drilling intrusion restrictions in place to determine if they are sufficiently protective of human health and the environment. This concern arises from a lack of documentation on the rationale used to establish the restricted regions. Standard oil and gas reservoir evaluations are poorly suited to analyze the problem as they focus on flow of fluids in the subsurface, whereas the question here is one of transport of contaminants. Significant advances in understanding contaminant transport in the subsurface have been made in the decades since the drilling restrictions were initially established.

Projects Rulison and Rio Blanco were located in west-central Colorado. At Rulison, a 40-kiloton nuclear device was detonated 2,568 m below the land surface in the Williams Fork Formation on September 10, 1969. At Rio Blanco, three 33-kiloton nuclear explosives were simultaneously detonated in a single emplacement well in the Mesaverde Group and Fort Union Formation, at depths of 1,780, 1,899, and 2,039 m below land surface on May 17, 1973. The objective of these reports was to estimate lateral distances that tritium released from the detonations may have traveled in the subsurface and evaluate the possible effect of postulated natural-gas development on radionuclide migration. Other radionuclides were considered in the analysis, but the majority occur in relatively immobile forms (such as nuclear melt glass). Of the radionuclides present in the gas phase, tritium dominates in terms of quantity of radioactivity in the long term and contribution to possible whole body exposure.

The models only replicated subsurface processes and did not account for additional factors such as mixing and dilution in a hypothetical gas production well, nor did they account for exposure scenarios (e.g., transmission and dilution in a pipeline, inhalation routes from gas use) required to assess either exposure limits or doses.

2001 Preliminary Report Pertaining to Rio Blanco, DRI Pub. 45186; also DOE/NV/13609-15

The first report in the series is an outline of an approach to developing models for both the Rio Blanco and Rulison sites, followed by a very preliminary set of simulations of gas, water, and

tritium transport following the three simultaneous 33-kiloton nuclear detonations in 1973 at the Rio Blanco site. A preliminary conceptual flow and transport model was developed that recognized that the gas 'reservoir' is actually in rock of very low matrix permeability and that the dominant permeable pathways for fluids are through a network of fractures created by regional tectonism. The gas-in-place is basin-centered, meaning that much of it is located downdip from water-saturated regions in the formation(s), there are few obvious gas-water contacts, and there are no obvious trapping mechanisms, as gas is present mostly in lenticular reservoirs from tens to hundreds of meters in length.

The intrinsic permeability of the formation was estimated prior to the test as being between 10^{-15} to nearly 8×10^{-18} m^2. This is an average value that considers flow through both the sandstone and shale, and flow through both fractures and matrix (although fractures probably dominated flow). The degree of heterogeneity was largely unknown, except that the formation contained both sand and shale lenses (i.e., the actual values of permeability of the individual units was not known). Post-test drilling indicated that there was no connectivity among the three cavities. The initial tritium radioactivity release from the three simultaneous detonations was estimated as 3,000 Ci (curies). Forty percent of the radioactivity was trapped in the melt, and thorough discussion of partitioning was given in The nuclear test description matrix and fractures were largely unknown, and the ignored, and instead gas and liquid water were assumed to flow through a network of fractures, modeled as an equivalent porous medium.

Two-dimensional flow and transport was modeled through a single formation, the Upper Cretaceous Mesaverde Group, with an intrinsic permeability of 3×10^{-17} m^2 and a porosity of 0.105. Although the upper device was detonated in the Ohio Creek Member of the Upper Cretaceous Fort Union Formation, the member status of the lower two devices was unknown. Results of the simulations are not discussed here as they were entirely superseded by the results presented in the 2005 Rio Blanco report.

2004 Letter Report Documenting Rulison Results

A letter report was submitted in 2004 describing a small study to investigate the gross behavior of tritium transport away from a chimney created by the Rulison nuclear detonation. This report set the tone for the 2007 report. A conceptual model was developed, in which the detonation occurred in the Williams Fork Formation, the chimney was modeled with the same properties as the nuclear-stimulated fractures (chimney properties were unknown), and a hydraulic fracture zone was included outward from the production well, which was located 457 m (1,500 ft) from the emplacement hole. The results showed that for a period of 35 years following the detonation, molecular diffusion controlled tritium transport (a natural horizontal or vertical gradient, if present, was unknown) traveled about 125 m from the detonation (or working) point, but never extended beyond the drilling exclusion zone. A period of gas production from the hypothetical well resulted in minimal tritium migration, which also did not reach the exclusion boundary. The results are considered obsolete, as the intrinsic permeability of the nuclear-stimulated zone of fractures (modeled as an equivalent porous medium) was overestimated by two orders of magnitude and the permeability of the hydraulic (production) fractures was overestimated by a factor of two (as compared with the 2007 report). Most importantly, the 2007 report presented the results of Monte Carlo simulations through 500 separate random permeability and porosity fields.

2005 Report on Rio Blanco, DRI Pub. No. 45215; also DOE/NV/13609-45

The geologic model was improved over the 2001 letter report such that it included the Mesaverde Group and overlying Fort Union Formation. The upper device was detonated in the lower part of the Fort Union Formation, while the middle and lower devices were detonated in the Mesaverde Group (now Formation). Both formations are low-permeability shales (permeability ~10^{-17} square meters [m^2]), with lenses of slightly higher permeability sandstone spread throughout. The length of some of these lenses is as great as 1,000 m. The formations are hydrostatically pressured; horizontally, the pressure gradient(s) were not well known, as production tests were not run to completion due to the length of time required to reach quasi-steady state.

The geologic model was incorporated into a conceptual flow and transport model that included transport of radionuclides (tritiated water and krypton gas) in a two-phase (gas and liquid) system. The conceptual flow and transport model was developed into the numerical model. Radionuclides released from the cavity were transported in both liquid and gas phases, and were allowed to partition between phases in accordance with Henry's law. Two types of simulations were conducted: one that investigated flow away from the three nuclear cavities in a regional pressure field, and the other that investigated flow from only the middle cavity/chimney toward a producing gas well. The permeability and porosity, however, were that of the Fort Union Formation (the formation in which the upper detonation occurred) as its permeability is higher, and this would be a more 'conservative' simulation (i.e., transport would be exaggerated). The reason that flow was only investigated from the middle chimney is that symmetry was assumed in the model, as the upper and lower horizontal boundaries between the detonations were assumed to streamlines and that fluid flow and tritium transport would be identical in the other two chimneys, as the upper and lower boundaries were streamlines dividing flow between the upper and middle detonations, and middle and lower detonations, respectively. In addition, a few

simulations were conducted that included discrete fractures in the vicinity of the cavities. Results showed fractures to be important when flow-controlling fractures were spaced greater than 20 m apart. For a greater fracture density, flow through fractures and flow through matrix gas resulted in nearly identical concentrations, indicating that inclusion of discrete fractures in this model may be unnecessary. The reason is that matrix diffusion of tritium in the gas phase acts to make the concentration field more uniform between fractures and matrix. There is an extensive discussion of these simulations in the report.

Two types of models were developed: Type 1, in which methane gas and liquid water with a single radionuclide mixed in both phases migrated within the natural gas reservoir in response to chemical gradients (i.e., liquid and gas diffusion), slight regional pressure gradients, and radionuclide decay. In these simulations, transport was modeled away from all three cavity/chimneys. A second type of model was run (Type 2) in which flow and transport was through a narrow interval, 120 m high, away from a single cavity/chimney toward a producing gas well located outside the current drilling exclusion boundary. Drilling is currently prohibited within 183 m (600 ft) of the emplacement well. The well was located 291 m away from the center of the cavity/chimney, such that hydraulic fractures from the production well were assumed to reach the exclusion boundary. The Type 2 simulations were also used to conduct uncertainty analysis using the Monte Carlo method to address parametric uncertainty of porosity and intrinsic permeability.

The Type 1 simulations show that for various combinations of intrinsic permeability and slight regional pressure gradient, the leading edge of the tritium mass fraction (i.e., concentration) field never extends beyond 100 m from the center of the three cavity/chimneys (Figure 1). These results, however, did not address the impact of a hypothetical nearby gas-producing well. To address this scenario, three-dimensional Type 2 simulations were required.

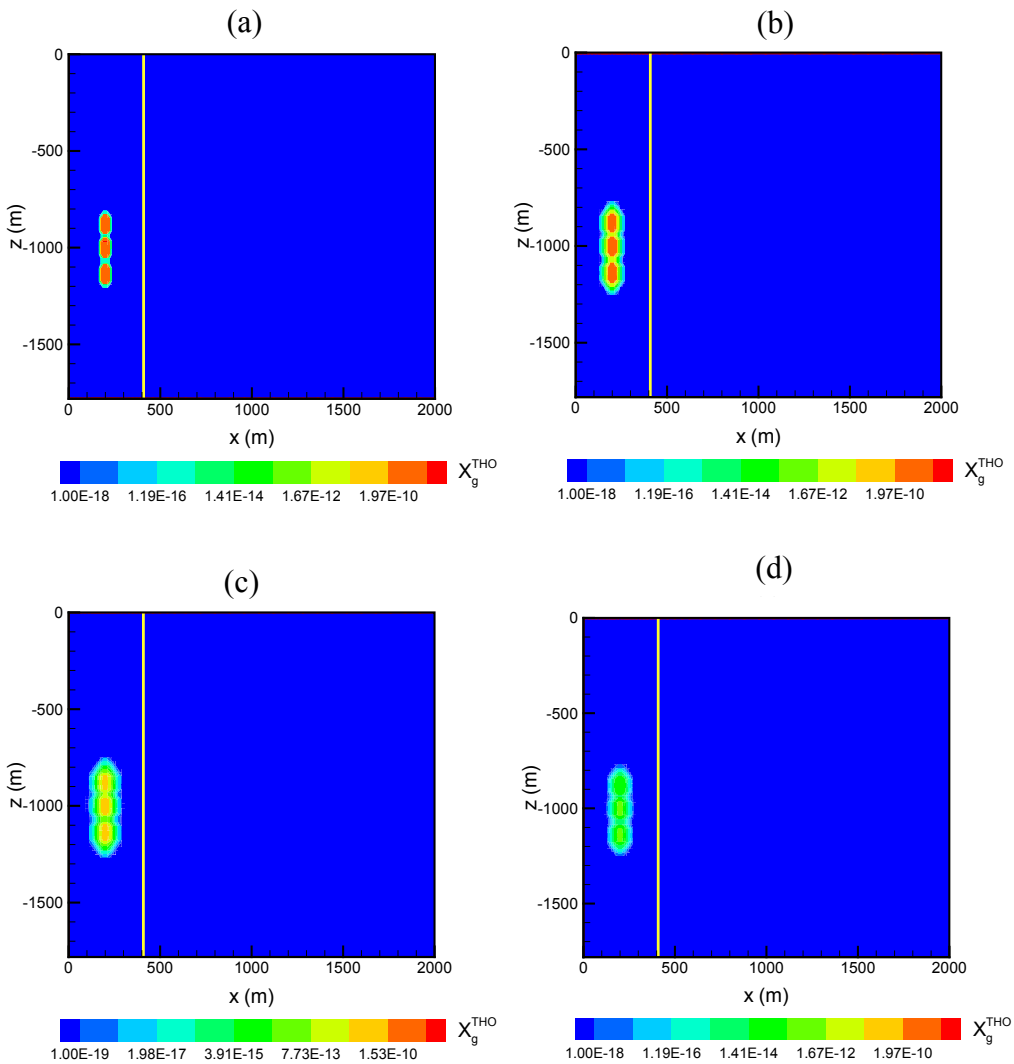

Figure 1. Results of a two-dimensional simulation showing mass fraction of tritiated water vapor, X_g^{THO}. The times are (a) 1 month, (b) 20 yr, (c) 100 yr, and (d) 250 yr. The vertical line located at x = 404 m shows the location of the drilling exclusion boundary with respect to the location of the detonations.

The three-dimensional Type 2 simulations modeled flow and transport away from a single cavity/chimney toward a production well (Figure 2). The reservoir properties were those of the Fort Union Formation, as intrinsic permeability is about an order of magnitude greater than for the Mesaverde Group. Several simulations were conducted that investigated sensitivity of permeability, production rate, initial and residual liquid saturation, and tortuosity. For example, a one order-of-magnitude increase in intrinsic permeability had little effect on the transport of tritium, as the Péclet number for gas transport (a relationship between diffusive and advective flow) was much less than one (the highest gas velocities were never greater than 10^{-8} m s^{-1}). The value of initial and residual liquid (and hence gas) saturation had an effect of diffusing tritium in the gas phase, but the distances varied only by several tens of meters or so. High gas saturation resulted in more spreading and mixing of tritium in the gas phase, and it allowed the center of the tritium "plume" to diffuse more rapidly than for cases where initial gas saturation was low. The choice of tortuosity model had the greatest effect on transport; a relative permeability based model resulted in radionuclide transport distances approximately 100 m greater than for a

saturation-dependent (Millington-Quirk) model. As little research has been conducted on tortuosity in two-phase systems in the past 45 years, a lack of understanding of tortuosity may be the greatest limitation in the models.

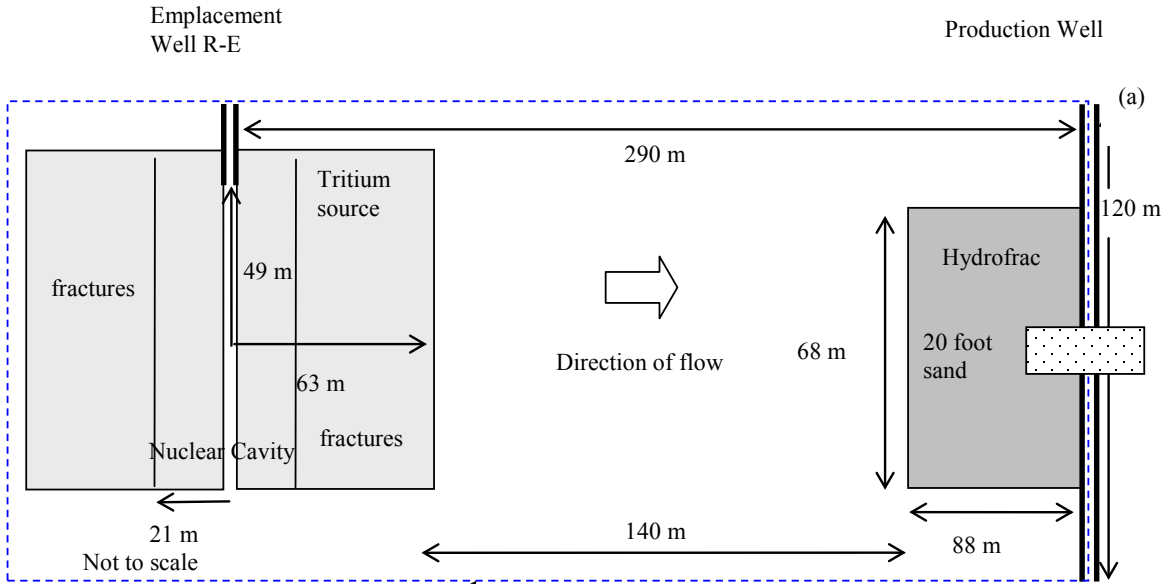

Figure 2. Model formulation for gas flow and tritium transport to a production well

Based on the Type 2 simulations with gas production, uncertainty of tritium transport in the gas reservoir was assessed using the Monte Carlo method. Permeability and porosity of the Fort Union Formation were considered as random parameters due to their heterogeneity in the site. Distributions of and the correlation between the two variables were identified based on their on-site core measurements from two boreholes, assuming that the measurements were representative. Five hundred realizations of correlated random fields of the two parameters were generated and used to construct the TOUGH2 input files. Except for these two random parameters, other model parameters remained the same as those of the Type 2 simulations with reference parameters. The stabilization of the statistics of quantities of interest obtained from the 500 realizations was examined empirically and the results suggested that 500 realizations were sufficient to yield meaningful statistics used to quantify tritium transport uncertainty. The 50th percentile represented the prediction of tritium transport in an average sense, while the 5th and 95th percentiles quantify associated predictive uncertainty caused by the uncertain values of permeability and porosity due to their heterogeneity at the site. The 5th and 95th percentiles were considered superior to the mean and variance of the mass fractions for uncertainty assessment in this project, since there is no evidence that the simulated mass fractions followed normal distributions. Whereas the 50th percentile tritium plume did not approach the production well during the entire simulation period, the 95th percentile tritium plume approached, but did not reach, the production well during and after the production period (Figure 3). The breakthrough curves of the 95th percentile of tritium mass fraction at the production well indicated that the tritium concentration could be several orders of magnitude higher than the mass fraction of deterministic Type 2 simulations, suggesting that the uncertainty was not negligible. Nonetheless, the peak mass fraction at the production well was close to the environmental background value. Additional uncertainties remain that could not be quantified by the Monte Carlo analysis either due to lack of data (e.g., the lateral gradient) or because they are a conceptual component (e.g., location of production well, presence of multiple wells).

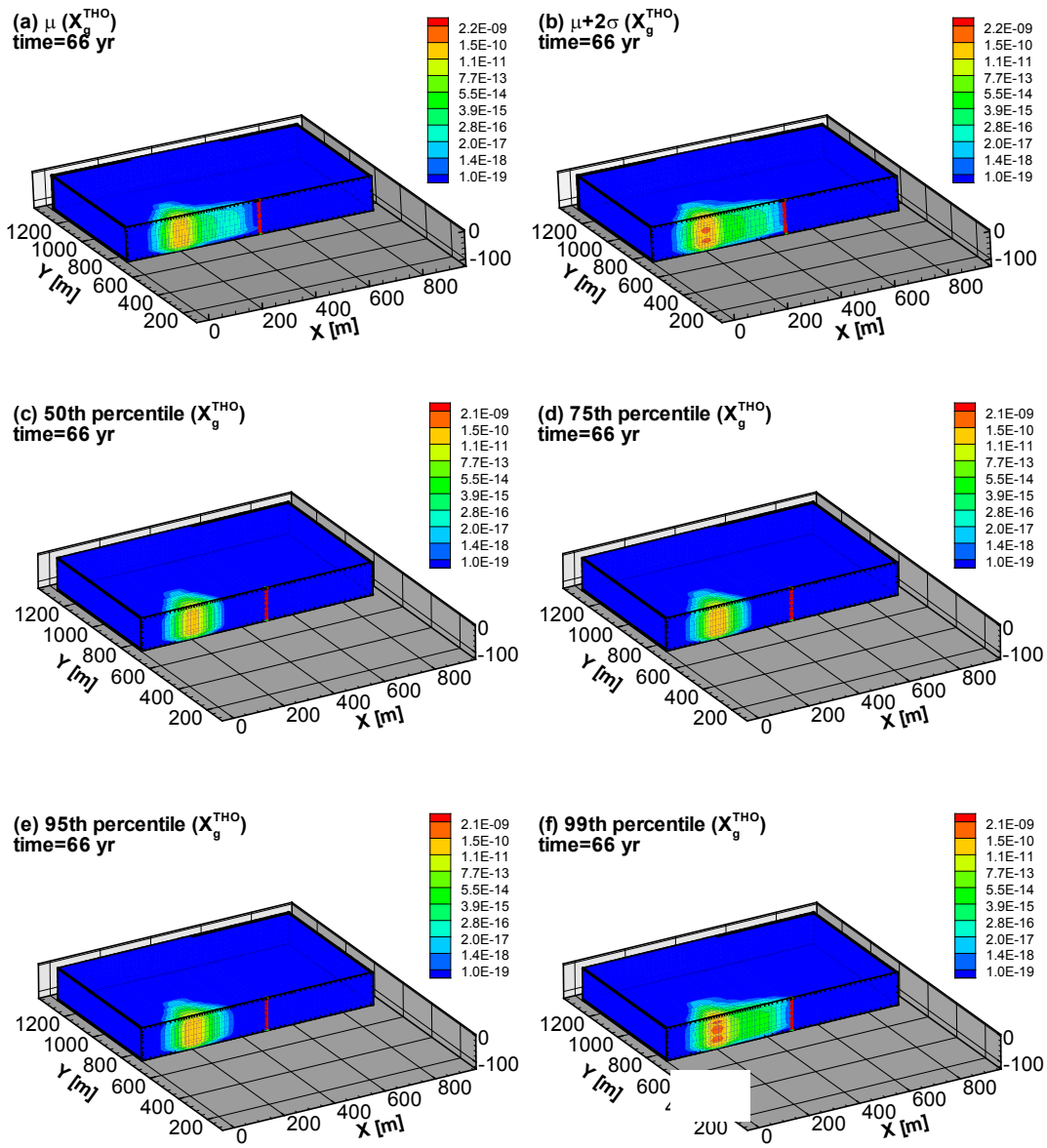

Figure 3. (a) Mean (μ), (b) upper bound of the 95 percent confidence interval (μ+2σ), (c) 50th percentile, (d) 75th percentile, (e) 95th percentile, and (f) 99th percentile of mass fraction of tritium in gas phase at 66 years after the detonation (one year after the end of gas production).

2007 Report on Rulison, DRI Pub. No. 45224; also DOE/NV/13609-54

The objectives of this work were to calculate the nature and extent of tritium contamination in the subsurface from the Rulison test from the time of the test through the year 2007, and to evaluate tritium migration under natural-gas production conditions to a hypothetical gas production well in the most vulnerable location outside the DOE drilling restriction. The natural-gas production scenario involves a hypothetical production well located 258 m horizontally away from the detonation point, outside the edge of the current drilling exclusion area. The production interval in the hypothetical well is at the same elevation as the nuclear chimney created by the detonation, in order to evaluate the location most vulnerable to tritium migration. The basic idea is similar to that of the Rio Blanco model, but the manner in which the model was implemented was more complex than that of the Rio Blanco model. The most important difference is that permeability and porosity were treated as spatially variable, such that the permeability fields were completely heterogeneous, in contrast to the Rio Blanco work in which permeability and porosity were uniform throughout each computer simulation. Other differences are the range of permeability and porosity was different, as was the distance from the detonation point to the hypothetical producing natural gas well.

A three-dimensional geologic model was developed of the local Williams Fork Formation at the Rulison site that includes a sequence of sandstone and shale lenses conditioned on observations at two site wells. The dominant flow and transport direction is east-west, in agreement with the direction of regional fractures in the area. The average sandstone lens length is approximately 161 m and mean thickness is 7.5 m. The sandstone lenses are characterized by very low intrinsic permeability in core measurements (on the order of 10^{-18} m^2), while reservoir tests indicated higher permeabilities (up to 10^{-16} m^2) presumably as a result of fractures encountered at the field scale. Porosity of Williams Fork sandstone units was to be between 0.01 and 0.1. Shale units are considered barriers to flow, with intrinsic permeability of 10^{-20} m^2.

A conceptual flow and transport model for the area around the emplacement well was developed to investigate the rates of tritium transport in the subsurface away from the chimney. As was the case for Rio Blanco, tritium is transported as the tritiated water molecule ^3HHO in both the gas and aqueous phases from the nuclear chimney (located in Lot 11) radially outward under a chemical concentration gradient for 38 years (the time from the nuclear test until 2007). At this time the hypothetical gas production well was placed in the model 258 m directly to the west, in Lot 12, and gas production was simulated for 30 years. During this time, transport was enhanced by the pressure gradient created by the production well.

The geologic and conceptual models were implemented in the numerical simulator TOUGH2, and an equivalent porous medium approximation was used to simulate the fractured environment. Permeability and porosity distributions were developed based upon a statistical analysis of core data. Distributions were also developed for fracture permeability and hydraulic fracture (fractures surrounding the hypothetical gas production well that are induced to enhance flow around the well bore) length based on a multiple of the core permeability data, and literature values, respectively. Five hundred realizations were solved in TOUGH2, each representing one equally likely combination of sandstone-shale geometry and parameter values. Each model realization was simulated to determine the most likely length and time scales of tritium transport away from the chimney.

The simulator allows for partitioning between phases as well as radioactive decay. Results show that for the first 38 years following detonation of the nuclear device, tritium transport is controlled by gas diffusion and radioactive decay. The shape of the tritium plume is not dependent on the permeability field, as diffusion is controlled by tortuosity, which is in turn controlled by gas saturation and porosity. Based on the 50th percentile of the 500 Monte Carlo simulations, the maximum travel distance of tritium was approximately 80 m from the nuclear detonation point during the 38 year period of diffusion. This is essentially the distance fractured by the nuclear detonation.

Production from the hypothetical gas well begins 38 years after the nuclear detonation (in the year 2007). Results of the Monte Carlo simulations suggest that tritiated water vapor above background concentrations will not reach the production well at the 95th percentile (Figure 4). The peak mass fraction of tritium (mass of tritiated water in the gas phase to mass of the gas phase per unit volume) in the gas phase at the 95th percentile is 1.01×10^{-21} g^{THO} g_{gas}^{-1}, as compared to the background mass fraction of tritium prior to nuclear testing, estimated at 10^{-20} (mass of tritiated water vapor to mass of gas, estimated from the background atomic ratio of 10^{-18} atoms of tritium to atoms of hydrogen). Breakthrough at the production well above background concentration was observed at the 99th percentile, with a peak mass fraction of 2.33×10^{-19} g^{THO} g_{gas}^{-1}, occurring 68 years after the nuclear test. Partitioning of tritium between the gas and liquid phases resulted in liquid phase mass fractions approximately two times higher than those in the gas phase.

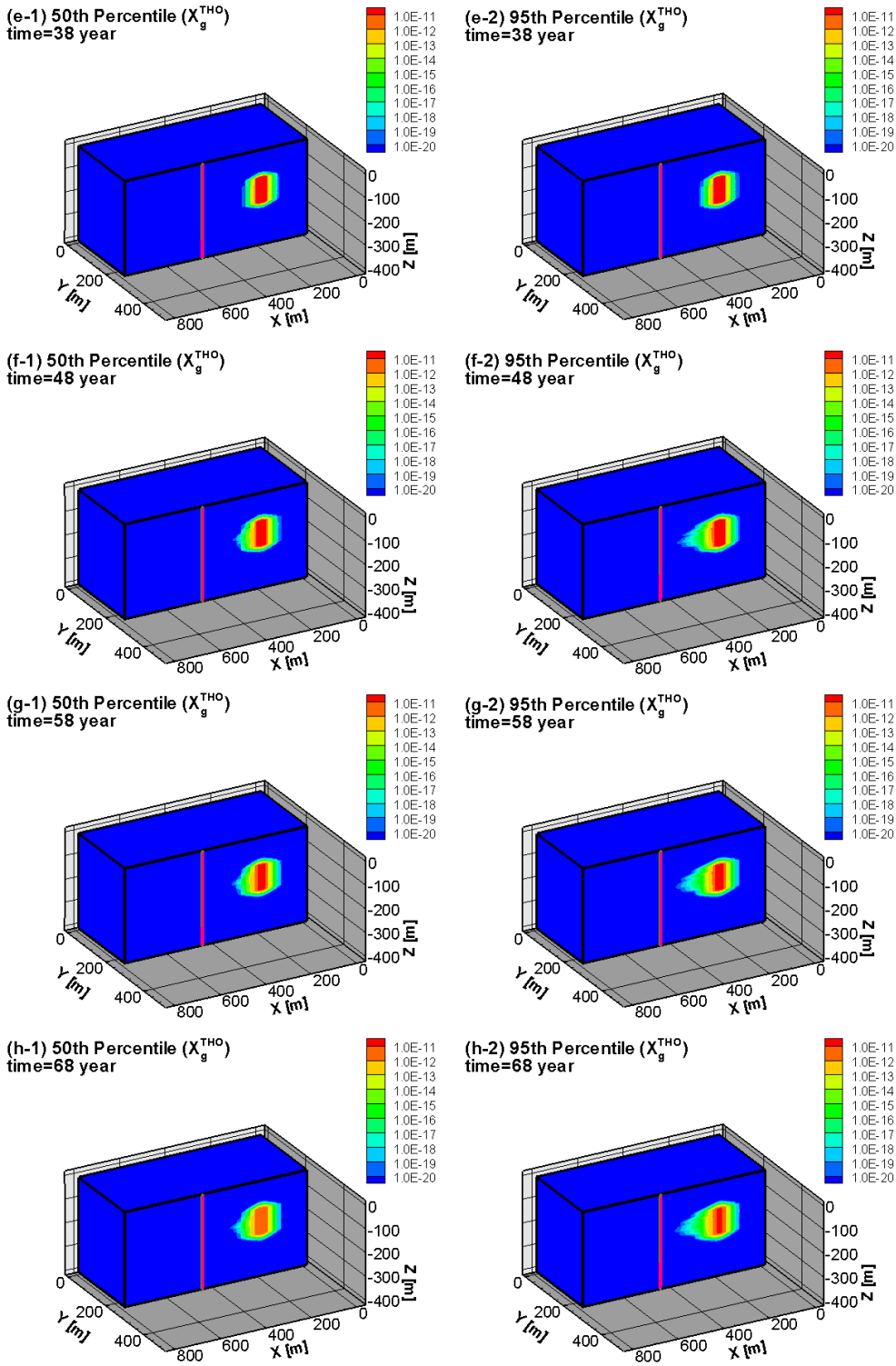

Figure 4. Results of Monte Carlo simulations showing the mass fraction of tritiated water vapor at the 50th (left column) and 95th (right column) percentiles for at the start of gas production (38 years after the nuclear detonation) through the end of gas production (68 years after the detonation). The top of the simulation is 2,368 m below the land surface.

2008 Addendum on Rulison

The results of the 2007 report discussed above suggested that there was less than five percent probability of tritium reaching a hypothetical gas production well located 258 m from the detonation point. Reviews of the model results indicated concerns with the value of the partitioning coefficient controlling the distribution of tritiated water between liquid and vapor phases, the assignment of effective porosity to hydraulically generated fractures surrounding the hypothetical production well, and the treatment of molecular diffusion in the partially saturated reservoir. These concerns were addressed in the 2008 addendum through additional computer simulations that tested the impact of these model features on the degree to which tritium is transported away from the detonation point.

Independent evaluation of the partitioning coefficient identified that the value used in Cooper et al. (2007) was inappropriate for the subsurface temperatures present in the gas reservoir at Rulison. A more correct value leads to no transport of tritium above background to the production well because tritiated water is strongly favored in the immobile aqueous phase (Figure 5).

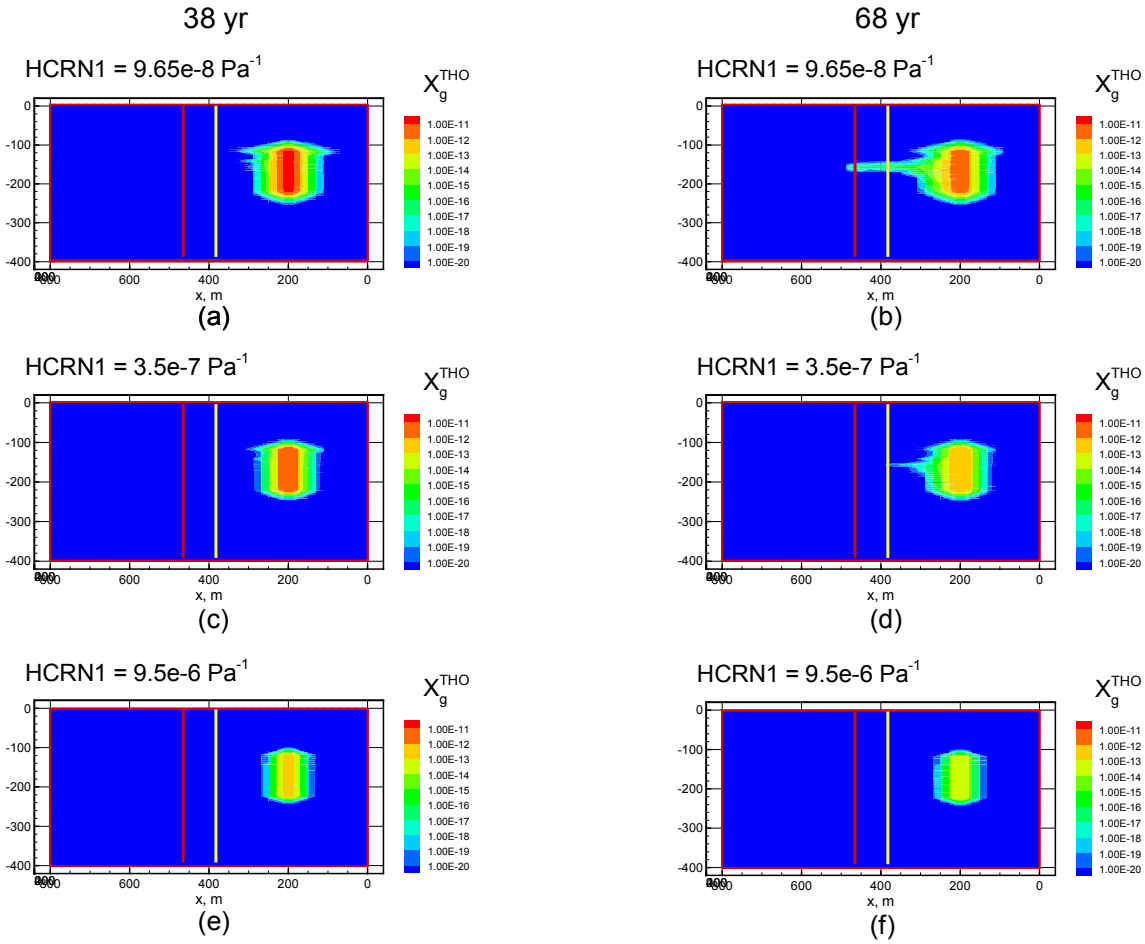

Figure 5. Results of three simulations in which the inverse Henry's law constant was changed. The three simulations used realization 10, which represents gas-phase tritium concentration at the 99th percentile in Cooper et al. (2007). The left-hand column shows the field of X_g^{THO} 38 years after the nuclear detonation while the right-hand column shows X_g^{THO} at 68 years. The first row, (a) and (b), shows the X_g^{THO} field for an inverse Henry's law constant appropriate for a temperature of 312 °C, while the second row shows the results for exactly the same simulation but with the inverse Henry's law constant equivalent to a temperature of 230 °C. The third row is the same as the first two, but for an inverse Henry's law constant appropriate for a reservoir temperature of 101 °C. The yellow vertical line in each figure depicts the location of the lot 11/12 boundary while the red vertical line shows the location of the gas production well.

Another limitation of the 2007 model was that the hydraulic fractures around the production well were assumed to have a porosity of 10 percent. This was changed in the 2008 Addendum to assume that the hydraulic fractures increased intrinsic permeability, but not porosity. This resulted in porosity values in the hydraulically fractured zone to be the same as the native formation. Reduction of this porosity to that of the host sandstone increases the velocity of the gas phase and accompanying tritiated water vapor (Figure 6).

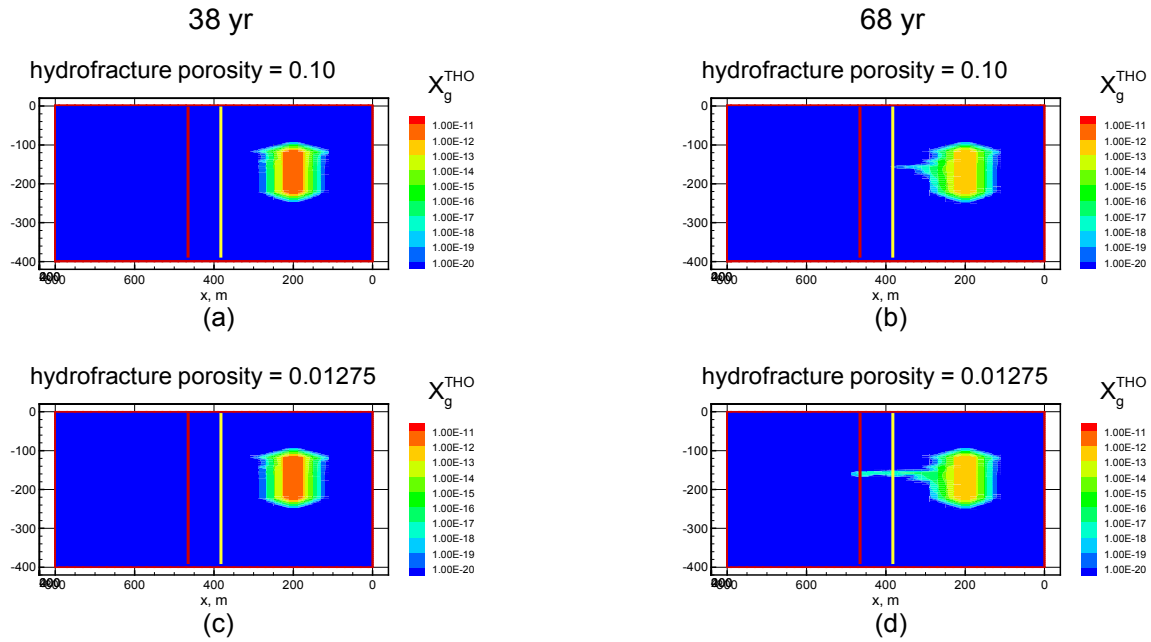

Figure 6. Results of two simulations that compare the effect of different hydraulic fracture porosity, based upon realization 10, and using partitioning for 230 °C. The upper row shows gas-phase tritium mass fraction toward a production well in which the EPM hydraulic fracture porosity is 0.10, while the lower row shows the same mass fraction field with a hydraulic fracture porosity equivalent to that of the native sandstone, in this case 0.01275. The yellow vertical line in each figure depicts the location of the lot 11/12 boundary while the red vertical line shows the location of the gas production well.

With respect to tritium diffusion, application of a tortuosity value that was constant and greater than the Millington-Quirk saturation-dependent model used previously resulted in greater diffusive spreading of the tritium plume. Both the hydraulic fracture porosity and diffusivity changes favored enhanced tritium transport away from the nuclear chimney, but their combined effects were overwhelmed by the effect of the partitioning coefficient, such that the new simulations predict *less* tritium transport than presented in Cooper et al. (2007). Only when partitioning was assumed to occur under the elevated temperature conditions that may be present in the bottom of the nuclear cavity, was transport observed at concentrations higher than that in Cooper et al. (2007) Figure 7 and Table 1. These conditions were not representative of the subsurface in the upper nuclear chimney or the surrounding formation. All of the additional simulations and sensitivity tests were performed with only the top ten of the 500 equally probable realizations considered by Cooper et al. (2007). Each of the 500 realizations presents an equally likely distribution of sandstone and shale; their porosity, permeability, and the length of the hydraulic fractured zone were selected from ranges possible for the formations. Focusing on only the ten realizations with the most transport neglected the importance of the sandstone-shale geometry in limiting transport from the nuclear chimney. Only in those few realizations with well-connected sandstone between the nuclear chimney and the production well was there any opportunity for transport. For those low probability cases, the new simulations showed that the tritiated water partitioning coefficient is the next dominant factor to control transport. Although low porosity and liquid water contents of the hydraulic fracture zone and small tortuosity values had the potential to increase tritium transport away from the chimney, they were much less

important than the configuration of the sandstone-shale geometry and partitioning of tritiated water between phases.

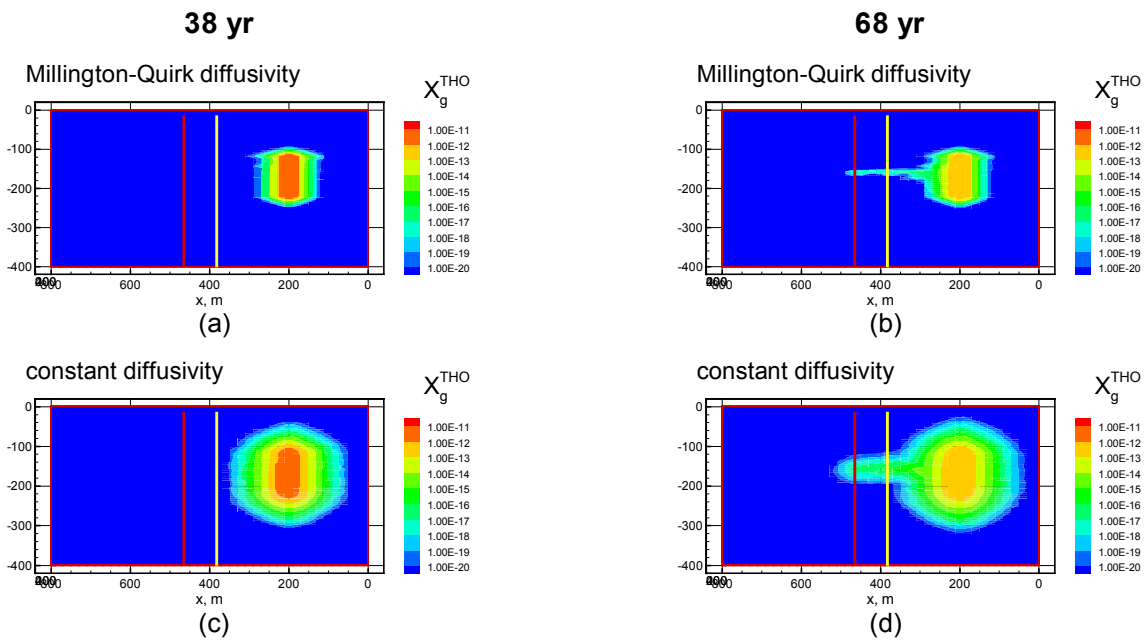

Figure 7. Results of two simulations in which the diffusivity model is compared. Realization 10, which was at the 98th percentile in breakthrough in the 2007 report was used for both simulations. The left-hand column shows the mass fraction of tritiated water vapor X_g^{THO} 38 years after the nuclear detonation while the right-hand column shows X_g^{THO} at 68 years. The first row, (a) and (b), shows the X_g^{THO} field for a simulation in which the Millington-Quirk tortuosity model was used, while the second row shows the results for a similar simulation in which the diffusivity was assumed constant. The yellow vertical line in each figure depicts the location of the lot 11/12 boundary while the red vertical line shows the location of the gas production well.

Table 1. Peak tritium mass fraction in the gas phase (X_g^{THO}) at the production well location for the ten Monte Carlo realizations with the most transport. Peak values occur between 48 and 68 years after the nuclear test. Three model results are shown for each realization: the results from Cooper et al. (2007); results with H_c^{-1} for 101 °C (realistic for most of the chimney except for the lowermost part), lower hydraulic fracture porosity, and constant diffusivity; and results for H_c^{-1} for 230 °C (probably only realistic for the lower part of the chimney where the detonation occurred), lower hydraulic fracture porosity, and constant diffusivity.

NMC	Cooper et al. (2007)$_x$ (X_g^{THO})	H_c^{-1} =101 °C $_y$ (X_g^{THO})	H_c^{-1} =230 °C (X_g^{THO})
10	2.33×10^{-19}	$\sim 10^{-30}$	9.25×10^{-17}
30	3.38×10^{-19}	$\sim 10^{-35}$	1.79×10^{-20}
80	5.48×10^{-18}	$\sim 10^{-30}$	5.10×10^{-17}
118	6.58×10^{-20}	$\sim 10^{-39}$	8.58×10^{-23}
143	1.08×10^{-19}	$\sim 10^{-37}$	1.53×10^{19}
185	2.77×10^{-19}	$\sim 10^{-27}$	3.95×10^{16}
303	5.64×10^{-20}	$\sim 10^{-30}$	6.83×10^{17}
321	2.16×10^{-18}	$\sim 10^{-37}$	1.07×10^{20}
372	1.48×10^{-17}	$\sim 10^{-30}$	6.99×10^{18}
493	1.09×10^{-19}	$\sim 10^{-36}$	3.62×10^{20}

2010 Letter Report Update on Rulison

In 2010, a second enhancement (beyond the Addendum, discussed above) was made to the 2007 model. In this case, twelve random permeability/porosity fields were generated based upon updated statistics of the sandstone percentage (assumed to be 40 percent as opposed to 49 percent in the 2007 Report and 2008 Addendum). The sandstone porosity and permeability were determined based upon calibration to post-shot production of gas from the chimney. Other model enhancements included the following:

- The tortuosity value was changed to a constant value, 0.047 (derived in the addendum), rather than a parameter that could be as low as 10^{-5} (as was used in the 2007 report)
- Tritium partitioning between the gas and aqueous phases was completely dependent upon temperature
- A single value of sandstone permeability and porosity is used, rather than a distribution, based upon the calibration
- Gas production was simulated using a deliverability approach (production against specified pressure) rather than prescribed flow
- Nuclear fracture and hydraulic fracture continua were simulated as having ellipsoidal shape in the horizontal plane rather than cylindrical, resulting in longer fracture lengths in the east-west direction
- The hydraulic fracture continua simulated fracturing of all rock within 100 m and an outer zone of increased permeability in only sandstone, rather than the single, smaller, increased-permeability zone in only sandstone simulated in the previous model
- Separate capillary pressure and relative permeability curves were used for sandstone, shale, hydraulic fractures, and the nuclear chimney

A plan view of the simulation domain is shown in Figure 8, showing the 'ellipsoidal' fracture fields. The maximum distance of the nuclear-generated (chimney) fractures in the east-west (i.e., x-) direction was 100 m from the detonation, while the distance in the y-direction was 60 m. In the original model, nuclear-generated fractures extended 80 m in both the x- and y-directions. With respect to the hydraulic fractures, two different zones were developed (Figure 8). Within the inner zone, it was assumed that both the sandstone and shale units would be fractured, while in the outer zone, it was assumed that the shale would be too plastic to be fractured, such that only the sandstone would be fractured. The result of this is that the intrinsic permeability of the fractures zones was changed. The details are presented in Table 1 of the Addendum.

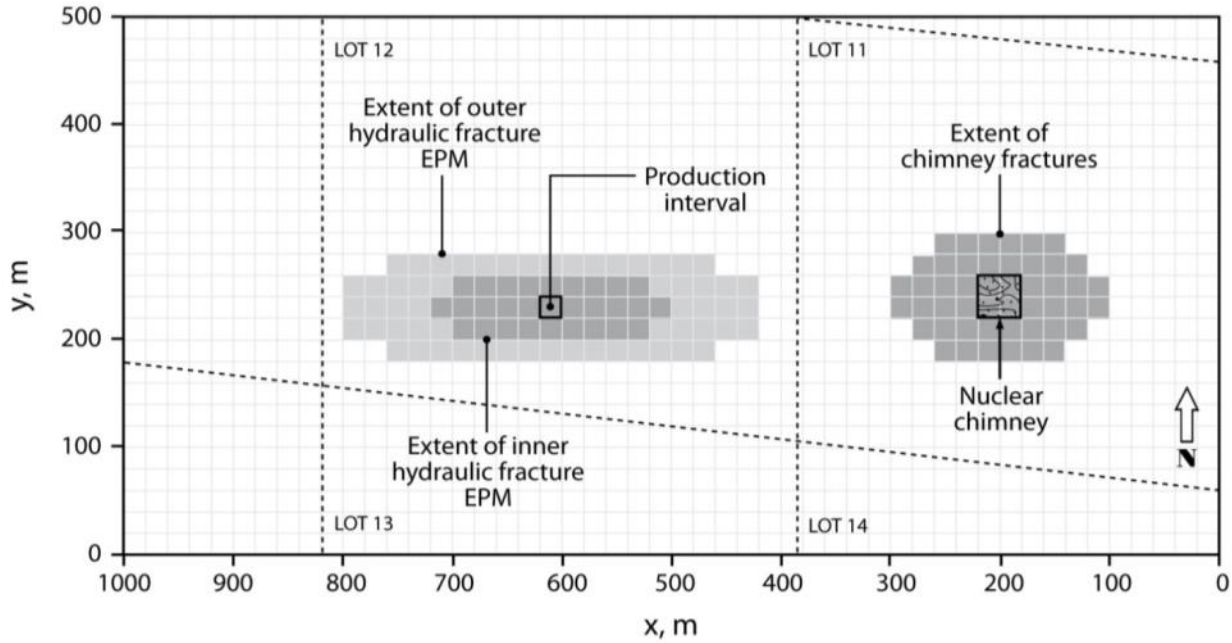

Figure 8. Plan view of the computational domain with nuclear chimney, chimney fractures, and inner and outer ellipsoidal fracture continua. Flow was from the nuclear chimney on the left toward the production well in the center of lot 12.

The model was calibrated against well test conducted subsequent to the nuclear detonation, in 1970 and 1971. The purpose of the calibration was to determine the best fit values for the native sandstone, the nuclear chimney, and the nuclear-generated (or explosion-related) fractures. The model was calibrated by prescribing a known flow rate to the re-entry borehole (the 'well' that was tested) and adjusting the permeabilities until the model pressure response matched that of the measured pressure during the test.

The tritium partitioning coefficient used in the 2007 report was for a temperature higher than that existing anywhere in the reservoir, and as a result, the simulations overpredicted tritium transport (i.e., they were overly conservative). This was changed in the Addendum to include a more realistic value for the reservoir temperature, realizing that the temperature in the cavity was much higher, and required a coefficient that would favor additional tritium in the gas phase. In the 2010 update, the issue was fully resolved by modifying the TOUGH2 program to handle temperature-dependent partitioning everywhere in the simulation domain. This was an important improvement over the manner in which partitioning was handled in the previous reports.

The results of the first 41 years of diffusive transport, prior to the implementation of a producing gas well, is shown in Figure 9. The results show that transport never extends beyond the boundary between lots 11 and 12. Although the simulation is for one permeability/porosity realization, the results are nearly identical for all 12 realizations, as diffusive transport is independent of permeability, and the porosity changes were so small between realizations that the differences in plume character is not discernible between simulations. The reason that the plume is now bell-shaped, in comparison to the results of previous simulations, is due to the higher temperature at the bottom of chimney, where the nuclear device was located, and the temperature is much hotter, favoring tritium partitioning into the gas phase.

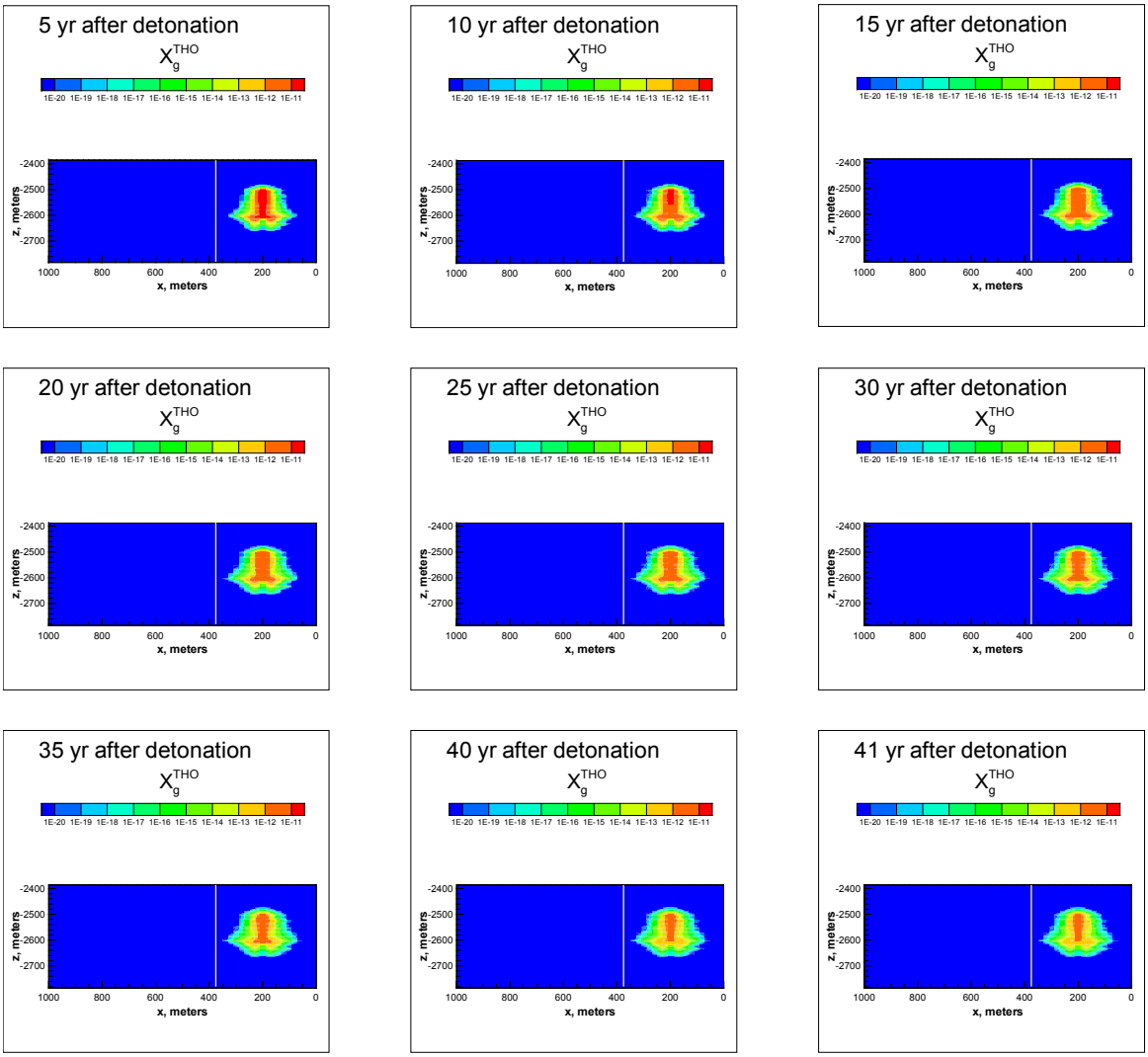

Figure 9. Mass fraction of tritiated water vapor in five-year increments for 41 years following the nuclear detonation for realization 1. Each pane shows a two-dimensional vertical east-west slice that cuts through the detonation point. Corresponding values in picocuries are 4 x 10^{10} picoCuries per liter (liquid water equivalent of condensed vapor) for X_g^{THO} =10^{-10} (the red end of the scale) to 4 pCi l^{-1} for X_g^{THO} =10^{-20} (the blue end of the scale). The vertical axis is depth below land surface, and the vertical yellow line depicts the boundary between lot 11 (to the right of the line) and lot 12.

Simulation results for all 12 permeability/porosity realizations are shown in Figure 10. Each panel in the figure is for the same time, 30 years after the start of gas production from the hypothetical gas well, which is the time of maximum transport. After 30 years, production was assumed to stop which would lead to a relaxation of the drainage gradient toward the well during production. In all twelve simulations, tritium did not extend beyond the boundary between lots 11 and 12, and therefore remained more than 200 m from the production well throughout the simulation. This is consistent with the results of the 2007 report, which showed that tritium would not reach the well in over 95 percent of the simulations.

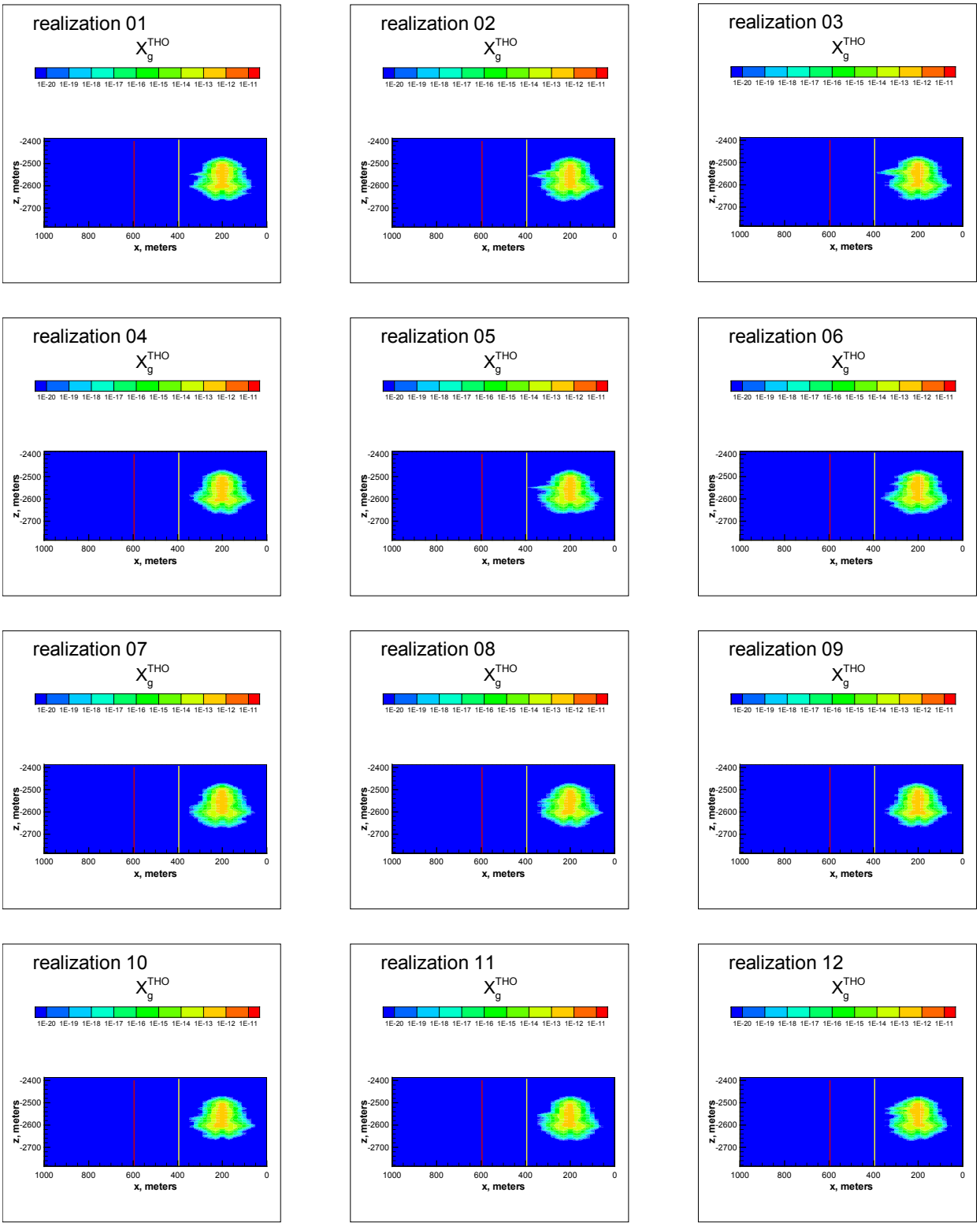

Figure 10. Mass fraction of tritiated water vapor after 30 years of gas production from the well, for all 12 realizations. The vertical axis is depth below land surface. The vertical yellow line is the boundary between lot 11 (to the right of the line) and 12, while the vertical red line shows the location of the hypothetical production well.

TOUGH2 Computer Program

The conceptual model includes flow and transport as coupled processes that must be solved simultaneously to get a realistic understanding of the radionuclide distribution. The TOUGH2 (**T**ransport **o**f **U**nsaturated **G**roundwater and **H**eat) integral finite difference simulator was used to implement the model as it handles three-dimensional, multiphase, multicomponent heat and mass transport through porous media in a fully coupled manner (Pruess et al. 1999). The code fully accounts for the movement of gaseous and liquid phases, their transport of latent and sensible heat, and phase transitions between liquid and vapor occurring under pressure, viscous, capillary, and gravity forces according to Darcy's law. The program provides options for specifying injection or withdrawal of energy (heat) and fluids. The equation of state module that was implemented (EOS7R) is capable of handling four components: water, air, solute and heat (although only isothermal flow was simulated). TOUGH2 is a DOE-sponsored code that has been used extensively to study heat and mass flow in geothermal reservoirs, saturated/unsaturated zones, and oil and gas reservoirs. Several changes were made to the TOUGH2 program in order for it to correctly simulate the important processes. The EOS7R module assumes the gas phase to be air and air/water mixtures. This was easily changed to replace air properties with those of methane, which are important in the density and viscosity correlations.

References

Cooper, C.A., and J. Chapman, 2001. Modeling approach for evaluating radionuclide transport in nuclear-stimulated gas reservoirs, DRI Publication no. 45186, also DOE/NV/13609-15, 36 pp.

Cooper, C.A., 2004., Scoping analysis of gas phase transport from the Rulison underground nuclear test, Desert Research Institute Letter Report, also DOE/NV/13609-LTR2004-01, 12 pp.

Cooper, C.A., M. Ye, J. Chapman, and C. Shirley, 2005. Radionuclide migration at the Rio Blanco Site, a nuclear-stimulated low-permeability natural gas reservoir, DRI Publication no. 45215, also DOE/NV/13609-45, 94 pp. plus three appendixes.

Cooper, C.A., M. Ye, J. Chapman, 2007. Tritium transport at the Rulison site, a nuclear-stimulated low-permeability natural gas reservoir, Desert Research Institute publication 45224, and DOE Office of Legacy Management, DOE/NV/13609-54, 102 pp.

Cooper, C.A., M. Ye, and J.B. Chapman, 2008. Addendum: Tritium transport at the Rulison Site, a nuclear-stimulated low-permeability natural gas reservoir, unpublished Desert Research Institute, Reno, Nevada, letter report, 18 pp. plus two appendixes.

Cooper, C.A., J.B. Chapman, Y. Zhang, R. Hodges, and M. Ye, 2010. Update of tritium transport calculations for the Rulison Site: Report of activities and results during 2009–2010, unpublished Desert Research Institute, Reno, Nevada, letter report, 24 pp.

Pruess, K., C. Oldenburg, and G. Moridis, 1999. *TOUGH2 User's Guide, Version 2.0*, LBNL-43134, Berkeley, California.

Ye, M., C.A. Cooper, J.B. Chapman, D. Gillespie, and Y. Zhang, 2009. Geologically based Markov chain model to simulate solute tracers in natural gas reservoirs with uncertain conditions, SPE Reservoir Evaluation & Engineering, 12(6), pp. 974–984, doi 10.2118/114920-PA.

This page intentionally left blank

Appendix B

Method Used to Create Sandstone - Shale Realizations

This page intentionally left blank

Transition-probability based geostatistical model for the Rulison and Rio Blanco Sites

Yong Zhang and David Gillespie

Desert Research Institute

April 8, 2011

In this study, logs from the Rulison emplacement well (R-E), the Rulison exploratory well (R-EX), and six recently drilled Noble Energy gas production wells (BM 26-33b, 26-33c, 26-33d, 26-34a, 26-34b, and 26-34c) are incorporated into TPROGS [Carle et al., 1998] to simulate the distribution of sandstone and shale facies. In comparison to traditional variogram-based geostatistical methods, the transition probability/Markov approach in TPROGS improves consideration of spatial cross-correlations and facilitates the integration of geologic interpretation of facies architecture into the model development process.

The results were used to generate several equally probable facies distribution realizations of the Rulison subsurface (upper and lower Williams Fork Formation) that were used to populate the model mesh. The wells within the Rio Blanco model domain do not reach the lower Williams Fork Formation. The statistics from the well data at Rulison were used with the well data at Rio Blanco to generate several equally probable facies distribution realizations of the Rio Blanco subsurface (Ft Union Formation, and the upper and lower Williams Fork Formation).

1. Upper Williams Fork Formation (UWF)

The average thickness for sandstone, 13.0 ft, is fitted by the measured transition probabilities along the vertical direction (Figure 1). Here the transition probability is defined by the following conditional probability

$$t_{ij}(h) = \Pr\{j \text{ occurs at } x+h \mid i \text{ occurs at } x\} \quad ,$$

where x is a spatial location, h is the lag (separation vector), and i, j denote facies.

In Figure 1, the intersection of the grey line (tangent of transition probability) with lag axes indicates the average thickness of each facies. The shale facies is treated as the background category in TPROGS, since it has a higher proportion than sandstone. The measured average thickness for shale is 16.46 ft.

The volumetric proportion of sandstone and shale is 44.4% and 55.6%, respectively. This is similar to the proportion observed in the UWF at Rio Blanco (which is 43.6% and 56.4% for sandstone and shale, respectively). In Figure 1, the dashed line denotes the proportion of each facies.

Figure 1 also shows that the Markov chain model fits the measured transition probabilities. The good agreement is due to the relatively abundant data along the vertical direction.

For the horizontal direction (Figure 2), the calculation of mean length for each facies contains intrinsic uncertainty, due to the sparse data along this direction (similar to many other sites). The facies distribution along the horizontal direction is assumed to be isotropic, since no data at present shows clearly the anisotropic pattern. The mean length along the horizontal direction is 650 and 823 ft for sandstone and shale, respectively. The 650-ft mean length for sandstone is estimated by the measured transition probabilities along the horizontal direction (Figure 2). It is also on the same order as the one (528-ft) used by Cooper et al. [2007] for the Rulison site. The 823-ft mean length for sandstone is the best-fit result of TPROGS, based on the measured transition probabilities (note that in the horizontal direction, shale can also be treated as the background category).

2. Lower Williams Fork Formation (LWF)

The average thickness for sandstone, 12.4 ft (see Figure 5), is smaller than that in the UWF unit. Similarly, the proportion of sandstone (42.5%, calculated by driller's logs), is relatively smaller than that in UWF. The calculated average thickness for shale is 16.7 ft.

Sandstone is less continuous in the LWF than the sandstone in the UWF. The mean length (along the horizontal direction) for LWF sandstone is 450 ft, which is 70% of the mean length in UWF. A shorter mean length in LWF than UWF is expected, since the LWF was deposited primarily in an alluvial system and the UWF in primarily a marine depositional system. Note again that the 450-ft mean length for sandstone is estimated by the measured transition probabilities (Figure 6), which contain high uncertainty and apparent noise due to the sparse data on the horizontal direction.

The volumetric proportion of sandstone and shale is 42.5% and 57.5%, respectively. Hence the LWF has less sandstone than the UWF.

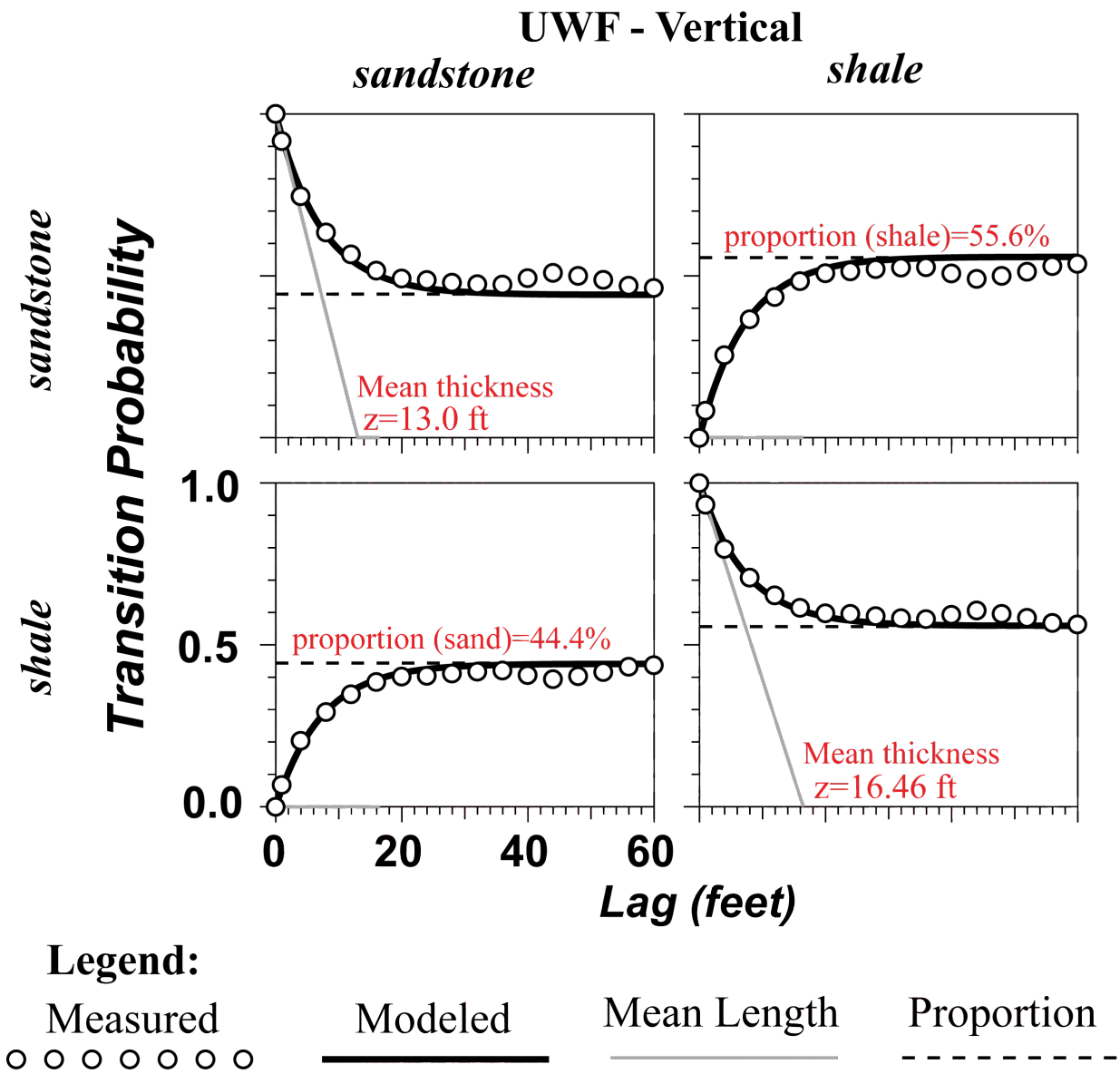

Figure 1. UWF-Vertical: The Markov Chain/Transition probability model along the vertical direction built for UWF, using 6 wells.

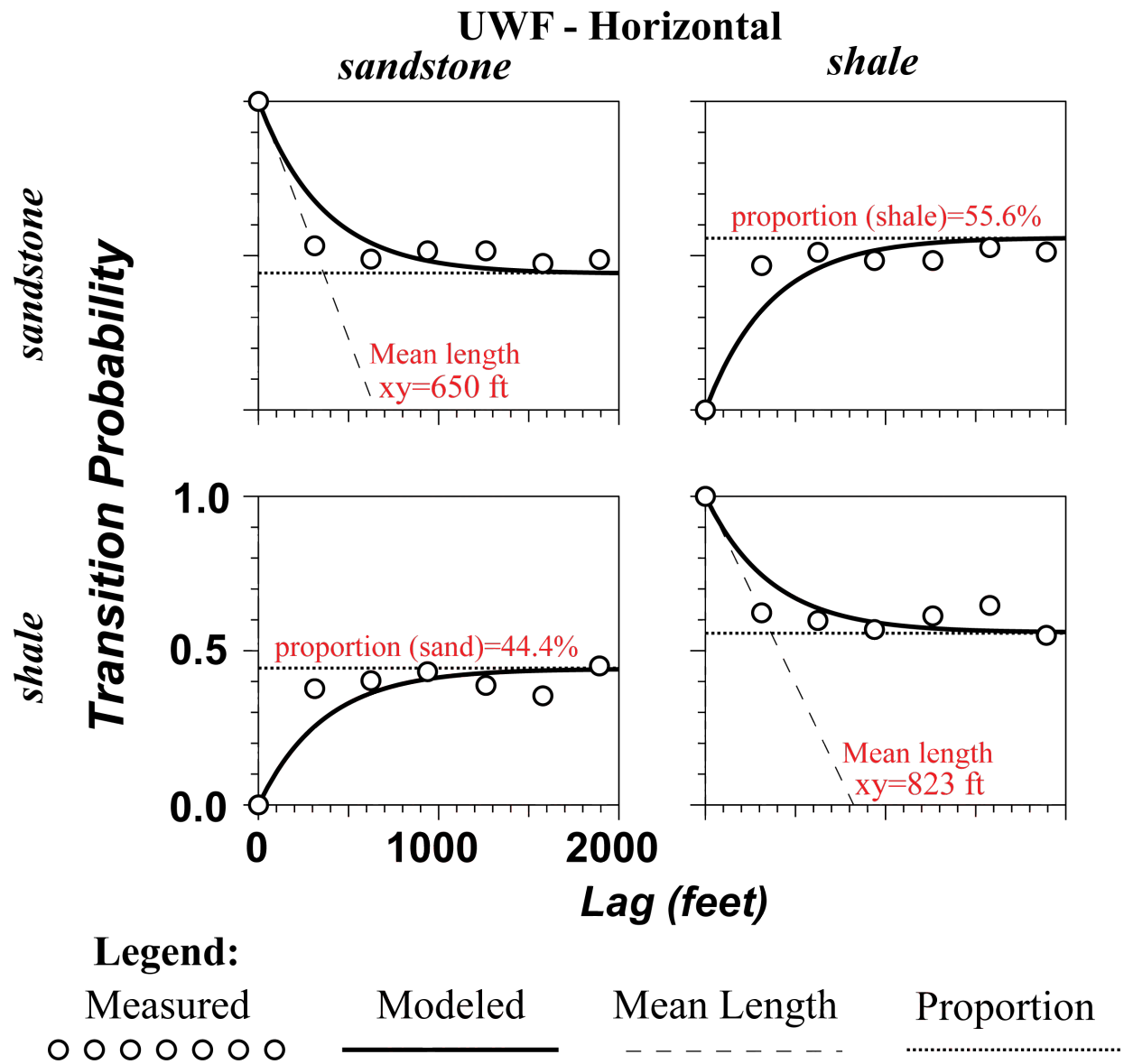

Figure 2. UWF-horizontal: The Markov Chain/Transition probability model along the horizontal direction built for UWF, using 6 wells.

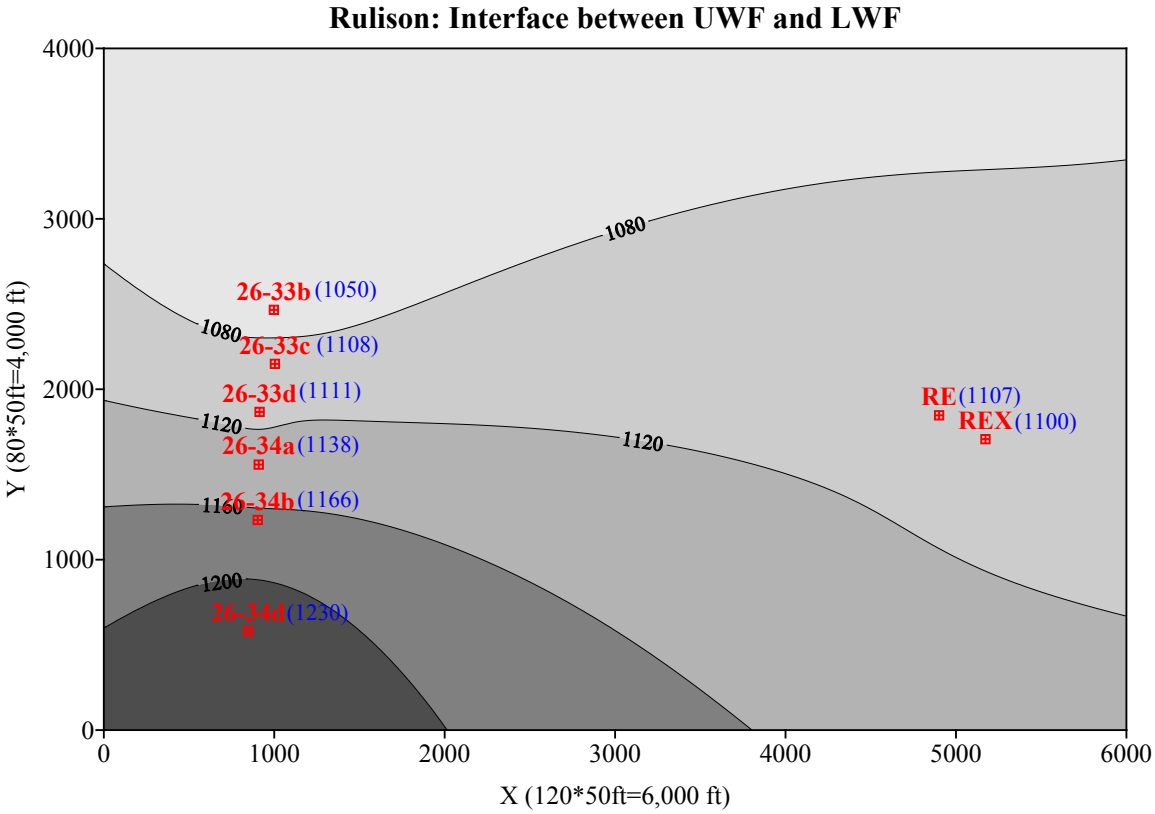

Figure 3. Elevation (feet) of the interface between the UWF and LWF. The contour was generated by interpolating the interface at the 8 wells, using Kriging method. The blue font on the right side of each well denotes the elevation of the interface. Note that the interface for well 26-33 and 26-34 was interpreted by: "*The topmost continuous sandstone unit was picked as the top of the WF. Around 1200 feet there is a silty zone that seem to separate the thicker more continuous units and thinner units below. The top of Gas was picked at the first continuous sandstone unit below the silty zone. The top of the Cameo was selected based on the bottom of the somewhat continuous sandstone units and the top of the discontinuous units below*". The interface for R-E and R-EX was picked as the first continuous sandstone unit below the silty zone.

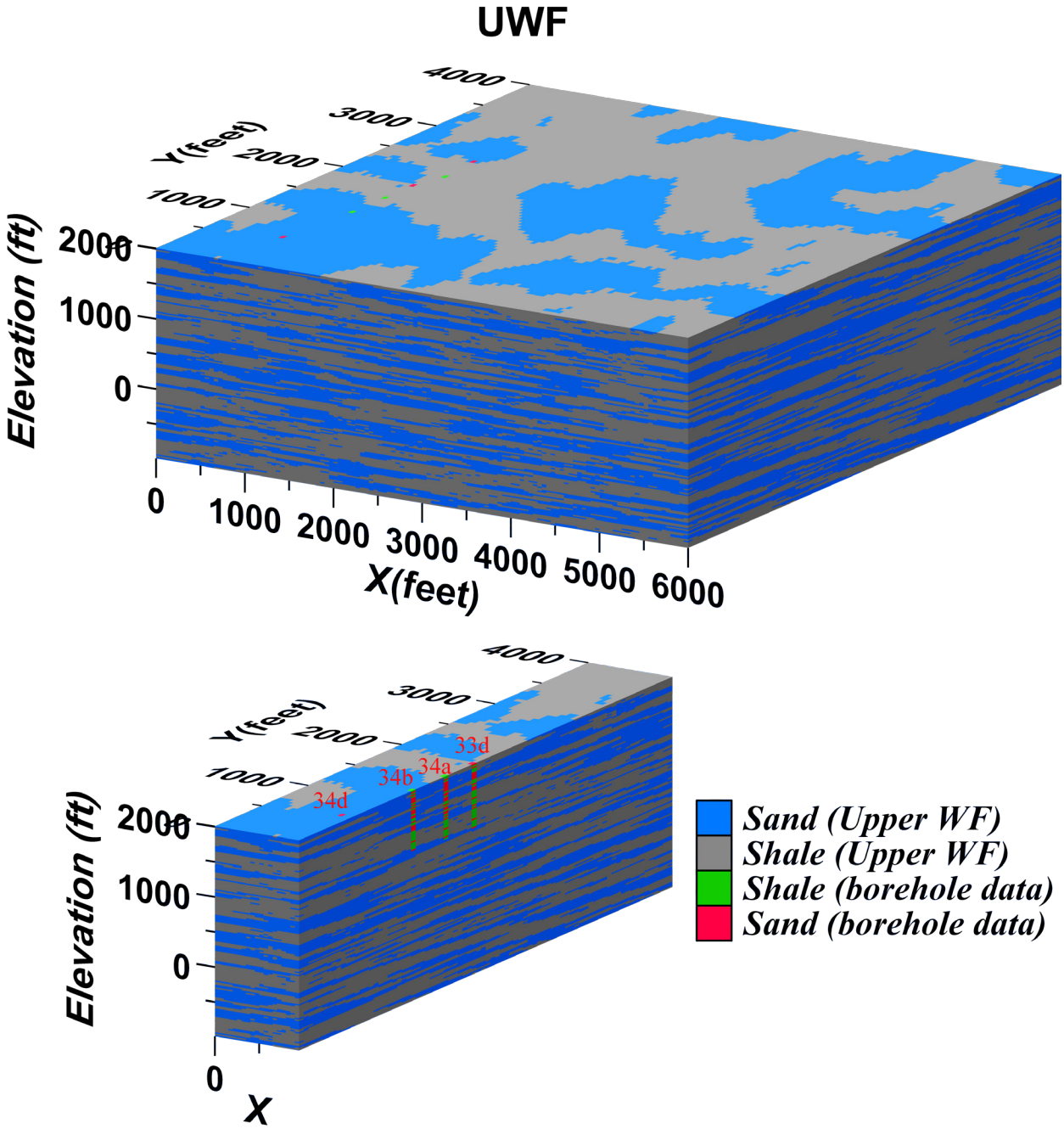

Figure 4. Rulison-UWF facies model (3-d view and an exploded view) built by TPROGS (using the model shown in Figure a 1 and Figure 2).

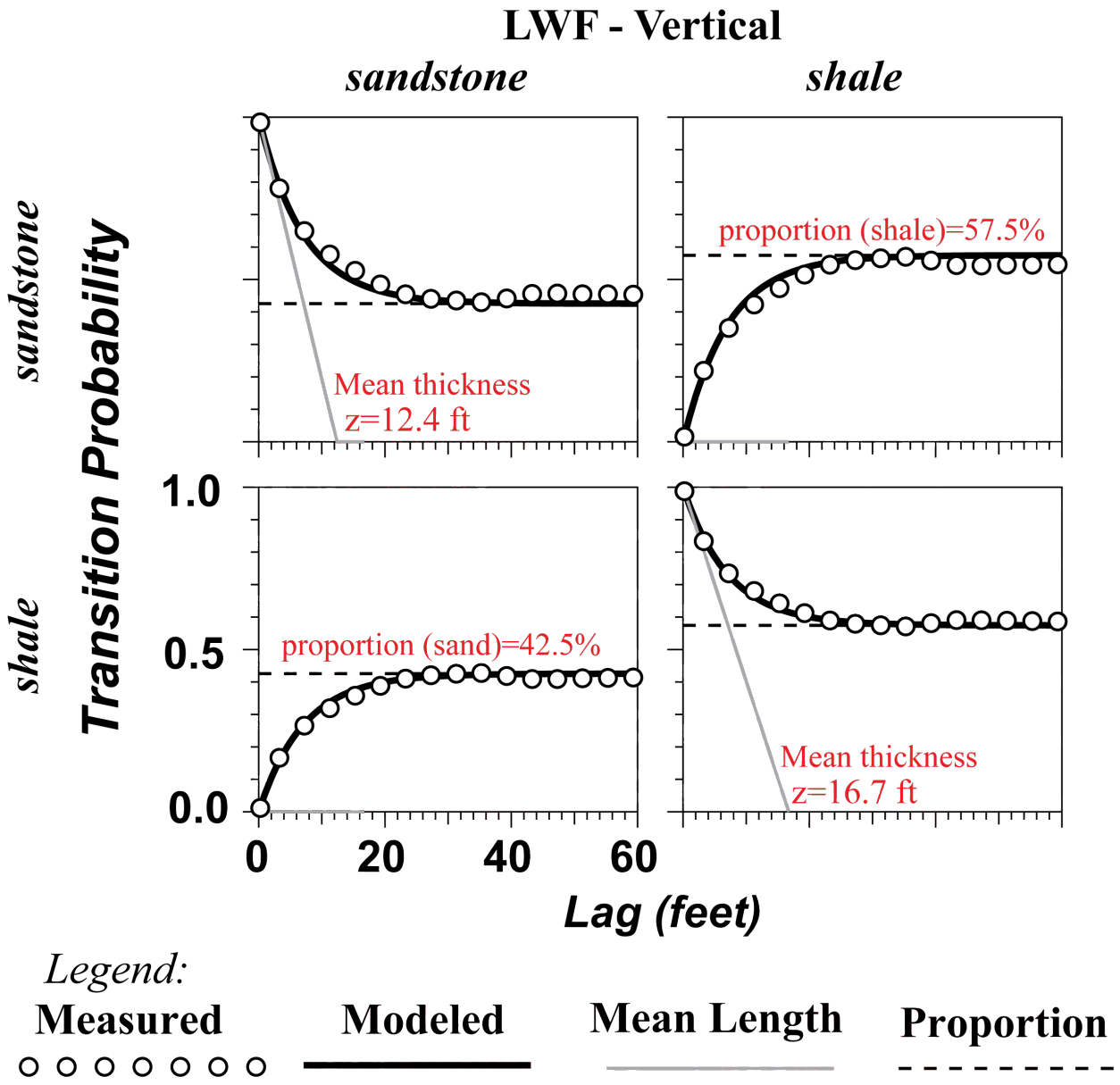

Figure 5. LWF-Vertical: The Markov Chain/Transition probability model along the vertical direction built for LWF, using 8 wells.

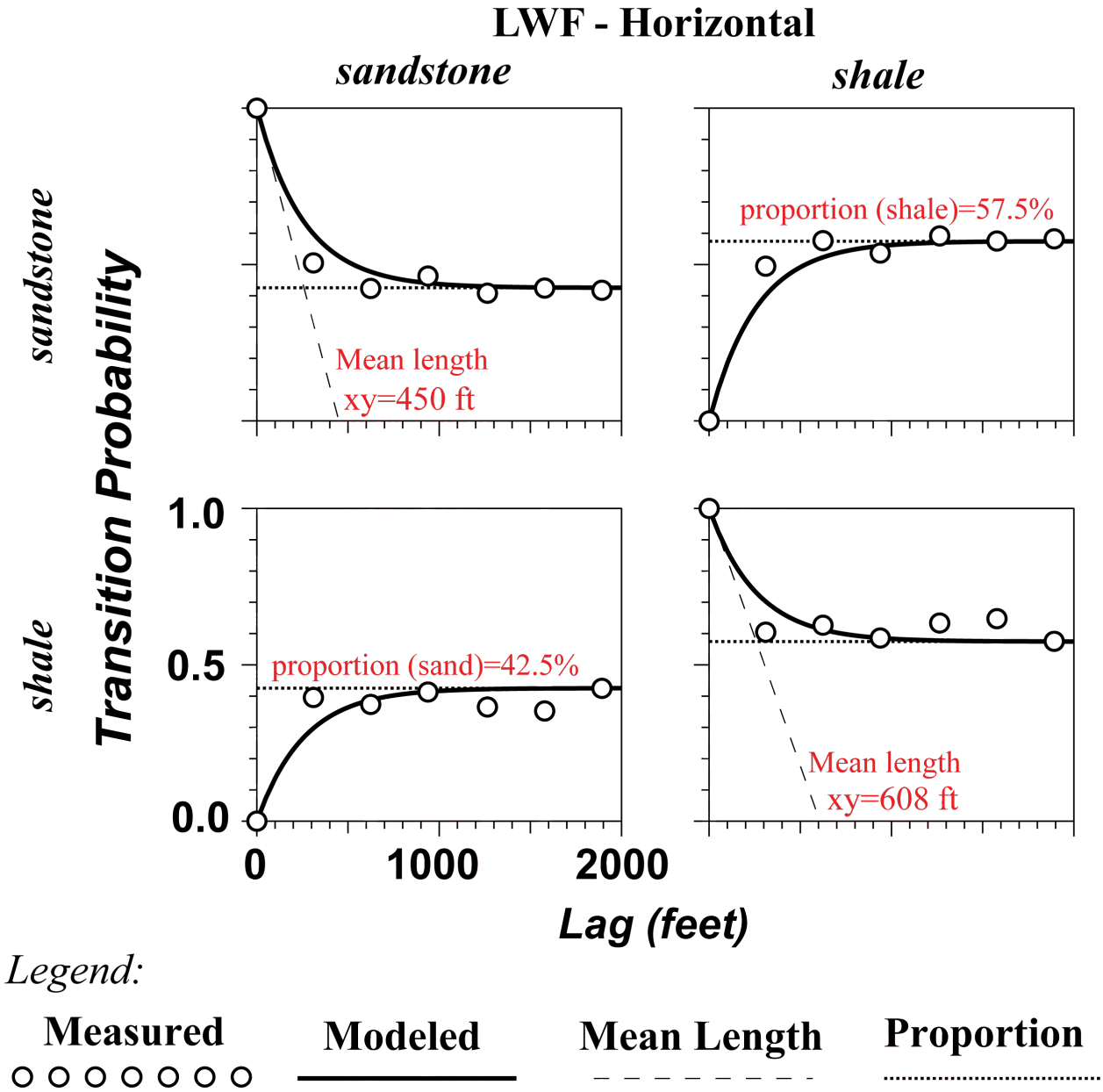

Figure 6. LWF-horizontal: The Markov Chain/Transition probability model along the horizontal direction built for LWF, using 8 wells.

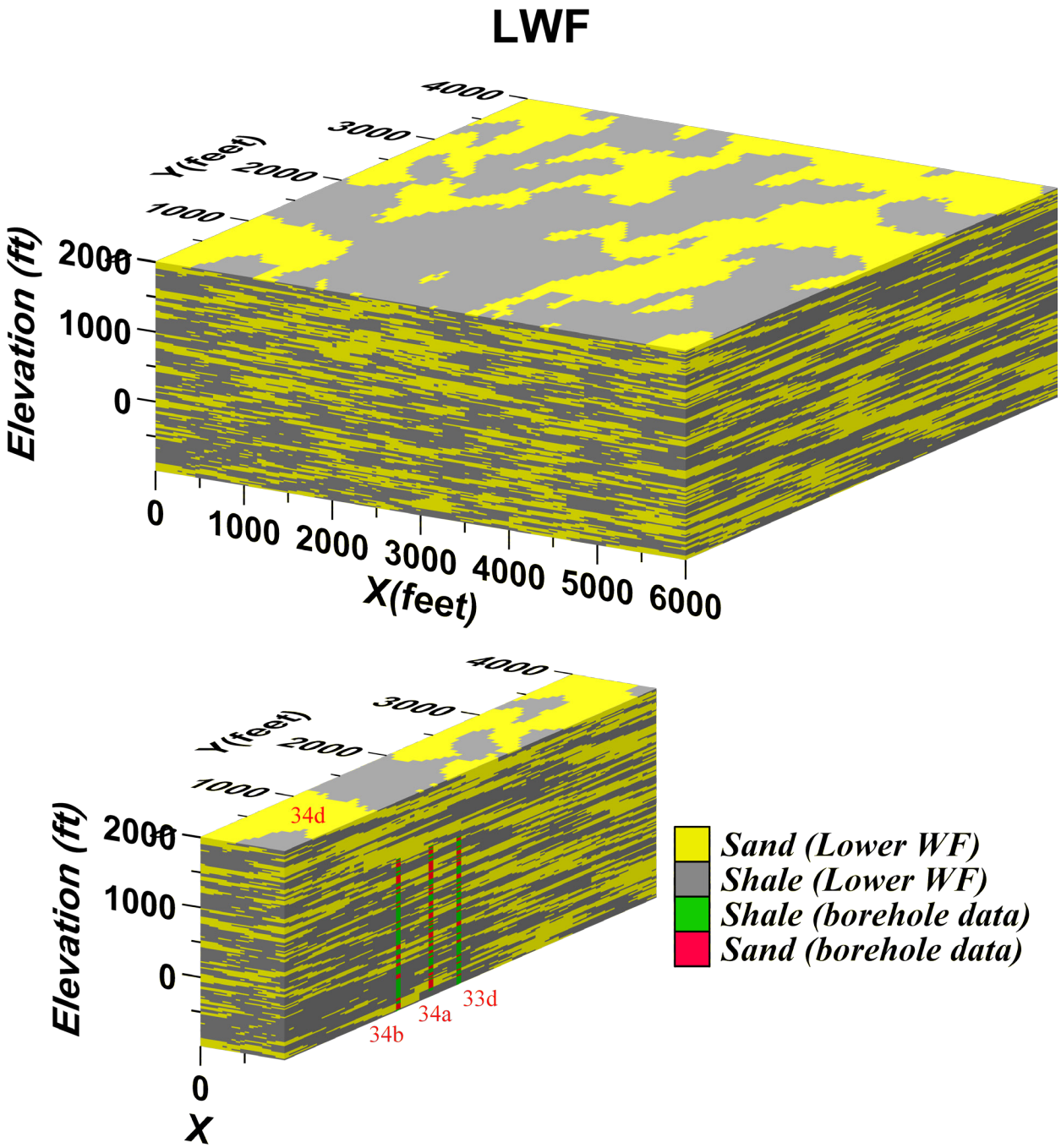

Figure 7. Rulison-LWF hydrofacies model (3-d view and the exploded view) built by TPROGS (using the Markov Chain models shown in Figure 5 and 6).

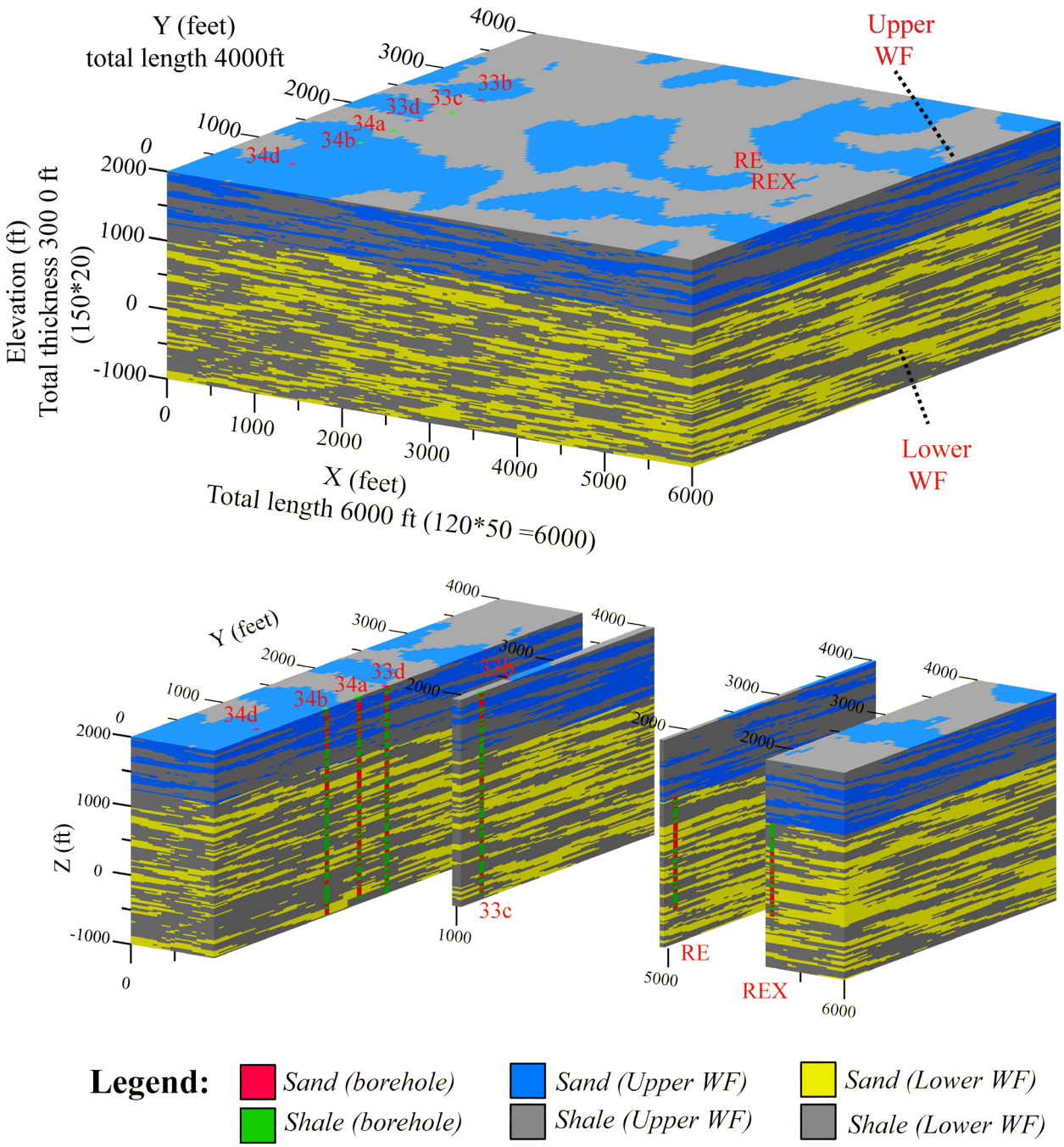

Figure 8. Combining Fig. 4 and Fig. 7 (with the interface shown by Fig. 3)) - Rulison facies model (3-d view and the exploded view) built by TPROGS. 8 wells (26-33b, 26-33c, 26-33d, 26-34a, 26-34b, 26-34d, RE, and REX) are used to build the transition probability model.

Reference

Carle, S. F., Labolle, E. M., Weissmann, G. S., Van Brocklin, D., and Fogg, G. E., 1998, Conditional simulation of hydrofacies architecture: a transition probability/Markov approach, In Fraser, G. S., and Davis, J. M., Concepts in Hydrogeology and Environmental Geology No. 1, SEPM (Society for Sedimentary Geology) Special Publication, p. 147-170.